Characterizing cysteine modifications in Parkinson's-linked parkin and their influence on dopaminergic cell health

Travis Fehr

A thesis submitted in partial fulfillment of the requirements for the Master's degree in Neuroscience.

Department of Cellular and Molecular Medicine
Faculty of Medicine
University of Ottawa

Abstract

Recessive mutations in *PRKN*, the gene coding for parkin, cause early-onset Parkinson disease (PD). Neuronal loss in parkin-deficient PD cases is restricted to specific dopamine-producing neuronal populations that have high oxidative stress. Our lab recently uncovered a role for parkin in redox biology, whereby the wild-type protein neutralizes reactive oxygen species (ROS) as well as reactive electrophilic species (RES), including dopamine itself and its metabolites. We propose that this may be an essential function that parkin confers in these vulnerable neurons. In the current work, I have further characterized parkin's redox function by using mass spectrometry (LC-MS/MS) to analyze the redox state of parkin's cysteines following exposure to H_2O_2 by differentially labelling oxidized vs. reduced cysteines; furthermore, I mapped adducts of reactive dopamine metabolites to specific cysteine residues. Using a differential labelling technique followed by LC-MS/MS analysis, we found that the redox state of parkin's cysteines is altered when exposed to oxidative stress. There, increased oxidation of parkin correlated with both aggregation and insolubility, a phenomenon also observed in adult human brain. Furthermore, by using LC-MS/MS, I have detected adducts of oxidized dopamine metabolites at various cysteine residues on parkin; there, one specific site, the primate-specific residue C95, showed a particular vulnerability to modification by dopamine. This evidence confirmed our previous biochemical assays that had suggested parkin can be directly modified by dopamine. Expanding on previous data generated in our lab, which showed that the presence of wild-type (WT) parkin promotes the formation of melanin *in vitro*, I created a C95A mutation-carrying, recombinant parkin protein and observed that its ability to promote melanin formation *in vitro* was abolished. Similarly, we found that p.C95A parkin is not able to protect cells from

dopamine-induced ROS stress as well as does WT parkin. Overall, these results suggest that parkin's ability to neutralize ROS, to sequester reactive dopamine metabolites (RES) and to promote melanin formation, all via its cysteine oxidation, may confer protection of vulnerable dopamine-producing cells in adult human brain.

Table of Contents

List of Figures

List of Abbreviations

AADC	Aromatic acid decarboxylase
ADH	Aldehyde dehydrogenase
ADP	Adenosine triphosphate
AM	Aminochrome
ATP	Adenosine triphosphate
CCCP	Carbonyl cyanide m-chlorophenyl hydrazone
CNV	Copy number variant
COMT	Catechol-o-methyltransferase
DA	Dopamine
DAQ	Dopamine Quinone
DASQ	Dopamine semiquinone
DAT	Dopamine transporter
DBS	Deep brain stimulation
DHI	Dihydroxyindole
DHIQ	Dihydroxyindolequinone
DNA	Deoxyribonucleic acid
DOPAC	3,4-Dihydroxyphenylacetic acid

DOPAL	3,4-Dihydroxyphenylacetaldehyde
DTT	Dithiothreitol
DβH	Dopamine-β-hydroxylase
ETC	Electron transport chain
GCase	Glucocerbrosidase
GSH	Glutathione
GSSG	Glutathione disulfide
HMW	High molecular weight
HVA	Homovanillic acid
IAA	Iodoacetamide
iPSC	Induced pluripotent stem cell
LC	locus coeruleus
LC-MS/MS	Liquid chromatography mass spectrometry
LDAC	Leukodopaminochrome
L-DOPA	L-3,4-dihydroxyphenylalanine
LRRK2	Leucine-rich repeat kinase 2
L-Tyr	L-tyrosine
MAO	Monoamine oxidase
MASSAD	Mass adduct due to an artifact of the same size as dopamine

MPP^+	1-methyl-4-phenylpyridinium
MPTP	1-methyl-4-phenyl-1,2,3,6-tetrahydropyridine
MS	Mass spectrometry
mtDNA	Mitochondrial DNA
NBT	Nitro blue tetrazolium
NE	Norepinephrine
NEM	N-ethylmaleimide
NM	Neuromelanin
PAGE	Polyacrylamide gel electrophoresis
PD	Parkinson's disease
PINK1	PTEN-induced putative kinase 1
PTM	Post translational modification
RES	Reactive electrophilic species
RING	Really Interesting New Gene
RNS	Reactive nitrogen species
ROS	Reactive oxygen species
r-Parkin	Recombinant human parkin
SDS	Sodium dodecyl sulfate
SEM	Standard error of the mean

SN	Substantia nigra
SOD	Superoxide dismutase
TMT	Tandem mass tag
TCEP	tris(2-carboxyethyl)phosphine
TH	Tyrosine Hydroxylase
TOM	Translocase of the outer mitochondrial membrane
Ubl	Ubiquitin-like domain
UPS	Ubiquitin proteasome system
VMAT2	Vesicular monoamine transporter 2
VTA	Ventral tegmental area

Acknowledgments

This thesis would not have been possible without the support and encouragement of many mentors, peers, friends, and family members.

First and foremost, I would like to thank my supervisor Dr. Michael Schlossmacher for giving me the opportunity to study and work in the lab. Thank you also to Dr. Julianna Tomlinson. You two have been super encouraging and have taught me so much over the past few years as I have developed as a young researcher. I am forever grateful.

Thank you also to my wife Jess. You're love, support, and scientific guidance have helped me get through the good and bad times.

To all my fellow colleagues in the Schlossmacher lab, thank you. You've been so supportive, helpful, and patient as I've learned and grown in the lab. To Daniel and Jackie, thank you for setting up such an amazing project for me to jump into.

Finally, thank you to my family for the support and many questions about my work. Especially, thank you for constantly asking me to explain how my work will help their loved ones living with Parkinson's. I find it easy in my day to day work to fixate only on the basic molecular biology of my own project, but you've helped to me keep the true end goal in mind: to improve the lives of patients.

Chapter 1 Introduction

1.1 Overview of Parkinson's Disease

Parkinson's disease (PD) is a complex neurodegenerative movement disorder. It was first described in 1817 by Dr. James Parkinson in "An Essay on the Shaking Palsy" [1]. In Canada, nearly 100,000 people currently live with PD, making it the second most common neurodegenerative disorder, and with an aging population, the prevalence of PD is forecasted to double by 2031 [2]. The primary symptoms of PD are related to movement and include a resting tremor, slow and stiff movements, impaired balance, and rigidity of the muscles. These symptoms result from a decrease in dopamine, a neurotransmitter that controls movement, due to the death of specific dopamine-producing neuronal populations. Despite its prevalence and decades of research, our understanding of the mechanisms of the disease remain limited, and there currently remains no cure or cause-directed therapy.

1.1.1 Etiology of Parkinson's disease

Most PD cases are known as "sporadic" or "idiopathic" and have no readily identifiable genetic or environmentally induced cause. Nevertheless, 5-10% of cases do have a clear genetic association and are known as "familial" or "heritable". In addition to genetic risk, several environmental risk factors have been identified that increase one's chance of developing idiopathic PD. These including pesticide exposure, prior head injury, rural living, beta-blocker use, an agricultural occupation, and heavy metal exposure. Many of these risk factors are

complementary and are consistent with two current areas of research looking at the effects of toxicant exposure (i.e., pesticides, heavy metals) and inflammation (i.e., immune response to prior infections). Other environmental factors reduce the risk of PD incidence, such as smoking and caffeine consumption [3].

Even though heritable cases comprise a small subset of the total PD patient pool, studying the impact of monogenic parkinsonism-associated mutations provides a valuable method of understanding disease pathogenesis in some of its forms. Parkin, DJ-1, PTEN-induced putative kinase 1 (PINK1), leucine-rich repeat kinase-2 (LRRK2), and α-synuclein are all proteins that have been strongly linked to the development of heritable PD [4-7]. Parkin, DJ-1 and PINK1 are linked to early onset, autosomal recessive disease, whereas LRRK2 and α-synuclein are linked to autosomal dominant forms of the disease. In total, there are nearly 20 genes that have been linked to familial PD [8].

1.1.2 Presentation and pathology of Parkinson's disease

Characteristic PD symptoms include tremor, slowness/stiffness, impaired balance, and muscle rigidity. Many PD cases also present with several non-motor symptoms including autonomic dysfunction, cognitive deficits, sensory abnormalities, and sleep disturbances [9]. The motor symptoms of PD result from the loss of specific dopaminergic neurons in the brain, leading to a deficiency in dopamine, a neurotransmitter that is involved in movement control. One of the pathological hallmarks of PD that can be visualized in *post mortem* brain is the loss of the dark pigment that colours the substantia nigra (SN) in healthy adults. This region of the midbrain has a dark colour due to the presence of neuromelanin, a substance composed largely of

oxidized dopamine. The formation of neuromelanin, its role in PD, and possible interactions of dopamine radicals with parkin will be discussed further throughout this thesis.

Another pathological hallmark of typical late-onset PD is the formation of Lewy bodies. These inclusions are composed largely of misfolded α-synuclein and are deposited in neurons of the brain, spinal cord, vagus nerve, and adrenal medulla [10]. While Lewy pathology has been universally associated with late-onset PD, these inclusions are notably absent in parkin-deficient cases.

1.1.3 Current Treatments and Therapies

Shortly after the discovery that dopamine was deficient in PD brains, it was recognized that patients could be treated with L-3,4-dihydroxyphenylalanine (L-DOPA; levodopa) as a form of dopamine replacement [11,12]. L-DOPA is a naturally occurring chemical precursor of dopamine and, unlike dopamine, can cross the blood brain barrier. This treatment alleviates some of the motor symptoms of PD and is currently considered to be the most effective treatment [13]. Despite its benefits, L-DOPA does not always aid all symptoms, its dose often needs to be increased over time, and it can lead to undesirable side effects such as nausea, vomiting, hypotension, and impulse control behaviour changes. Further, within 5 years of commencing L-DOPA treatment, up to half of PD patients develop motor fluctuations including dyskinesias [14]. Other pharmacological PD treatments include dopamine agonists and monoamine oxidase B inhibitors. These are often utilized in combination with L-DOPA [15].

A well-established surgical treatment for the motor symptoms of PD is deep brain stimulation (DBS). This involves the implantation of an electrode into the subthalamic nucleus, globus pallidus internus, or thalamus and has been shown to effectively regulate motor dysfunction in moderate to severe PD cases. One example of an indication for which this surgical treatment may be recommended is when a patient continues to respond to L-DOPA, but motor fluctuations and dyskinesia have become debilitating. However, DBS is invasive, expensive, and not effective in all patients; it can also have unintended side effects. As a result, it is typically pursued as a last resort in subjects younger than age 70 years with limited "on time" provided by pharmacotherapy. The average time from PD diagnosis to DBS surgical intervention is 10-13 years [16].

Additionally, physical therapy has proved useful in managing the motor symptoms of PD. Exercise, including both aerobic and strength training, has produced positive short and long term results by improving gait, balance, tremor, and motor coordination. Long term improvements have been linked to exercise-induced neuroplasticity [17].

Currently available PD treatments, including pharmacological, surgical, and lifestyle therapies, are useful for managing the symptoms of PD. However, they all have decreasing efficacy over time. This is largely because none of the current treatments address root causes of the disorder. Even with the available treatments, PD will continue to progress. Therefore, additional research is needed to further uncover the mechanism of neurodegeneration in PD. This should lead to target identification for future treatments, and hopefully one day, an intervention to bring PD to a halt.

1.1.4 Introduction to parkin-linked Parkinson's disease

The most common cause of monogenic familial PD is recessive mutations in *PRKN* (PARK2), the gene that codes for the parkin protein. These mutations lead to a form of early-onset PD, which presents as early as adolescence [5]. As mentioned, PARK2-linked PD does not usually present with Lewy-body pathology. Also absent are the cognitive and pervasive autonomic deficits that are often seen in typical late-onset PD [18,19]. Parkin-deficient PD is characterized especially by limb dystonia followed by the classical triad of PD features. Neuropathologically, this PD variant shows progressive and relatively selective loss of dopamine-producing neurons in the SN and Locus coeruleus (LC; where dopamine molecules are quickly processed into noradrenaline). Clinical reports have suggested that parkin-linked disease cases are particularly sensitive to L-DOPA treatment, but are also sensitive to early L-DOPA-induced dyskinesia [20,21]. Parkin's essential function that prevents these specific neurons from degeneration in healthy adults remains unknown.

The *PRKN* gene encompasses 12 exons separated by long intronic sequences. The entire gene spans more than 1.53 Mb, making it one of the longest genes in the human proteome [5,22]. Once transcribed, parkin is a 52 kDa protein composed of 465 amino acids, arranged into five major domains. These include an N-terminal ubiquitin-like domain (Ubl) as well as four RING (Really Interesting New Gene) domains termed RING0, RING1, IBR (in-between-RING), and RING2. Each of the four RING domains are stabilized by coordinating two zinc ions through interactions with seven cysteines and one histidine residue. Over the past few years, several crystal structures of parkin have shown that it adopts a compact structure, stabilized by multiple hydrophobic interactions [23]. The Ubl domain is joined to the four RING domains by a flexible 65-amino acid-long linker region. Movement of the Ubl domain via this flexible linker region

mediates inhibition and activation of parkin's E3 ligase activity. Over 200 mutations within the *PRKN* gene have been identified; however, which of these are pathogenic remains under review. Many of these mutational variants are 'copy number variants' (i.e., CNVs) of individual DNA stretches; point mutants are spread across its domains [24-26]. Many of these mutations affect parkin's structural stability and solubility. Parkin is expressed throughout the body, including notably high expression in the midbrain, cortex, skeletal and cardiac muscle, kidney, and testis [5,27].

1.1.5 Parkin as an E3 Ligase

Parkin is best known for its role as a cytosolic E3 ubiquitin ligase. Previous experiments overexpressing parkin have suggested that is serves as part of the ubiquitin-proteasome system (UPS) where it transfers activated ubiquitin peptides onto lysine residues or the N-terminal amino group of damaged or otherwise unnecessary proteins. Ubiquitination is a common post-translational modification (PTM) that targets these 'to be degraded substrates' for proteasomal degradation or autophagy [28]. Parkin has also been suggested to work with PINK1, another protein that has been linked to autosomal recessive PD, to regulate mitochondrial quality control and promote the selective autophagic elimination (mitophagy) of damaged or depolarized mitochondria [29]. It is believed that during basal conditions, PINK1 is imported into mitochondria by translocase of the outer mitochondria (TOM) complexes [30], where it is cleaved by various mitochondrial proteases [31,32]. As a result, PINK1 levels are low in healthy cells [33]. During these steady-state conditions, parkin is free in the cytosol and its ubiquitin-ligase activity is repressed [34]. However, when the mitochondrial membrane is depolarized, the importation of PINK1 is

inhibited, and instead the protein remains bound to the outer mitochondrial membrane, stabilized in a manner such that the phosphorylation domain of PINK1 is open on the cytosolic face [35,36]. The accumulation of PINK1 and its kinase activity have been shown to recruit activated parkin to the outer mitochondrial membrane. Parkin activation is mediated by phosphorylation of S65 in its Ubl domain leading to conformational change and exposure of its active site in the RING2 domain [37]. At this point, parkin can ubiquitinate various outer mitochondrial membrane proteins, as studied in cellular paradigms. This ultimately leads to autophagic elimination of the depolarized mitochondrion [34,38,39].

Parkin's role as an E3 ubiquitin ligase, and specifically its role in the clearance of damaged mitochondria, is seemingly beneficial to neurons as well as specific cell types that express parkin. For instance, the parkin-dependant removal/turnover of mitochondria in the developing mouse heart has been shown to be critical [40]. However, the absence of parkin's E3 ligase function does not explain the selective vulnerability of SN and LC neurons in parkin-deficient PD. In most cases, the number and structure of mitochondria appear to be normal in the absence of parkin. Further, most parkin mutations that have been linked to PD do not significantly alter its function as an E3 ligase, and some even increase its E3 function [26]. As such, the specific mechanism by which parkin allows at risk cells, dopamine producing neurons, to survive remains unclear. There is considerable evidence that the vulnerability of SN and LC dopamine-producing neurons may lie in their elevated oxidative stress. Our lab also has evidence, currently under review [41,42], that parkin may act as a redox active molecule, and we propose that parkin's critical function may lie in managing these oxidative stressors. The unique oxidative environment of SN dopamine neurons and parkin's redox capabilities will be explored in the following sections.

1.2 Oxidative stress

Since the development of PD is slow and progressive, it is highly unlikely that any sort of acute toxicity is responsible for the death of dopaminergic neurons in typical PD. Rather, ongoing stressors, such as excess pro-oxidant forces, are more likely to be responsible for the progressive neuronal death observed in PD. Redox stress has long been associated with PD; hence, the sources of oxidative radicals, their mechanisms of action, and relevant physiologic antioxidant defenses remain important areas of research. A large subset of reactive oxygen species (ROS) in disease brain is caused by abnormal iron metabolism [43-45]. Iron is a transition metal that is essential for normal cellular function due to its ability to participate in electron-transfer reactions by cycling between ferrous and ferric oxidation states. This is essential for various functions including oxygen transport and storage, electron transport during mitochondrial respiration, DNA repair, and neurotransmitter synthesis (including dopamine), among other functions. However, excess iron can have harmful effects by generating excess ROS. This can occur through mechanisms such as the Fenton reaction which converts hydrogen peroxide into the highly reactive hydroxyl radical. The role of iron in ROS generation is in line with observed increases in iron in specific regions of the aging brain, including the SN [45,46]. Further increases in iron concentration have been described in PD brains [43,47].

1.2.1 Characteristics of vulnerable neuronal populations

A critical question in the field is why dopaminergic neurons of the SN and LC are selectively lost in the absence of parkin, while other regions, including dopamine-producing neurons of the Ventral Tegmental Area (VTA), are mostly unaffected.

One hypothesis is that the selective vulnerability of certain neuronal populations, particularly dopaminergic neurons of the SN, are selectively vulnerable due to their relatively high level of metabolic activity, leading to higher than average oxidative stress. These cells are autonomous pacemakers that fire regularly at 2-4 Hz (even in the absence of synaptic input). This maintains dopamine levels in brain regions innervated by the SN, particularly the striatum; however, this process is metabolically demanding. Particularly, this firing utilizes voltage-dependent Cav1.3 L-type calcium channels, leading to extensive calcium influx. This is distinct from most neurons, including dopaminergic neurons in the neighbouring VTA, which rely exclusively on monovalent cation channels to drive pacemaking. Further, among cells that utilize L-type calcium channels, the channels with the Cav1.3 subunit are relatively rare (~10% of L-type calcium channels) and are unique in that they open at a relatively depolarized potential. This allows them to contribute towards driving the membrane to firing; however, this comes at a metabolic cost due to fluctuating cytosolic calcium concentrations [48]. Because cellular calcium is involved in diverse functions ranging from regulating enzyme activity to programmed cell death, its concentration is tightly regulated around 100 nM (10,000x lower than in the extracellular space). Therefore, excess cytosolic calcium must be removed, and this process is ATP-dependant [48-50]. It is believed that this removal of higher than average amounts of cytosolic calcium leads to high oxidative stress in these neurons [51,52].

Another complementary hypothesis proposes that these neurons are selectively vulnerable due to their uniquely high axonal arborization [53-55]. Nigrostriatal axons are unmyelinated and are orders of magnitude larger than other neuronal populations [56]. The axon of one SN dopamine neuron can give rise to more than one million synapses and exceed four meters in total length [57]. Computational models have suggested that the energy requirement for action potential propagation is not linearly related to axon length or surface area, but rather increases according to a power law with regards to the branching and the complexity of axon morphology [53].

In support of data from these computational analyses, *in vitro* work has shown that vulnerable SN dopamine neurons have a higher basal rate of oxidative phosphorylation, a smaller reserve capacity, a higher density of mitochondria in axons, and an elevated level of basal oxidative stress compared to less vulnerable VTA dopamine neurons. The same study found that artificially reducing axonal arborization also reduces basal oxidative phosphorylation and the susceptibility of murine primary neurons to MPP^+ and rotenone, two toxicants that act as mitochondrial electron transport chain inhibitors [58]. Subsequent research from the same group found that in parkin-knock out dopamine neurons, basal oxidative phosphorylation was increased, and survival was reduced in neurons that had complex axonal arborization. This previews parkin's role in antioxidant defences, a concept that will be further explored in following sections. In this study, neurons that survived had a lower expression of the dopamine transporter, which in turn led to reduced vulnerability to the neurotoxin MPP^+. Together, these data suggest that elevated ROS levels caused by extensive axonal arborization and greater dopamine reuptake (oxidative stress due to dopamine will be explored in the following section) may contribute to chronic stress in these neurons. The absence of parkin further increases the

oxidative stress and reduces survival. VTA dopamine neurons, which are far less vulnerable to degeneration, did not show altered survival in the absence of parkin, suggesting that the absence of parkin is potentially lethal only in neurons that exhibit higher energetic demands and higher oxidative stress associated with profuse arborization [59].

1.2.2 Cellular consequences of elevated reactive oxygen species

ROS are normal metabolites produced by cells, and when at appropriate levels and in regulated situations, are a necessary component of cellular homeostasis and signalling. However, excess ROS can have detrimental effects by leading to oxidative stress, which represents an imbalance between ROS production and antioxidant defences. High ROS levels can facilitate the random oxidation of various cellular macromolecules which can damage cellular structures leading to cell death. Previous studies have reported elevated levels of oxidized lipids and DNA in the brains of both familial and sporadic PD patients [60,61]. Oxidative stress can increase the chance of spontaneous DNA mutations, which in turn can make cells more prone to dysfunction [62]. Further, the direct oxidation of proteins can alter or inhibit their activity leading to dysfunction and/or neuronal death. Another sign of oxidative stress is the carbonylation of proteins, lipids, and nucleic acids. Excess carbonylation can lead to malfunction of these biomolecules, toxicity, and activation of inflammation and immune responses [63]. An increase in the incidence of protein carbonyls has been observed in the brains of PD patients [64], including parkin deficient human cases as shown by our team [41].

The electron transport chain (ETC) within the inner mitochondrial membrane is a critical means of energy production but is also a target for ROS-induced damage. During this series of

redox reactions, electrons are passed between multiple protein complexes, resulting in the translocation of protons across the membrane. This proton gradient powers ATP synthase, which phosphorylates ADP into ATP. One significant source of mitochondrial oxidative stress results from the premature leakage of electrons from complexes I and III to oxygen, producing superoxide anions (O_2^-) [65,66]. This ROS production as a by-product of ETC energy production is sufficiently managed under normal physiologic conditions; however, in cases of mitochondrial damage, the ROS production from ETC leakage can be detrimental to energetically demanding cells.

Mitochondria are uniquely susceptible to damage due to ROS. Unlike nuclear DNA, mitochondrial DNA (mtDNA) is not protect by histones, and as a result is more easily oxidized [67]. It also lacks many of the repair mechanisms that nuclear DNA possesses and as a result, mutations in mtDNA accumulate much more rapidly with age [68,69]. Since most proteins coded for by mtDNA are involved with the ETC, these mutations are likely to further disrupt energy production and increase ROS.

The involvement of mitochondria in PD pathogenesis gained attention after certain individuals exposed themselves to illicit preparations of narcotics that were contaminated by the neurotoxicant 1-methyl-4-phenyl-1,2,3,6-tetrabydropyridine (MPTP) and developed PD-like symptoms soon after. *Post mortem* analyses revealed selective destruction of the SN in the brains of these individuals. The selective degeneration of the SN and/or LC following systemic administration of MPTP was further demonstrated using several primate models [70-72]. Subsequent studies revealed that MPTP is able to enter SN neurons via the dopamine reuptake system and undergoes oxidation by monoamine oxidase B [73]. 1-Methyl-4-phenylpyridinium (MPP+), the

oxidized, active form of MPTP, inhibits complex I of the mitochondrial electron transport chain, resulting in electron leakage and ROS generation [74]. While the relevance of MPTP as a parkinsonian phenotype-replicating agent in animal models to the pathogenesis of typical PD has been extensively debated, these findings demonstrate the effect that mitochondrial health and ROS generation have on SN neuronal health, including their survival. In support of this, it has been shown that inhibition of mitochondrial biogenesis in flies similarly leads to the loss of dopaminergic neurons and motor dysfunction [75].

Another compound that has been linked to PD is rotenone, a pesticide. Rotenone is hydrophobic and can cross biological membranes independently of a transporter. The compound's toxicity, both in its functional effect in killing pests and its consequential effect in humans, results from inhibition of Complex I of the mitochondrial ETC. Notably, mice treated with rotenone show similar neurodegeneration patterns to PD, with degeneration specific to SN dopamine neurons while other neuronal populations, including VTA dopamine neurons, are relatively spared [76].

Redox stress in the SN has also been observed in human brain. Even in the SN of healthy individuals, the concentration of oxidized proteins was found to be twice as high as in the caudate, putamen and frontal cortex [77]. It is believed that increases in this redox stress and/or deficits in the capacity of these cells to manage and reduce ROS is implicated in the loss of these neurons in PD. In addition to observations of oxidized cellular metabolites in the midbrain neurons of both familial and sporadic PD cases, additional evidence for oxidative stress being implicated in the development of PD comes from observations of altered redox states due to mutations in various PD-linked proteins. One study utilized induced pluripotent stem cells

(iPSCs) derived from patients with parkin or PINK1 mutations. They observed mitochondrial dysfunction, increased sensitivity to CCCP (an inhibitor of oxidative phosphorylation), and dopamine accumulation in PD iPSCs versus control cell lines [78]. Another study used iPSCs with a G2019S LRRK2 mutation (PD-linked) and observed elevated expression of various genes involved in oxidative stress regulation as well as reduced survival when treated with oxidative stressors such as H_2O_2, 6-hydroxydopamine, or MG132, a proteasome inhibitor. Another protein linked to recessive familial PD, DJ-1, is known to be a redox-active sensor of oxidative stress. DJ-1 can be oxidatively modified at several of its cysteine residues [79]. Oxidized DJ-1 has been shown to prevent MPP+ induced cell death [80]. Multiple observations can be made from these results: (1) A single mutation can significantly disrupt cellular redox homeostasis. (2) Various PD-linked genes individually have implications in redox homeostasis. (3) This suggests that even in the absence of monogenic PD-linked mutations (i.e. sporadic PD cases), PD progression is likely impacted by altered interactions between these proteins and other redox-active cellular metabolites in oxidatively demanding neurons.

1.2.3 Known redox sensors and antioxidants

In order to manage oxidative stress, cells across the body utilize various antioxidants. Superoxide dismutase (SOD) converts O_2 into the slightly less reactive hydrogen peroxide. Catalase is a heme-containing enzyme that catalyzes the decomposition of hydrogen peroxide to water. Similarly, glutathione peroxidases and peroxiredoxins detoxify hydrogen peroxide into oxygen and water. Glutathione (GSH) and thioredoxin are both thiol-containing proteins that act

as antioxidants through cysteine-thiol disulfide exchange. They reduce ROS through the direct oxidation of their cysteine residues.

Alongside increasing ROS levels in the aging SN, a reduction of key antioxidants, including superoxide dismutase, glutathione peroxidase, glutathione reductase, and reduced glutathione, have all been observed in *post mortem* SN of healthy, aged individuals compared with younger individuals. Despite this moderate age-dependant reduction in antioxidant capacity in healthy SN, a much more drastic reduction has been observed in the SN of PD patients. This includes a ~40% reduction in glutathione levels, suggesting that glutathione production and recycling is either impaired and/or is unable to match hydrogen peroxide production. There is also evidence that superoxide anion (O_2^-) clearance is impaired in PD SN due to SOD1 enzymatic dysfunction and aggregation [81-84]. A reduction in the level and function of catalase has also been observed in PD SN [85].

Whether or not the decline in antioxidant capacity in PD SN is the result of or the cause of increased ROS levels is not entirely clear. With regards to non-enzymatic proteins such as glutathione, it is plausible that the decrease in the level of reduced glutathione molecules (GSH) is directly correlated to an increase in oxidized glutathione molecules (GSSG). Overall, there is strong evidence that the resulting oxidative stress is implicated in PD pathogenesis. Our has evidence that parkin contributes to the cellular thiol pool and thereby functions as an antioxidant. This critical function would serve a clear benefit to oxidatively demanding cells in the SN and LC.

1.3 Dopamine Metabolism and Toxicity

Dopamine was first identified as a neurotransmitter in the 1950's [86] after previously being considered to only be a precursor to epinephrine and norepinephrine. It was later established that dopamine-containing neurons were central to pathways involved in motor functions, reward, and cognition [87]. Dopamine depletion was linked to PD in the 1960's [88,89]. We now know that the loss of dopamine-producing neurons in the SN, leading to dopamine deficiency in the caudate nucleus and putamen, results in the prominent motor symptoms of PD. Degeneration of neurons in the LC, which utilize norepinephrine as a neurotransmitter, also occur in PD and are believed to contribute to both the motor and non-motor symptoms of PD [90,91].

1.3.1 Normal Dopamine Metabolism

The primary dopamine production pathway begins with L-tyrosine, whose phenol ring is hydroxylated by tyrosine hydroxylase (TH) to produce L-DOPA [92]. This is followed by decarboxylation by aromatic acid decarboxylase (AADC) to produce dopamine [93]. Dopamine can then be packaged into vesicles for use as a neurotransmitter, or in applicable neurons, dopamine can be converted to norepinephrine through hydroxylation by dopamine β-hydroxylase (DβH) [94,95]. Under normal physiologic conditions, the dominant pathway of dopamine degradation occurs through oxidative deamidation by monoamine oxidase (MAO), producing 3,4-dihydroxyphenylacetaldehyde (DOPAL), another very reactive metabolite. This reaction also produces hydrogen peroxide and ammonia, two potentially neurotoxic species. DOPAL is subsequently converted to a less reactive acid species (DOPAC) by aldehyde dehydrogenase (ADH). Catechol-O-methyltransferase (COMT) converts DOPAC to homovanillic acid (HVA), a

nonreactive metabolite. The pathways and intermediates outlined here are shown in Figure 1.1. Various minor pathways of dopamine production or degradation have been discovered and are described in review articles [96-99].

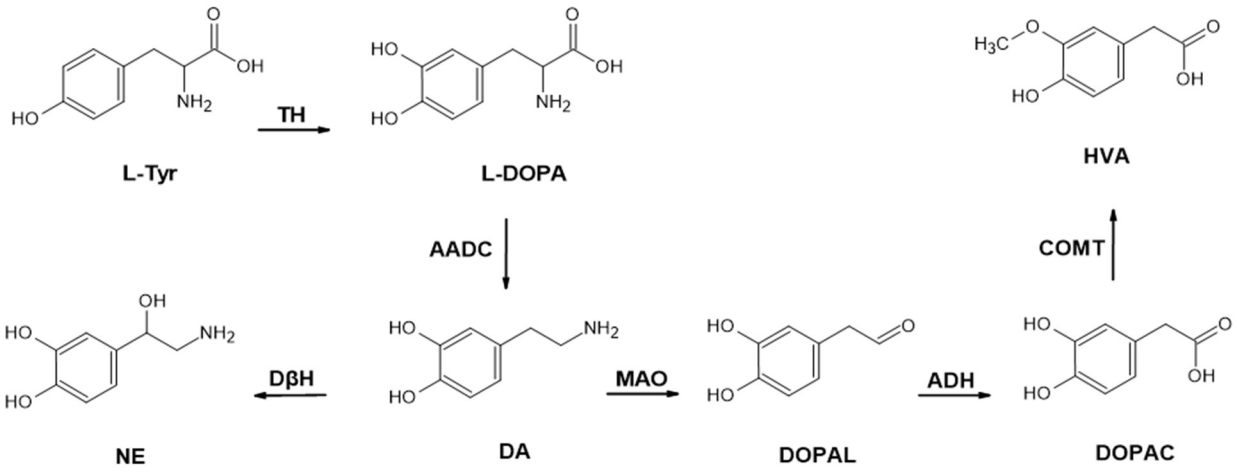

Figure 1.1: Pathway of normal dopamine production and metabolism.

L-Tyr: L-tyrosine; **TH**: Tyrosine hydroxylase; **L-DOPA**: L-3,4,-dihydroxyphenylalanine; **AADC**: Aromatic acid decarboxylase; **DA**: Dopamine; **DβH**: Dopamine β-hydroxylase; **NE**: Norepinephrine; **MAO**: Monoamine oxidase; **DOPAL**: 3,4-dihydroxyphenylalanine; **DOPAC**: 3,4-dihydroxyphenylacetic acid. **HVA**: Homovanillic acid.

1.3.2 Dopamine Signalling

In dopaminergic neurons, dopamine is produced in the cytosol but then imported into synaptic vesicles by vesicular monoamine transporter 2 (VMAT2), where it is stored until needed for signalling. There is evidence that VMAT2 physically associates with TH and AADC,

two enzymes involved in the synthesis of dopamine as previously described [100,101]. Upon excitation of dopaminergic neurons, these synaptic vesicles fuse with the plasma membrane, releasing dopamine into the extracellular space where it performs its function as a neurotransmitter. Signalling is attenuated as dopamine is removed from the extracellular space by the dopamine transporter (DAT). Once in the cytosol, dopamine can be once again sequestered into vesicles by VMAT2 or degraded by the pathway previously described. Dopamine removal from the extracellular space and subsequent degradation can also be mediated by astrocytes [102].

1.3.3 Neuromelanin formation

Dopamine production and metabolism take place in the cytosol, and its uptake into vesicles or enzymatic degradation is not instantaneous. This results in low levels of free dopamine in the cytosol of dopamine neurons. Dopamine has a relatively low free energy barrier to oxidation making it susceptible to spontaneous auto-oxidation. This is avoided in dopamine storage vesicles due to their acidic environment. Factors such as increased ROS, decreased antioxidants such as GSH, and increased concentrations of metals such as copper and iron can all increase the rate of dopamine auto-oxidation. Notably, all these factors have been linked to the degeneration of vulnerable neuronal populations in PD.

Dopamine can undergo either one electron oxidation to dopamine semiquinone (DASQ), a radical species, or two electron oxidation to dopamine quinone (DAQ). The amino group of DAQ cyclizes quickly to form aminochrome (AM; dopaminochrome) through the unstable intermediate leukodopaminochrome (LDAC) [103]. While still quite reactive, aminochrome is more

stable than the preceding intermediates. Aminochrome can accumulate to a degree, but can also be further rearranged to 5,6-dihydroxyindole and oxidized to 5-,6-dihydroxyindolequinone [96,104]. Further oxidation and polymerization of these dopamine metabolites leads to the formation of neuromelanin. This oxidative pathway is outlined in Figure 1.2.

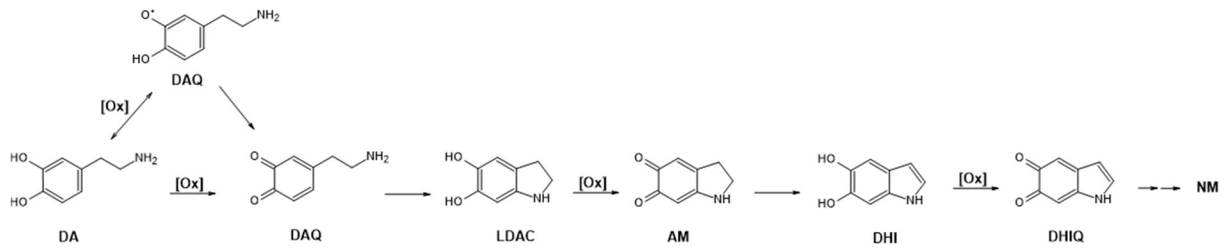

Figure 1.2: Dopamine oxidation pathway associated with neuromelanin formation.

DA: Dopamine; **DAQ**: Dopamine quinone; **LDAC**: Leukodopaminochrome ; **AM**: Aminochrome; **DHI**: 5,6-dihydroxyindole; **DHIQ**: 5,6-dihydroxyindolequinone; **NM**: Neuromelanin.

The protective effects of neuromelanin can be ascribed to the elimination of these intermediate reactive metabolites from the cytosol. Neuromelanin can also conjugate and trap potentially toxic metal ions, including copper and iron. This can help prevent further cellular ROS generation and dopamine oxidation. The polymerized dopamine may be further elaborated by conjugating protein and lipid species and sequestered into specialized neuromelanin autophagic-lysosomal organelles [105].

Dopamine neuron populations with higher VMAT2 expression (VTA > substantia nigra pars reticularis > SN) have a corresponding lower level of neuromelanin synthesis (SN >

substantia nigra pars reticularis > VTA) [96]. On the surface this suggests that the vulnerability of dopamine neurons is related to their neuromelanin content; however, it is much more likely, and widely accepted, that dopamine neuron vulnerability is more directly related to higher concentrations of oxidized dopamine species (i.e. the intermediates leading to neuromelanin formation). Cytosolic dopamine concentrations need to be kept relatively low to maintain neuronal health. Intracellular patch electrochemistry recordings have suggested that neuromelanin synthesis occurs when cytosolic dopamine concentrations are above 3 μM [96]. If cytosolic dopamine exposure is elevated for too long, dopamine toxicity will potentially outpace available protective, neutralizing mechanisms resulting in neuronal death. Some known mechanisms that neurons use to limit cytosolic dopamine concentrations include sequestration into synaptic vesicles by VMAT2, catabolic breakdown by MAO, allosteric feedback inhibition by dopamine on tyrosine hydroxylase, and dopamine metabolite sequestration by antioxidants such as glutathione (GSH).

1.3.4 Dopamine Reactivity and Toxicity

Dopamine is a very reactive metabolite, and when it is not sequestered into vesicles or degraded as previously described, can be a significant stressor to vulnerable neuronal populations. As previously described, dopamine can be oxidized to various highly reactive and toxic metabolites such as dopamine quinone and aminochrome [106,107]. These can be detrimental to protein function. For example, one study showed that the lysosomal enzyme glucocerebrosidase (GCase), itself an important PD risk factor, can be modified by dopamine quinones, reducing its activity. This was demonstrated using recombinant GCase as well as in

iPSCs from a PD patient with a homozygous loss-of-function mutation in DJ-1. This mutation significantly increased mitochondrial oxidant stress, resulting in increased levels of oxidized dopamine which covalently modified and inhibited GCase [108].

Another study used 2D-gel electrophoresis and nitro blue tetrazolium (NBT) staining to compare dopamine quinone modifications in the SN of 2-month old vs. 15-month old rats. Of the five protein spots that showed the most prominent increase in NBT staining intensity, four of these corresponded to proteins involved in energy metabolism and mitochondrial function. Two of these enzymes, lactate dehydrogenase and malate dehydrogenase, were selected for further analysis. It was determined that modification of these enzymes by dopamine quinone had a significant impact of their activity, and that this inhibition could be reversed by the addition of GSH [109].

1.4 Parkin as a redox-active molecule

Considering the extraordinary degree of oxidative stress that dopamine neurons of the SN and LC face due to high levels of reactive metabolites such as ROS and RES over decades in humans, and the selective neuroprotective role of parkin in these cells, our lab has pursued parkin's role in protecting these vulnerable neuronal populations against oxidative stress. Parkin contains an unusually high proportion of cysteine residues, at 7.5% (35/465) of its amino acids. Cysteines are highly reactive thiol-containing residues. Thiols are vulnerable to oxidation and can to participate in redox chemistry. In a typical redox reaction, the oxidation of one substrate, leads to the reduction of the other. Oxidation of parkin has been shown (discussed below). Previous and ongoing studies in the lab tested our hypothesis that parkin protects these cells

specifically, by acting as a redox sensor, to detect and neutralize redox stress, including toxic, reactive metabolites related to ROS, RES or RNS (reactive nitrogen species), and that it does so through the donation of its own thiols leading to its own oxidation.

While parkin oxidation has been described before, these were always interpreted as loss-of-function events. For example, previous studies found that dopamine can modify parkin in cell culture, decreasing parkin's solubility and inhibiting its E3 ubiquitin ligase function [110]. Similarly, dopaminergic cells treated with hydrogen peroxide reduced parkin's solubility, correlating with decreased E3 ligase activity. Notably, parkin was found to be uniquely susceptible to ROS and dopamine induced inactivation/insolubility among various E3 ligase proteins [111]. It has also been shown that RNS stress can lead to S-nitrosylation of parkin *in vitro* and *in vivo.* This includes in mice treated with MPTP vs. controls, as well as in human PD brains compared to age-matched healthy brains [112,113]. Interestingly, it has been reported that this modification of parkin leads to an initial increase in its E3 ligase activity, but subsequently and ultimately inactivates this function [113]. Until now, the field has largely interpreted these ROS, RNS and dopamine-induced parkin modifications as loss of function. In direct contrast, we proposed that parkin oxidation reflects an important, neuroprotective function for this protein: parkin oxidation could confer antioxidant protection to the cell.

A study looking at dopamine neuron integrity in parkin-mutant *Drosophila* provided further evidence that parkin may contribute to the cellular antioxidant pool. Dopamine neuron death was observed in the high energy PPL1 neurons of these flies. Further inhibition of glutathione S-transferase S1, which has been suggested to play a role in detoxifying products of oxidative damage, enhanced the observed neurodegeneration. This supports the hypothesis that

the observed neuronal death in the absence of parkin is linked to increased oxidative stress [114]. Furthermore, in mice, parkin deficiency has revealed various metabolic abnormalities, including deficits in mitochondrial function, decreased levels of other proteins involved in protection from oxidative stress, lipid peroxidation, and overall decreased serum antioxidant capacity [115].

In our own studies, summarized in the following paragraphs and under peer review [41,42], *post-mortem* analysis of human control brains (i.e., the cause of death was non-neurological), revealed that parkin was predominantly insoluble in brains from older individuals. We looked at brains from across the lifespan and found that parkin solubility correlates with age. In young human brain, parkin is present mostly in the more soluble fractions, while in mid age and older human brain, parkin is present mostly in the less soluble fractions. This lack of soluble parkin in older human brains was not due to the absence of parkin mRNA. In addition to transitioning from the soluble to insoluble cellular fraction with age, parkin was also detectable in high molecular weight (HMW) aggregated "smears". These HMW parkin aggregates were collapsed to the monomeric size by the addition of DTT prior to Western blot analysis, suggesting that reversible oxidative modifications, such as inter-molecular disulfide bond formation, were largely responsible for parkin's aggregation. This is hypothesized to occur due to increasing oxidative stress in the brain as one ages.

The formation of HMW parkin aggregates and its transition from the soluble to insoluble fraction due to oxidative stress was previously modeled by our team in vitro using recombinant human parkin (r-parkin). Treatment with H_2O_2, aminochrome, CCCP, or rotenone all caused parkin to aggregate and become progressively insoluble. A similar shift in solubility was seen in cells expressing human parkin and treated with H_2O_2, as well as in the brains of mice that had

increased ROS due either to an acute exposure to MPTP or haploinsufficiency at the SOD2 locus. We showed *in vitro*, and in cells, that H_2O_2-induced changes in solubility were thiol-dependent, as if the r-parkin or cells were pre-incubated with n-ethylmaleimide (NEM), a compound that binds to and blocks cysteine thiol groups, and then treated with H_2O_2, no parkin aggregation was observed, and parkin remained soluble. Structural changes due to parkin oxidation were independently confirmed by collaborators using dynamic light scattering and far-UV-circular dichroism. These experiments confirmed multimer formation as well as a shift from α-helically ordered and unstructured protein in the soluble fraction to increased β-pleated sheet positive r-parkin in the insoluble fractions.

The redox hypothesis was such that we predicted that oxidation of parkin conferred a protective benefit to the cells. Indeed, in vitro assays have also revealed that parkin directly reduces hydrogen peroxide to water. This occurs in a concentration and time-dependant manner. This ability is diminished if parkin is previously oxidized or treated with NEM to block its cysteine residues. This further suggests that parkin becomes oxidized by the direct oxidation of its cysteines, and that through its own oxidation, parkin may confer cellular benefit by reducing otherwise harmful reactive species.

In addition to ROS (H_2O_2) stress, our lab was particularly interested in how parkin could protect against reactive dopamine metabolites. Previous sections outlined the metabolism of dopamine, including one pathway by which its progressive oxidation can lead to the formation of neuromelanin. Since several intermediate species in this pathway are extremely reactive and potentially toxic, while neuromelanin is a stable species, it would follow that molecules that help to promote the formation of neuromelanin would have a protective effect. Using an absorbance-

based assay that measures the spontaneous oxidation of dopamine to neuromelanin over time, our team demonstrated that the presence of r-parkin significantly increases the rate of neuromelanin formation compared to dopamine alone or in the presence of other proteins, suggesting that it could participate in neuromelanin formation in dopamine cells. While not proof, studies in our lab using newly created monoclonal antibodies against parkin, led to the discovery that parkin is physically associated with neuromelanin in human dopamine neurons.

These previous findings from our lab, described above, strongly suggest that parkin is uniquely sensitive to oxidative stress. Rather than this being detrimental to parkin's function as has long been the dominant view in the field, our lab believes that parkin's redox capabilities provide functional benefit to metabolically demanding dopamine-producing neurons that are vulnerable in PD. This view explains the selective vulnerability of these neuronal populations as well as the protective effect that parkin has on their survival. In light of this view, my project has sought to extend and further validate parkin's redox capabilities by using mass spectrometry to quantify, map and characterize the redox state of cysteine residues on parkin.

I hypothesize that: i) the solubility and reducing capacity of the parkin protein is dependent on the redox state of its cysteine residues; ii) that parkin's reducing capacity is beneficial to at-risk neurons, such as through covalent conjugation of highly reactive dopamine radicals; and iii) that in this process parkin plays a direct role in the formation of neuromelanin.

The objective of my current project has been to validate and extend the aforementioned findings by using mass spectrometry to further analyze the state of parkin's cysteine residues at baseline and following exposure to stressors such as ROS and RES. This has been accomplished through two aims: **Aim 1** has quantitatively analyzed the redox state of parkin's cysteines at

baseline and following exposure to H_2O_2 by differentially tagging reduced vs. oxidized residues. **Aim 2** has optimized the detection of dopamine metabolite post translational modifications (PTM) on parkin following exposure to aminochrome *in vitro*.

Chapter 2 Materials and Methods

Recombinant protein expression in pET-SUMO vector

Wild-type human parkin was expressed as a 6-His-Smt3 fusion protein in *Escherichia coli* BL21 (DE3) Codon-Plus RIL competent cells (C2527, New England Biolabs) as previously described [116-118]. The C95A parkin mutant in the pET-SUMO vector was generated using site-directed mutagenesis. The cells containing the overexpressed, His-tagged parkin protein were grown at 37°C in 2% Luria Broth containing 30 mg/L kanamycin and 0.5 mM $ZnCl_2$ until OD600 reached 0.6, at which point the temperature was reduced to 16°C. Once OD600 reached 0.8, protein expression was induced with 25 μM isopropyl β-D-1-thiogalactopyranoside. The culture was left to express protein for 16-20 hours. Cells were harvested by centrifugation (4000 x g at 4°C for 10 min), lysed by incubation with 1:1000 lysozyme (stock made at 100 mg/mL) for 30 min followed by sonication (Amplitude: 50%, 4 minutes total, pulse: 30 seconds ON, 10 seconds OFF), and collected on Ni-NTA agarose beads by batch binding for 1 hour at 4°C. The beads with His-SUMO recombinant protein bound were washed 6 times with T500 buffer (50 mM Tris, 500 mM NaCl, 250 μM TCEP, 25 mM imidazole) and 2 times with T200 buffer (50 mM Tris, 200 mM NaCl, 250 μM TCEP, 25 mM imidazole). Purified recombinant protein was eluted from the beads by a 10 min incubation with T200 buffer containing 250 mM imidazole. For most experiments (except those indicated in the results section), the His-SUMO tag was removed by the addition of ULP1 protease and overnight dialysis at 4° in dialysis buffer (50 mM Tris, 200 mM NaCl, 250 μM TCEP). The cleaved tag was collected on Ni-NTA beads, the

purified protein was collected, and its stability confirmed by silver staining. Aliquots were stored at -80 °C.

Recombinant protein preparation

Prior to all in vitro stress experiments, the recombinant protein was prepared by removing TCEP (tris(2-carboxyethyl)phosphine), present in the elution and storage buffers, using repeat centrifugations (8 times 14,000 x g at 4°C for 5 min) in 30 kDa MWCO filters. The protein concentration was measured using a bicinchoninic acid (BCA) assay and adjusted as appropriate. In vitro stress experiments were performed with a final protein concentration of 30 µM. Recombinant parkin was incubated with H_2O_2 or aminochrome for 30 or 60 minutes respectively at 37°C, at varying concentrations as indicated in the results. Control samples were also incubated at 37°C with equal volumes of water. For applicable experiments, EDTA was prepared fresh and incubated with samples for 30 minutes at 37°C prior to aminochrome treatment. Aminochrome was synthesized freshly from dopamine as indicated below.

For experiments where soluble and insoluble fractions were separated, following the initial incubation, samples were centrifuged at 21,000 x g for 15 minutes. The supernatant was transferred to a fresh tube and the remaining pellet was extracted with 10 % SDS (Sodium dodecyl sulfate), using a volume equal to that of the supernatant. The pellets were incubated in SDS for 30 min at 37°C. Laemmli buffer (with DTT or gels labelled as “reducing conditions” and without for those labelled “non-reducing conditions”), was added to both the soluble and pellet fractions and samples were separated by SDS-PAGE.

For differential labelling experiments, following separation of the soluble and insoluble fractions, samples were treated sequentially with 5 mM iodoacetamide (IAA), 40 mM

dithiothreitol (DTT), and then 90 mM n-ethylmaleimide (NEM). Samples were incubated for 30 minutes at 37°C following each of the IAA, DTT, and NEM addition steps. All reagents were prepared fresh. NEM in particular was prepared within minutes of use of use.

Aminochrome synthesis

A solution of 0.1 M sodium phosphate buffer pH 6.0 was prepared from a mixture if 12 mL of 1 M NaH_2PO_4 and 88 mL of 1 M Na_2HPO_4. The reaction buffer (0.067 M sodium phosphate pH 6.0) was prepared by adding 33 mL of 0.1 M sodium phosphate buffer to 17 mL water. A solution of 10 mM dopamine in reaction buffer was prepared by adding 19 mg of dopamine hydrochloride to 1 mL of reaction buffer. Oxidation was activated by adding 20 µL of tyrosinase (25,000 U/mL) and the mixture as incubated at room temperature for 10 min. The tyrosinase was removed by centrifugation (14,000 x g for 10 min) using a 10 kDa MWCO filter. The absorbance of the filtrate was measured at a wavelength of 475 nm using an Ultrospec 2100 pro spectrophotometer and the concentration of aminochrome was determined using the Beer-Lambert equation and extinction coefficient of 3058 L x mol^{-1} x cm^{-1}.

Silver staining

All proteins were separated on pre-cast 4-12% Bis-Tris SDS-PAGE gels (Invitrogen) using MES running buffer (650 mM MES, 50 mM Tris, 1 mM EDTA, and 0.1 % SDS, pH 7.3) and Laemmli loading buffer (10% SDS, 20% glycerol, 0.1% bromphenol blue 0.125 M Tris HCl).

Proteins were stained in gel using a SilverQuest Silver Staining Kit (LC6070; Invitrogen) using the following protocol (“Fast” protocol as per kit instructions, volumes modified): The gel

was transferred into a plastic container, 50 mL of Fix solution (all solutions were prepared as per the kit instructions) was added, the gel was heated for 30 seconds in a microwave at full power, and was then incubated on a rocker for 5 min. the liquid was discarded, and 50 mL of 40% ethanol was added, the gel was heated in a microwave for 30 seconds at full power and then incubated on a rocker for 5 min. The liquid was discarded and 50 mL of "Sensitize" solution was added, the gel was heated in a microwave for 30 seconds at full power and then incubated on rocker for 2 minutes. The liquid was discarded, 50 mL of water was added, the gel was heated in a microwave for 30 seconds at full power and then incubated on a rocker for 2 minutes. This wash step in water was repeated one more time. The liquid was discarded, 50 mL of "Stain" solution was added, the gel was heated in a microwave for 30 seconds at full power and then incubated on a rocker for 5 minutes. The liquid was discarded, 50 mL of water was added and incubated for 1 minute. The liquid was discarded, 50 mL of "Developer" solution with "Developer Enhancer" was added, and the gel was left until protein bands were visible at an appropriate intensity. The reaction was quenched by adding 5 mL of "Stopper" solution and left for 10 minutes. The liquid was discarded, and the gel was washed with 50 mL if water for 10 minutes on a rocker. The gel was then imaged.

Peptide analysis by LC-MS/MS

Proteomics analysis was performed at the Ottawa Hospital Research Institute Proteomics Core Facility. Proteins were digested in-gel using trypsin (Promega) according to the method of Shevchenko [119]. Peptide extracts were concentrated by Vacufuge (Eppendorf). LC-MS/MS was performed using a Dionex Ultimate 3000 RLSC nano HPLC (Thermo Scientific) and Orbitrap Fusion Lumos mass spectrometer (Thermo Scientific). MASCOT software version 2.6.2 (Matrix Science, UK) was used to infer peptide and protein identities from the mass spectra. For

detection of dopamine metabolites on Parkin, the following variable modifications were included: 5,6-indolequinone (+$C_8O_2NH_3$, m/z shift +145), aminochrome (+$C_8O_2NH_5$, +147), aminochrome +2H (+$C_8O_2NH_7$, +149), and dopamine quinone (+$C_8O_2NH_9$, +151). The observed spectra were matched against human sequences from SwissProt (version 2018-05) and also against an in-house database of common contaminants. The results were exported to Scaffold (Proteome Software, USA) for further validation and viewing.

For applicable experiments, the raw MS data files were further processed with MaxQuant software version 1.6.5 and searched with the Andromeda search engine [120]. The reference fastas were set to uniprot-human (version 2019-02-12) and uniprot-E.coli. The *E. coli* proteome was included to account for bacterial proteins present in the recombinant protein samples. The 'second peptides' and 'match between runs' settings were enabled. All other settings were left as default. Selected variable modifications included oxidation (Met), acetylation (protein N-terminus), and carbamidomethyl (Cys), as well as custom modifications for pyro-carbamidomethyl (N-terminal Cys), N-ethylmaleimide (Cys), and NEM+water (Cys).

Western blotting

Proteins were separated by SDS-PAGE using 4-12% SDS gels in MES buffer. Proteins were transferred to PVDF membranes and blotted for parkin using the Prk8 antibody (Biolegend 808503, 1: 5,000) or parkin clone E (Biolegend A15165E 1:1000).

Nitro blue tetrazolium (NBT) Staining

Proteins conjugated to redox-cycling molecules were stained using the following NBT stain protocol: Following transfer from gel to a PVDF membrane, the membrane was washed

twice with water, covered from light and incubated with rocking for 45 min in NBT solution [8-9 mg of NBT added to 14 mL of 2 M potassium glycinate buffer (75 g glycine in 0.4 L water and pH adjusted to 10.0 with KOH)]. The membrane was washed twice with destain solution (0.16M sodium borate) and incubated in fresh destain solution for 16-24 h. The membrane was washed once with water and imaged before drying.

Sequence alignment

FASTA sequences for parkin molecules of various species were obtained form Uniprot (https://www.uniprot.org/). Sequence alignment between species was performed using T-Coffee (Center for Genomic Regulation of Barcelona; http://tcoffee.crg.cat/apps/tcoffee/do:regular). Output multiple sequence alignments were formatted using BoxShade (ExPASy – SIB Bioinformatics Resource Portal; https://embnet.vital-it.ch/software/BOX_form.html).

Statistical analyses

All statistical analyses were performed using GraphPad Prism version 6 (GraphPad Software, San Diego, CA, USA, www.graphpad.com). Differences between two groups were assessed using an unpaired t-test. Differences among 3 or more groups were assessed using a one-way or two-way ANOVA followed by the Tukey's multiple comparison test or Sidak multiple comparison test to identify statistical significance. Subsequent post hoc tests are depicted graphically and show significance between treatments. For all statistical analysis a cut-off for significance was set at 0.05. Data is displayed with p values represented as *$p < 0.05$, **$p < 0.01$,***$p < 0.001$, and ****$p < 0.0001$.

In vitro melanin formation assay

The recombinant protein samples were first prepared by exchanging the T200 protein buffer (50 mM Tris, 200 mM NaCl and 250 μM TCEP, pH 7.5) for T200-TCEP (50 mM Tris and 200 mM NaCl, pH 7.5) using repeat centrifugations (8 times 4000 x g at 4°C for 10 min) in Amicon Ultra 30 kDa MWCO filters. The protein concentrations were measured and adjusted to 20 μM using T200-TCEP. A 0.067 M sodium phosphate buffer, pH 6.0, was prepared by adding 33 mL of 0.1 M sodium phosphate buffer to 17 mL water and adjusting the pH using HCl. A stock solution of 100 mM dopamine HCl was prepared in 0.067 M sodium phosphate buffer.

Samples and controls were prepared in 100 μL total volume and contained: 10 μL of 20 μM protein or T200-TCEP, 10 μL of 100 mM dopamine or 0.067 M sodium phosphate buffer, and 80 μL T200-TCEP. The final concentration of protein was 2 μM and the final concentration of reagents was all 10 mM. The samples and controls were plated in triplicate, and absorbance read at 405 nm every 90 sec for 1 h and up to 4 h.

Chapter 3 Results

Dithiothreitol (DTT) induces parkin insolubility

Our lab had previously shown that excessive oxidative stress, including treatment with H_2O_2, rotenone, or CCCP, causes parkin to aggregate and become insoluble and that this is cysteine-dependent, suggesting that parkin's cysteines are redox reactive. I next wanted to examine whether excess reducing conditions have any effect on parkin's stability and solubility. I tested this by incubating recombinant parkin with increasing concentrations of dithiothreitol (DTT) for 30 min at 37°C. The soluble and insoluble fractions were separated by centrifugation and the insoluble pellet was resuspended in 10% SDS. Samples were resolved by SDS-PAGE and visualized by silver staining. As expected, excessive DTT exposure caused parkin to transition from the soluble to the insoluble fraction (Figure 3.1). This transition occurred largely between 100 mM and 1 M DTT concentrations.

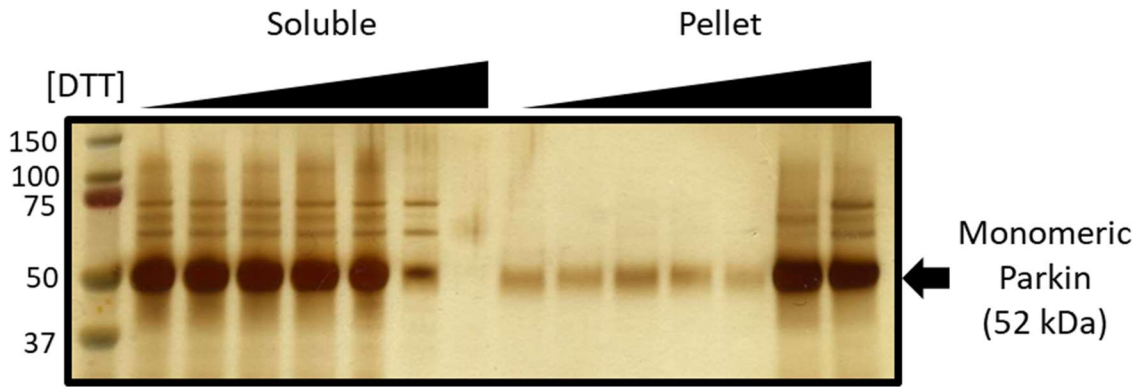

Figure 3.1: Incubation with DTT causes parkin to transition from the soluble to the insoluble fraction *in vitro*.

R-parkin was incubated with increasing concentrations of DTT (0, 100 μM, 1 mM, 10 mM, 100 mM, 1 M, 10 M) for 30 min at 37°C. The soluble and insoluble fractions were separated by centrifugation and the insoluble pellet was resuspended in 10% SDS. Protein was resolved by SDS-PAGE (non-reducing conditions) and visualized by silver staining.

Decrease in free cysteines in oxidized and insoluble parkin samples

Oxidation of parkin by H_2O_2 results in higher molecular weight species and loss of its solubility. This was sensitive to DTT (dithiothreitol), suggesting it was mediated by the redox state of its cysteine residues. To directly test the effect that oxidative stress has on parkin's cysteine residues and how that correlates with its solubility, I used a cysteine-fingerprinting method, coupled to LC-MS/MS analysis. Mass spectrometry was performed by Dr. Lawrence Puente at the Ottawa Hospital Research Institute Proteomics Core Facility. Methods and analysis were optimized in collaboration with Dr. Puente. There, r-parkin was exposed to various concentrations of H_2O_2 and then centrifuged to separate the soluble fraction from the insoluble pellet, which was resuspended in 10% SDS. Soluble and insoluble samples were then incubated sequentially with IAA (iodoacetamide), DTT, and then NEM (n-ethylmaleimide) for 30 minutes each in order to differentially label reduced and reversibly oxidized cysteines with IAA and NEM respectively. Following the labelling steps, all samples were separated by SDS-PAGE and the proteins were visualized by silver staining. This confirmed previous observations by showing that with increasing ROS exposure, parkin transitions from the soluble fraction into the insoluble fraction (Figure 3.2).

Relevant silver staining bands were excised and subjected to trypsin digestion followed by LC-MS/MS analysis. This data revealed adducts of IAA (representing reduced residues; Figure 3.3 A,B) and NEM (representing oxidized residues; Figure 3.3 C,D) at most cysteine residues on parkin. Across MS runs 5B, 11, and 12A, all cysteines on parkin have been identified with an IAA modification and 30/35 have been detected with an NEM modification. Direct oxidation of methionine residues has also been observed (Figure 3.3 E,F).

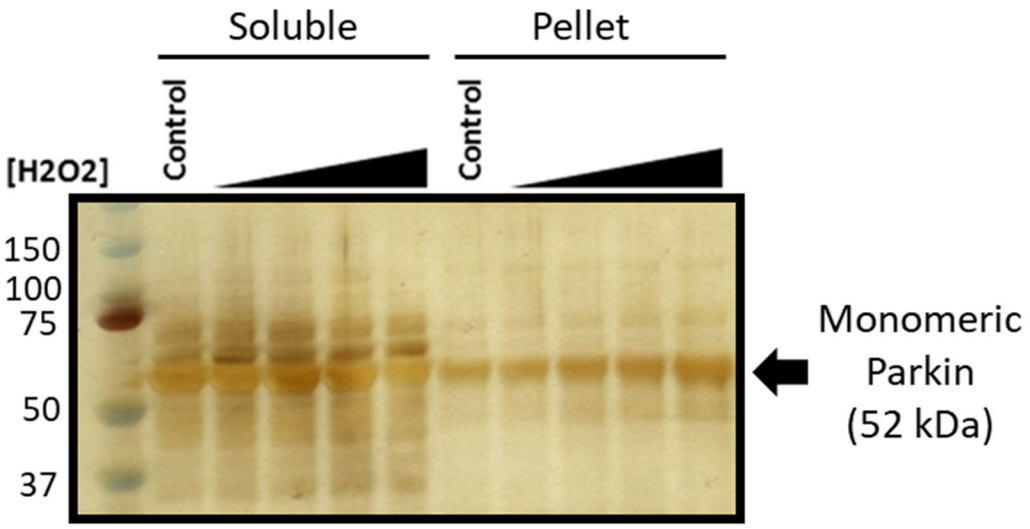

Figure 3.2: Recombinant parkin transitions from the soluble to insoluble fraction when treated with increasing concentrations of hydrogen peroxide.

R-parkin was treated with increasing concentrations of H_2O_2 (0, 10 µM, 100 µM, 1 mM, 10 mM). Samples were centrifuged to separate the soluble fraction from the insoluble pellet, which was resuspended in 10% SDS. Samples were separated by SDS-PAGE (reducing conditions) and visualized by silver staining.

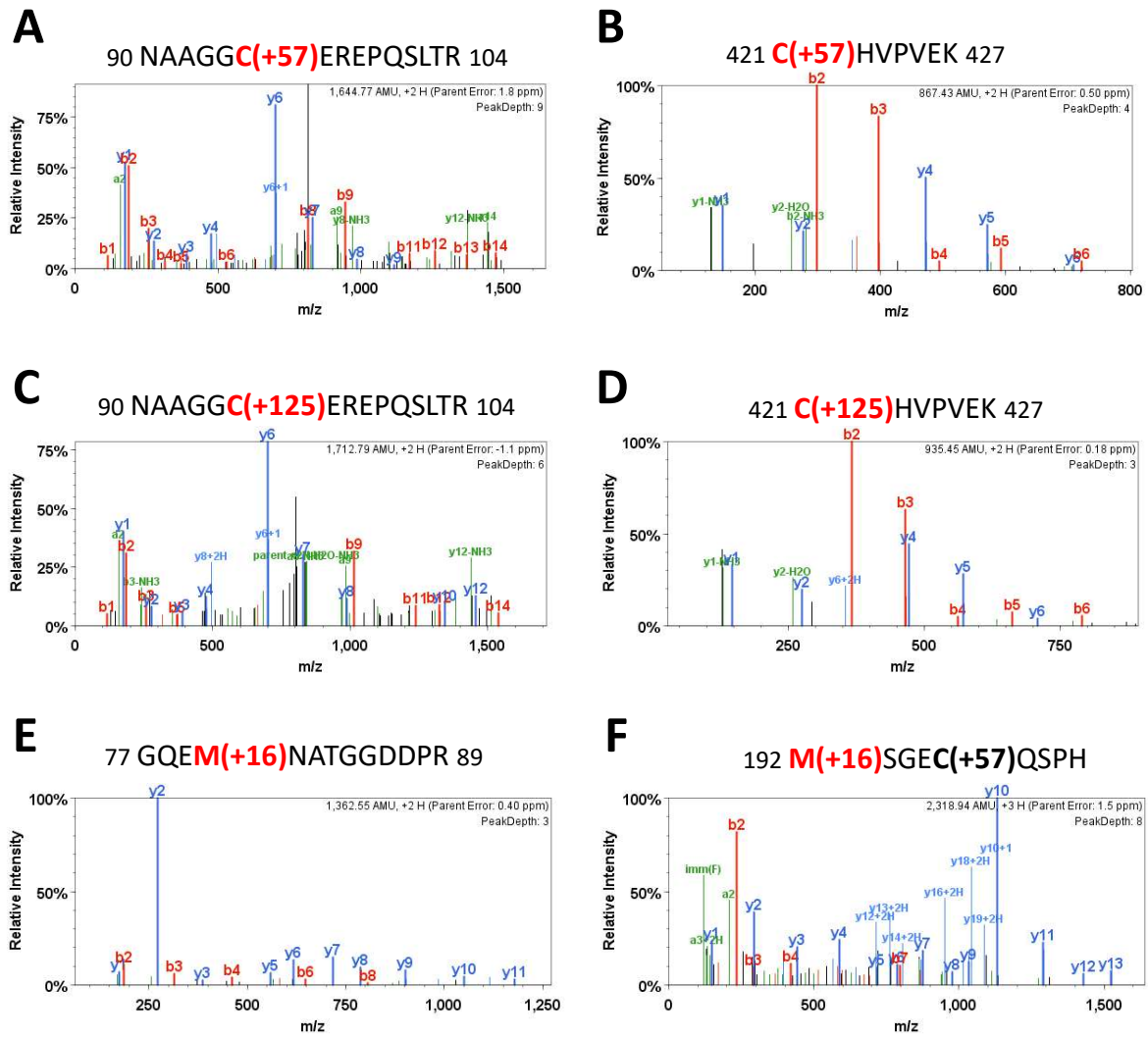

Figure 3.3: Spectra indicating parkin modifications by IAA, NEM and oxidation of methionine residues.

Following MS analysis and data processing, LC-MS/MS spectra were extracted from Scaffold PTM to highlight examples of various PTMs observed on parkin. (**A**) IAA at C95 (**B**) IAA at C421 (**C**) NEM at C95 (**D**) NEM at C421 (**E**) Methionine oxidation at M80 (**F**) Methionine oxidation at M192.

Following initial analysis by LC-MS/MS, the raw MS data files were further analyzed using the MaxQuant software platform developed by Cox et al [120]. The relevant output file lists all peptides that contain a PTM mass shift matching that expected for a carbamidomethyl (IAA) modification at a cysteine residue, indicating a 'reduced' or free thiol in the original sample. This file was filtered to remove any non-parkin peptides and relevant data was extracted to compare the intensity of IAA modified peptides across samples at individual parkin cysteine residues.

No significant difference in IAA intensity was observed between the three individual soluble or pelleted samples (Figure 3.4 B,C). However, when the IAA intensities of the three soluble fractions were combined and compared to the three pelleted fractions, significantly less IAA intensity was observed in insoluble parkin (Figure 3.4 D). This demonstrates that parkin's transition to the insoluble fraction correlates with fewer of its cysteine residues being in a reduced state (i.e., more are oxidized). I also probed for NEM modifications in the MS data to quantify the abundance of reversible oxidized cysteines; however, coverage of NEM modified cysteine residues was not sufficient for accurate quantification.

As a further confirmation of the effect that H_2O_2 treatment has on parkin's free cysteine thiols, raw LC-MS/MS data from an experiment previously performed in our lab was reanalyzed using the new MaxQuant analysis platform. The samples in this experiment were treated with H_2O_2 or water as a control; however, the soluble and insoluble fractions were not separated. Samples were then treated with IAA to label cysteines that remained reduced after the ROS exposure. In this case, analysis of the MaxQuant data showed significantly lower IAA intensity following H_2O_2 treatment (Figure 3.4 E), demonstrating that H_2O_2 exposure promotes the oxidation of parkin cysteine residues in the total pool of parkin.

These results using r-parkin treated with H_2O_2 were supported with MS analysis of human and mouse tissue, performed in parallel by a member of our lab, which demonstrated *in vivo* oxidation of parkin's cysteine residues.

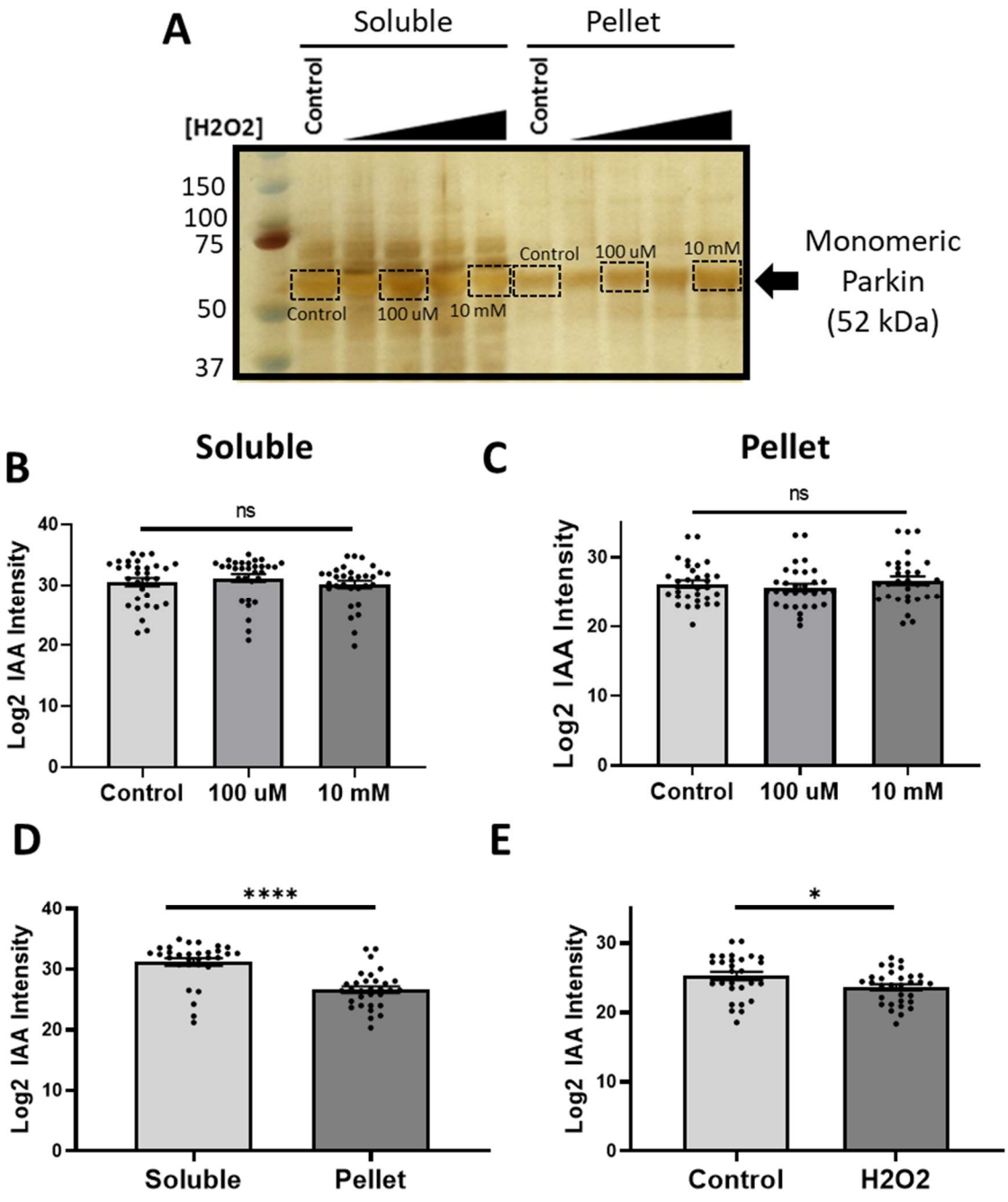

Figure 3.4: Fewer of parkin's cysteines are in a reduced state in oxidized and insoluble parkin samples.

R-parkin was exposed to increasing concentrations of H_2O_2. The soluble and insoluble fractions were separated by centrifugation and the insoluble pellet was resuspended in 10% SDS. (**A**) The

silver stained gel from Figure 3.2 is shown again with relevant bands that were excised for LC-MS/MS analysis labelled. (**B-C**) MS data was analyzed using MaxQuant. IAA intensity values were extracted and compared between samples. Data points represent the IAA intensity calculated at an individual cysteine residue (n=31 cysteines quantified). (**D**) IAA intensity between soluble and insoluble fractions were compared. Data points represent the average IAA intensity from the three soluble or insoluble fractions at an individual cysteine residue (n=31 cysteines quantified). (**E**) R-parkin was treated with H_2O_2 or water and remaining free cysteines were labelled with IAA. Raw MS data files were analyzed using MaxQuant software, and IAA intensities for each cysteine residue were extracted and compared between samples. Data points represent the IAA intensity calculated at an individual cysteine residue (n=28 cysteines quantified and matched in both treatment groups). Statistics for A and B were analyzed using an RM one-way ANOVA with the Tukey multiple comparison test. Statistics for C and D were analyzed using a paired t-test. Error bars represent mean +/- SEM.

MASCOT parameter set selection impacts PTM spectral counts

Aside from the MaxQuant-analyzed data presented above, the workflow I employ to detect PTMs on parkin includes searching the raw LC-MS/MS data using the MASCOT search engine. This involves selecting up to 9 possible variable modifications per search. Later sections will outline my efforts to detect dopamine-metabolite PTMs on parkin. Knowing that the choice of variable modifications could impact coverage and the discovery of my PTMs of interest, I included common contaminants, artifacts, and other common oxidative PTMs (selected in collaboration with proteomics expert Dr. Lawrence Puente). With one of my recent experiments, multiple MASCOT searches were performed on the same raw data set, allowing me to compare how spectrum count data is impacted when the combination of variable modifications changes. The analysis presented below was performed as a *post-hoc* review of aminochrome-treated samples in MS run 10 to test the degree of variability that results from changes to MASCOT parameter sets. Detailed results from this aminochrome-treatment experiment are presented in later sections; however, this analysis is intended solely to demonstrate optimization of our methodology and test the degree to which a specific parameter set impacts spectrum counts.

Four distinct MASCOT searches were performed on the raw MS data as shown in Figure 3.5 A. For searches A, C, and D, the spectral counts are shown separately for the technical replicates; however, for search E, the raw MS data and spectral counts for technical replicates within a specific sample type were combined during the data analysis stage. In cases where the same PTM was included in various MASCOT searches, Figure 3.5 B compares the spectral count data for that particular PTM across searches. This analysis confirms that spectral counts do in fact vary based on the parameter set searched; however, in most instances the differences are not significant and trends between samples and treatments appear to be mostly consistent

between searches. This was calculated statistically for total parkin spectra and trioxidation modified peptides. (Figure 3.5 C,D). In most instances the differences in spectral counts between MASCOT searches was not significant with one exception being spectral counts of trioxidation modified peptides in control samples, as indicated. Overall, this analysis suggests that the PTM data we have observed is robust and trustworthy since the observation of PTMs of interest is not entirely dependant on the inclusion or exclusion of other specific variable modifications. Nevertheless, it does highlight the importance of educated inclusion of redox-related modifications that are likely to occur in MS samples, and importantly, of maintaining the same set of variable modifications across experiments.

A

Parameter Set	Modification	1	2	3	4	5	6	7	8	9	10	11	12	16	13	14	17	18	15	19
		Control			AM - 52 kDa			AM - HMW			EDTA Control		EDTA AM - 52 kDa		EDTA AM Shifted				EDTA AM - HMW	
A	Aminochrome (+149)	0	0	0	1	2	2	0	0	0	0	0	0	0	0	0	0	0	1	0
A	Aminochrome (+147)	0	0	0	2	1	1	3	0	0	0	0	6	3	2	3	3	3	1	2
A	Dopamine Quinone	0	0	0	1	1	0	0	0	0	0	0	0	2	1	0	0	0	1	0
A	Indolequinone	0	0	0	6	4	5	4	0	2	0	1	6	4	4	3	4	5	4	5
	Total DA	***0***	***0***	***0***	***10***	***8***	***8***	***7***	***0***	***2***	***0***	***1***	***12***	***9***	***7***	***6***	***7***	***8***	***7***	***7***
A	Trioxidation	75	125	119	165	156	139	158	134	125	106	114	177	132	149	130	92	79	166	102
A	Oxidation (M)	72	68	59	66	67	56	49	36	35	62	55	66	47	43	37	23	39	34	44
A	Cys->Dha	89	90	89	118	117	111	132	117	90	81	90	111	138	119	129	81	58	129	84
A	Total parkin spectra	1550	1566	1586	1321	1253	1047	870	759	802	1488	1451	1230	1039	959	965	690	554	1037	611
C	Indolequinone	0	1	2	5	4	5	4	0	2	0	1	5	5	4	3	4	5	3	5
C	Trioxidation	51	107	100	146	140	134	165	132	132	94	108	163	124	156	135	86	80	176	102
C	Oxidation (M)	70	87	74	70	82	72	77	60	56	87	101	103	40	69	71	30	50	74	59
C	Total parkin spectra	1613	1612	1606	1345	1303	1104	963	799	852	1592	1597	1326	1072	1032	1063	719	593	1142	687
D	Trioxidation	53	108	94	147	143	131	158	126	133	85	106	161	129	143	145	89	74	181	97
D	Oxidation (M)	45	43	38	45	52	41	38	31	34	36	40	51	27	36	36	17	29	37	33
D	Dioxidation (W)	54	81	69	48	63	56	53	48	57	91	104	64	54	46	63	53	35	81	40
D	Phosphorylation (ST)	130	114	109	100	115	69	124	94	96	109	108	133	129	128	104	58	41	154	66
D	Cys->Dha	83	108	98	134	146	142	165	143	123	97	128	153	166	140	146	100	72	174	95
D	Total parkin spectra	1602	1590	1591	1348	1304	1067	958	802	870	1530	1526	1310	1132	1046	1057	710	566	1183	622
E	Indolequinone	0			16			8			2		11		15				8	
E	Aminochrome (+147)	0			6			6			2		9		13				7	
E	Trioxidation	353			604			566			282		404		610				326	
E	Oxidation (M)	196			221			156			114		138		223				115	
E	Dioxidation (W)	263			209			186			230		135		236				139	
E	Sulfoxidation (STY)	621			600			568			347		511		716				360	
E	Cys->Dha	292			401			408			214		310		490				257	
E	Unmodified	3287			2350			1488			2008		1458		2023				1049	
E	Total parkin spectra	4943			4026			3004			3165		2741		3844				1999	

B

Modification	Parameter Set	Control			AM - 52 kDa			AM - HMW			EDTA Control		EDTA AM - 52 kDa		EDTA AM Shifted				EDTA AM - HMW	
Total parkin spectra	A	1550	1566	1586	1321	1253	1047	870	759	802	1488	1451	1230	1039	959	965	690	554	1037	611
	C	1613	1612	1606	1345	1303	1104	963	799	852	1592	1597	1326	1072	1032	1063	719	593	1142	687
	D	1602	1590	1591	1348	1304	1067	958	802	870	1530	1526	1310	1132	1046	1057	710	566	1183	622
	E	4943			4026			3004			3165		2741		3844				1999	
Aminochrome (+147)	A	0	0	0	2	1	1	3	0	0	0	0	6	3	2	3	3	3	1	2
	E	0			6			6			2		9		13				7	
Indolequinone	A	0	0	0	6	4	5	4	0	2	0	1	6	4	4	3	4	5	4	5
	C	0	1	2	5	4	5	4	0	2	0	1	5	5	4	3	4	5	3	5
	E	0			16			8			2		11		15				8	
Trioxidation	A	75	125	119	165	156	139	158	134	125	106	114	177	132	149	130	92	79	166	102
	C	51	107	100	146	140	134	165	132	132	94	108	163	124	156	135	86	80	176	102
	D	53	108	94	147	143	131	158	126	133	85	106	161	129	143	145	89	74	181	97
	E	353			604			566			282		404		610				326	
Cys-Dha	A	89	90	89	118	117	111	132	117	90	81	90	111	138	119	129	81	58	129	84
	D	83	108	98	134	146	142	165	143	123	97	128	153	166	140	146	100	72	174	95
	E	292			401			408			214		310		490				257	

C

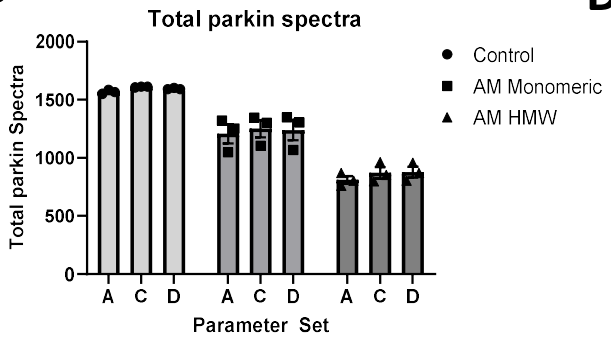

D

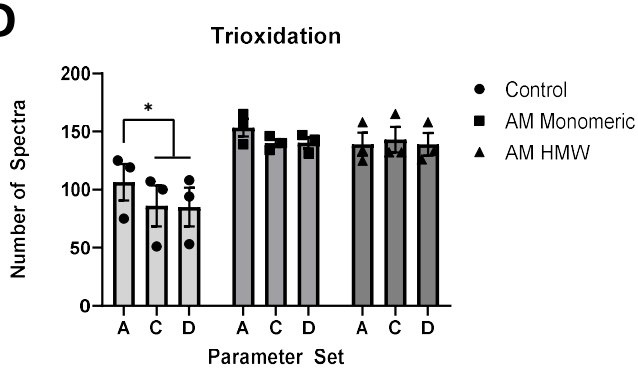

Figure 3.5: Spectrum counts vary slightly, but not significantly, based on the selected MASCOT PTM parameter set.

During the analysis of MS run 10, four distinct MASCOT parameter sets were searched. (**A**) Spectrum counts for various control and aminochrome-treated samples are sorted by MASCOT parameter set. (**B**) Spectrum counts are sorted by variable modification to highlight the degree of variability in spectrum counts for the same modification in the context of various MASCOT parameter sets. (**C,D**) The total number of parkin spectra (**C**) and the number of spectra corresponding to a trioxidation PTM on parkin (**D**) are plotted by sample fraction and MASCOT parameter set. The parameter sets indicated in the x-axis of C and D refer to the MASCOT parameter sets outlined in A. Statistics for C and D were calculated using a two-way ANOVA with a Tukey multiple comparison between parameter sets calculated within each distinct sample fraction (i.e. soluble, AM monomeric, AM HMW). No significant differences were observed unless indicated. Error bars represent mean +/- SEM (n=3).

Cysteine alkylating agents produce false positive dopamine adducts on parkin

In addition to the effects of H_2O_2 on parkin, we had a specific interest in dopamine-dependent modification of parkin, and mapping these covalent adducts using LC-MS/MS. These experiments, including the preparation of dopamine-metabolite-modified parkin and the subsequent preparation of samples for LC-MS/MS, required optimization, which was done over the course of several experiments.

One parameter that was optimized for the detection of dopamine metabolite adducts was the LC-MS/MS method itself, which was switched from a standard collision induced dissociation (CID) MS method to a higher energy collisional dissociation (HCD) method. The injection volume was also increased above that used in a standard MS experiment. This optimization was done in close collaboration with Dr. Lawrence Puente (OHRI proteomics Core Facility).

Another parameter that was optimized was the post-translational modification mass shifts for dopamine metabolites that are used when probing the raw LC-MS/MS data using MASCOT software. There is limited evidence in the literature identifying dopamine-metabolite PTMs at distinct chemical mass shifts, so based on knowledge of dopamine oxidation metabolites, as outlined in section 1.3.4, the four structures and mass shifts outlined in Figure 3.6 were included in MASCOT searches. These corresponding to dopamine quinone, aminochrome (protonated and unprotonated forms), and indolequinone.

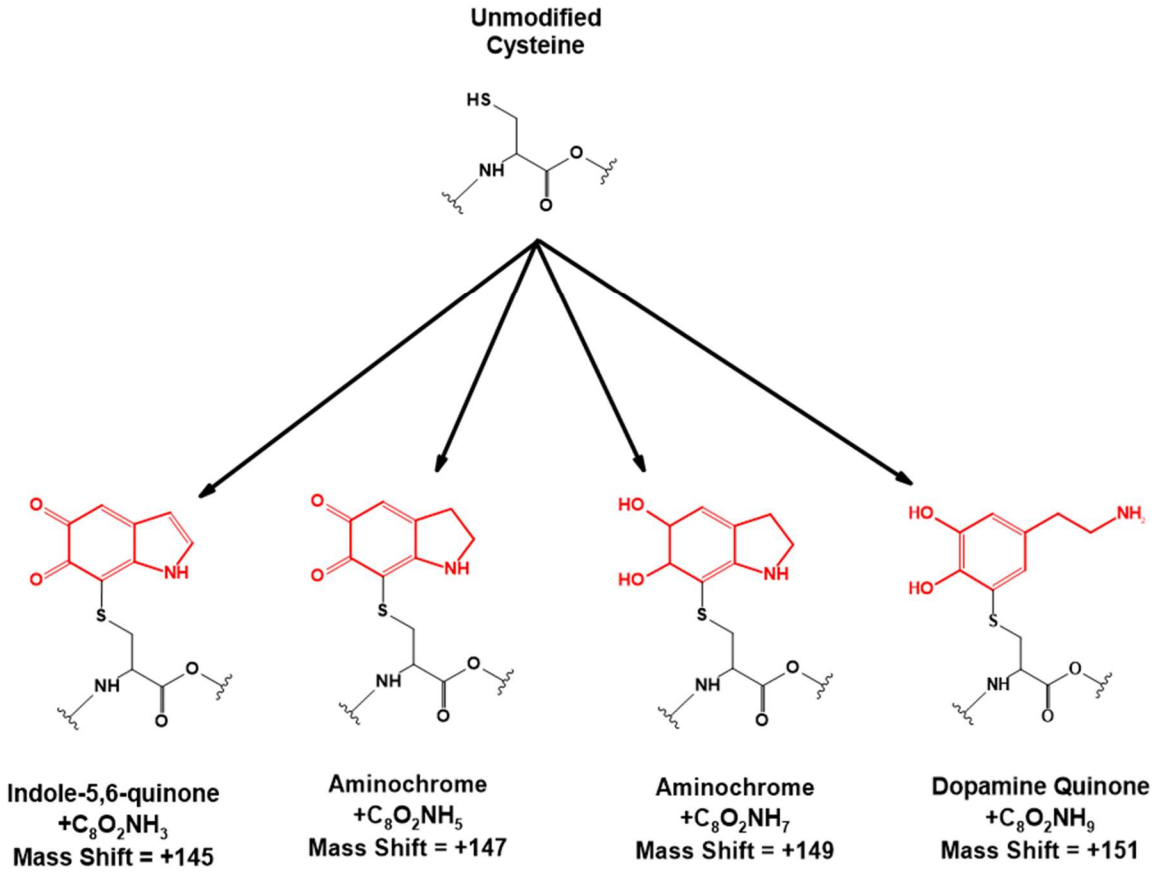

Figure 3.6: Structures of four predicted dopamine metabolite adducts that were probed for in LC-MS/MS data.

The chemical structure of four dopamine metabolite adducts that were pre-selected for detection/analysis by LC-MS/MS. The mass shifts indicated refer to that added to an unmodified cysteine residue.

Recombinant parkin was treated with water (control) or aminochrome for 1 hour at 37°C. Soluble and insoluble fractions were separated by centrifugation, and the insoluble pellet was resuspended in 10% SDS as was done for H_2O_2-exposed r-parkin above. Proteins were resolved by SDS-PAGE and visualized by silver staining. At 200 μM aminochrome treatment, parkin mostly transitioned into the insoluble fraction, and also formed HMW aggregates in distinct bands (Figure 3.7 A). Western blot analysis of select samples further highlighted several distinct HMW bands in the 200 μM AM treated insoluble fraction (Figure 3.7 B).

Select bands were excised from the silver stained gel and prepared for LC-MS/MS analysis, as indicated in Figure 3.7 A. During the process of peptide extraction and digestion for MS analysis, samples were treated with DTT and IAA in order to block unmodified cysteine residues and thus prevent oxidation artifacts due to processing. This is a standard practice during MS sample preparation. The raw MS data were analyzed using MASCOT and Scaffold PTM software (MS runs 4 and 7). This revealed many PTMs with mass shifts matching those predicted to be dopamine metabolite adducts on parkin; however, these adducts appeared in all samples, including non-aminochrome treated controls (Figure 3.7 C). This suggested that the covalent dopamine modifications observed here may be false positives, mistakenly calculated as being dopamine adducts by the peptide identification software used. This could result from combinations of PTMs on cysteines that contain multiple cysteine sites that together result in a mass shift statistically similar to that expected for one of our predicted dopamine metabolite PTMs. Throughout this thesis, these mass adducts that were detected and calculated to match one of my four predicted dopamine-metabolite adducts, but we ultimately believe to be false-positives, will be referred to as MASSADs (mass adducts due to artifacts of the same size as dopamine adducts).

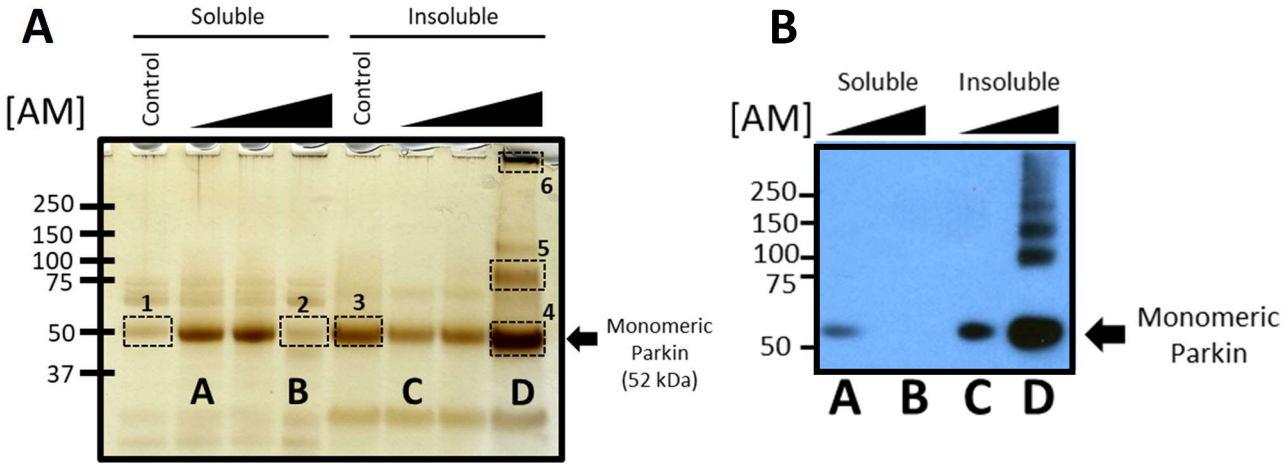

C

	Sample	DA Modified	Total Spectra	% Modified
1	Control Soluble	74	488	15.16 *
2	AM Soluble	34	275	12.36
3	Control Pellet	237	1483	15.98 *
4	AM Pellet Monomeric	223	974	22.90
5	AM Pellet HMW 1	91	571	15.94
6	AM Pellet HMW Top	50	396	12.63

Figure 3.7: False-positive mass changes matching expected shift for dopamine adducts, as detected in both control and aminochrome-treated parkin samples.

R-parkin was exposed to increasing concentrations of aminochrome (1 µM, 10 µM, 100 µM, 200 µM) for 1 hour at 37°C. The soluble and insoluble fractions were separated by centrifugation and the insoluble pellet was resuspended in 10% SDS. (**A**) Protein was resolved by SDS-PAGE (reducing conditions) and visualized by silver staining. The indicated bands were excised for LC-MS/MS analysis. (**B**) Select samples (1 µM and 200 µM aminochrome treatment, soluble and insoluble fractions) were further analysed by Western blot (IB: parkin clone E, 1:1000). (**C**) Following MS analysis, MASCOT software was used to infer peak and peptide identities from

the mass spectra. The number of spectra corresponding to dopamine-modified parkin peptides (as calculated by MASCOT; I propose that these represent largely false positive MASSADs), the total number of spectra corresponding to parkin peptides, and the percent of parkin peptides that are predicted to be dopamine modified are shown for each MS sample. * denotes control samples that were never treated with dopamine or aminochrome.

I predicted that treatment with IAA to block unmodified cysteines may be causing the MASSADs that were observed. In order to test this, I analyzed untreated r-parkin as well as parkin treated with DTT or DTT plus one of several compounds that are known to form irreversible, covalent adducts on cysteines. These included IAA, NEM, acrylamide, and tris(2-carboxyethyl)phosphine (TCEP). Importantly, these samples were never exposed to dopamine or aminochrome. All samples were then run on a gel, visualized by silver staining, and appropriate bands were excised and prepared for MS analysis without further exposure to DTT or IAA.

MASCOT software was used to infer peptide identities from the mass spectra. This analysis revealed many PTMs matching dopamine metabolite adducts on parkin in the four samples treated with a cysteine-modifying compound (Figure 3.8). Since these samples were not treated with dopamine, I concluded that the dopamine PTMs observed here are false positive MASSADs. No dopamine adducts were detected in the untreated parkin sample, or the sample that was only treated with DTT. As expected, these two samples did show a slight reduction in protein coverage as well as a slight increase in false discovery rate (FDR, an estimate of the expected fraction of discoveries for which the observations are the result of chance). This experiment demonstrates that various cysteine-modifying compounds can form complex sets of PTMs on parkin which can be misinterpreted by the spectra identification software as our predicted dopamine adducts. We therefore concluded that I must avoid exposing any dopamine-treated parkin samples to any of these cysteine-modifying compounds at any point during the experiment or during MS sample preparation.

Sample	Treatment	False Discovery Rate	Sequence Coverage	Peptide Sequence Matches	DA Metabolite Matches
1	None	2.4%	85%	3817	**0**
2	DTT	2.6%	83%	3110	**0**
3	DTT + IAA	1.8%	98%	3178	**76** *
4	DTT + NEM	1.8%	96%	3034	**59** *
5	DTT + acrylamide	2.1%	98%	3366	**23** *
6	TCEP	1.1%	98%	2740	**35** *

Figure 3.8: Various cysteine-modifying compounds can form false-positive dopamine adduct-like PTMs.

R-parkin was treated with or without DTT and the indicated cysteine-modifying compound. All incubation steps were performed for 30 minutes at 37°C. Following MS analysis, MASCOT software was used to infer peptide identities from the mass spectra as reported here. All dopamine-metabolite adducts listed are presumed MASSADs.

Additional secondary MASCOT searches were performed on select samples using altered PTM parameter sets (Figure 3.9). Some of these searches showed very limited numbers of MASSAD in the control and DTT treated samples, but still far less than in any of the samples treated with cysteine-modifying compounds. This further highlights the complexity of PTM formation on parkin and suggests that we must gauge dopamine modifications based on a clear increase in adduct formation in treated samples compared to controls rather than any single occurrence. Subsequent searches for dopamine-metabolite adducts in the following sections were all performed using MASCOT parameter set A as outlined in Figure 3.9 B, which showed no MASSADs in the absence of IAA, NEM, acrylamide, or TCEP treatment.

A

Sample	Treatment	Mascot Parameter Set	False Discovery Rate	Sequence Coverage	Peptide Sequence Matches	DA Metabolite Matches
1	none	B	2.6%	88%	4084	**4**
2	DTT	B	2.5%	85%	3386	**4**
3	DTT+IAA	B	2.0%	98%	3620	**121**
6	TCEP	B	3.3%	92%	1684	**38**
1	none	C	2.8%	84%	4153	**n.a.**
2	DTT	C	2.5%	84%	3445	**n.a.**
6	TCEP	C	3.6%	81%	1613	**n.a.**
5	DTT+acrylamide	D	2.0%	98%	3496	**15**
4	DTT+NEM	E	1.5%	98%	4063	**73**
5	DTT+acrylamide	F	2.3%	98%	2847	**5**
1	none	G	2.4%	95%	4558	**3**
2	DTT	G	2.4%	92%	3790	**4**
3	DTT+IAA	G	2.2%	98%	3519	**72**
5	DTT+acrylamide	G	2.3%	98%	3606	**17**
6	TCEP	G	1.8%	98%	2717	**31**

B

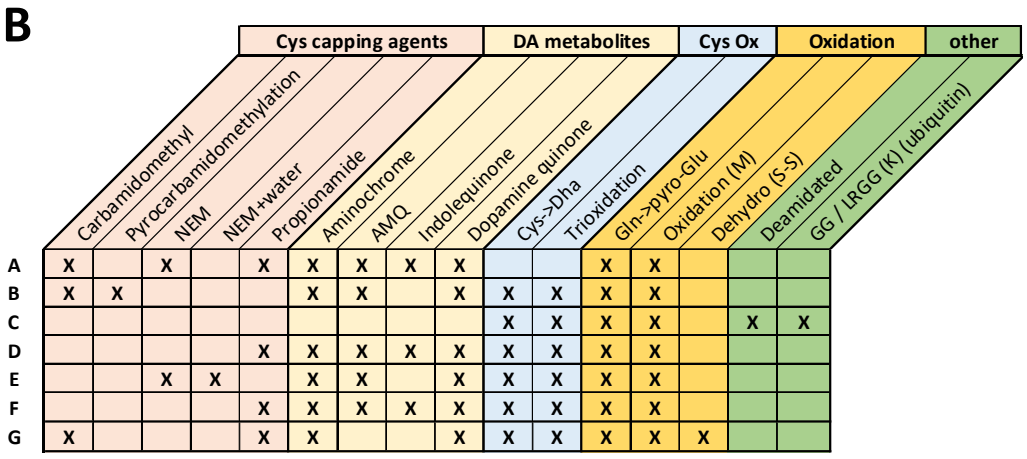

Figure 3.9: Additional MASCOT searches of data following r-parkin treatment with cysteine-modifying compounds without dopamine treatment.

R-parkin was treated with or without DTT and a cysteine-modifying compound. All incubation steps were performed for 30 minutes at 37°C. Following MS analysis, MASCOT software was used to infer peak and infer peptide identities from the mass spectra. (**A**) Additional MASCOT searches were performed on the same raw MS data set (in addition to that presented in Figure

3.8). All dopamine-metabolite adducts listed are presumed MASSADs. (**B**) The variable modifications included in each MACOT search are outlined. Parameter set A corresponds to the data presented in Figure 3.8.

Parkin forms covalent adducts with dopamine at cysteine 95

Having demonstrated that treatment with cysteine alkylating agents can produce MASSADs as predicted by LC-MS/MS analysis software, the initial experiments were repeated, this time omitting the use of DTT, IAA, NEM, or acrylamide at any point during the sample preparation stage or during the protein digestion and LC-MS/MS preparation stage. This omission leaves any unmodified cysteine residues exposed and vulnerable to greater intermolecular reactivity during MS analysis, which can reduce peptide coverage. However, I concluded that the added reliability of any observed dopamine PTMs would be worth any reduction in coverage.

Triplicate samples of r-parkin were incubated with either water (control) or 200 μM aminochrome for 1 hour at 37°C. The samples were mixed by pipetting in order to capture both the soluble and insoluble species and then run on a gel and visualized by silver staining. The indicated bands were excised and prepared for LC-MS/MS analysis. For the aminochrome treated samples, a high molecular weight (HMW) gel-excluded fraction was also excised in addition to the band matching monomeric parkin (Figure 3.10 A).

As an initial indicator of dopamine modification, a portion of each sample was also analyzed by NBT staining, which selectively binds to quinone species. This showed a clear enhancement in staining intensity in the aminochrome-treated samples (Figure 3.10 B).

Analysis of the LC-MS/MS data (MS experiment 9A) using Scaffold 4 and Scaffold PTM software revealed evidence of 14 total peptides containing PTM mass shifts matching one of our four predicted dopamine metabolite adducts (Figure 3.10 C). In addition to direct

modification by dopamine metabolites, other oxidative PTMs such as cysteine trioxidation (sulfonic acid) were observed in aminochrome-treated samples (Figure 3.10 D).

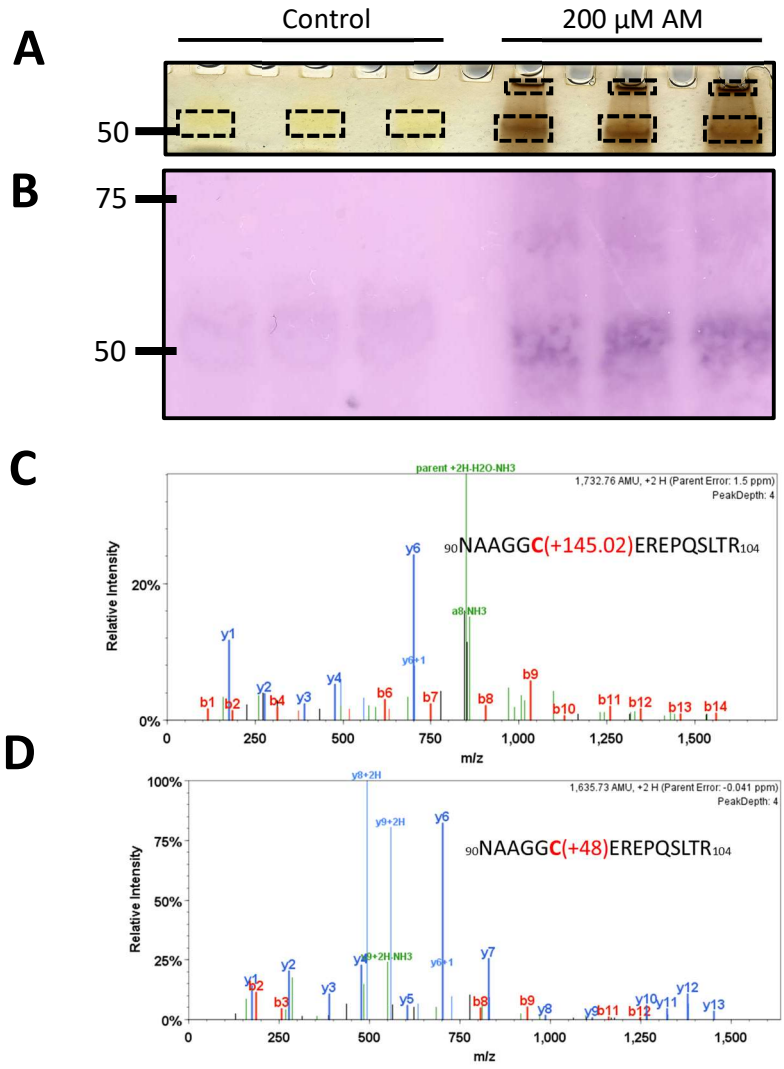

Figure 3.10: *Bona fide* dopamine metabolite adducts are detected on r-parkin following aminochrome treatment.

R-parkin was exposed to water (control) or 200 µM aminochrome. Samples were resolved by SDS-PAGE (non-reducing conditions) but were run only ~2 cm into the gel in order to capture as many modified parkin species as possible. (**A**) Protein was visualized by silver staining. Indicated bands were excised for MS analysis. (**B**) Fractions of each sample were visualized by NBT staining. (**C,D**) LC-MS/MS analysis revealed evidence of dopamine metabolite adduct

formation at C95. Shown are two MS spectra matching to the same parkin peptide (aa 90-104), one with an indolequinone modification at C95 (**C**) and the other with a non-dopamine PTM (trioxidation) at C95 (**D**).

All matches occurred in the aminochrome-treated samples rather than controls, suggesting that these PTMs can reliably be attributed to covalent modification by dopamine or its oxidized metabolites. Interestingly, all 14 of these dopamine metabolites adducts occurred at the residue C95 on parkin. As expected, the total number of parkin spectra observed, and coverage of the parkin protein was reduced in the samples that were not treated with IAA to block unmodified cysteines (Figure 3.11 A).

In order to verify these observations, two additional sets of control and aminochrome-treated r-parkin samples were prepared and analyzed in the same manner. These experiments revealed 39 additional peptides with PTM mass shifts matching one of our predicted dopamine adducts. Once again, all of the dopamine PTMs occurred in AM treated samples rather than control samples, further increasing confidence in the covalent dopamine modifications observed. These experiments further highlighted the sensitivity of C95 to dopamine adduct formation, with 82% (32/39) of dopamine PTMs occurring at that residue. The other 7 modifications observed occurred at 6 other cysteine residues: namely, C166, C169, C212, C238, C360, and C365 (Figure 3.11 B). Spectra corresponding to all unique dopamine-modified parkin peptides are shown in Appendix 2 and a list of all instances of dopamine-modified parkin peptides with validating information are shown in Appendix 3.

A

	MS Run 7 *Treated with IAA during sample preparation to block unmodified cysteines						MS Run 9A *Never exposed to IAA		
	1	2	3	4	5	6			
	Control Soluble	AM Soluble	Control Pellet	AM Monomeric	AM B	AM HMW	Control	AM Monomeric	AM HMW
Total parkin spectra	1071	851	2897	2184	1420	1003	1408	749	387
% Coverage	94%	93%	96%	88%	85%	85%	77%	64%	73%

B

Peptide sequence	Variable Modifications	Observed m/z	Spectrum charge	Actual peptide mass (AMU)	Peptide Identification probability	Mascot Ion Score	Scaffold Peptide Score	Quantity
76 KGQEmNATGGDDPRNAAGGcEREPQSLTR 104	M80 Oxidation (+16), **C95 Aminochrome (+147)**	802.8554	4	3,207.39	99.70%	33.3	41.69	1
76 KGQEmNATGGDDPRNAAGGcEREPQSLTR 104	M80 Oxidation (+16), **C95 Aminochrome (+149)**	642.8917	5	3,209.42	97.40%	27.7	18.71	1
76 KGQEmNATGGDDPRNAAGGcEREPQSLTR 104	M80 Oxidation (+16), **C95 Dopamine Quinone (+151)**	803.8625	4	3,211.42	97.80%	28.4	64.11	1
90 NAAGGcEREPQSLTR 104	**C95 Indolequinone (+145)**	867.3880	2	1,732.76	99.70%	59.5	130.03	31
90 NAAGGcEREPQSLTR 104	**C95 Aminochrome (+147)**	579.2650	3	1,734.77	99.70%	37.3	87.17	10
90 NAAGGcEREPQSLTR 104	**C95 Dopamine Quinone (+151)**	580.6098	3	1,738.81	99.50%	27.7	72.14	2
162 LRVQcSTcRQATLTLTQGPSCWDDVLIPNR 191	**C166 Aminochrome (+149)**, C169 Cys->Dha (-34)	1164.2490	3	3,489.73	99.30%	83.9	42.91	3
162 LRVQcSTcRQATLTLTQGPScWDDVLIPNR 191	**C166 Aminochrome (+149)**, **C169 Dopamine Quinone (+151)**, C182 Cys->Dha (-34)	1214.6033	3	3,640.79	99.20%	31.4	25.73	1
212 cGAHPTSDKETSVALHLIATNSRNITcITCTDVR 245	**C212 Dopamine Quinone (+151)**, **C238 Dopamine Quinone (+151)**	1310.9731	3	3,929.90	99.10%	27.8	19.84	1
350 VTcEGGNGLGcGFAFcREcKEAYHEGEcSAVFEASG TTTQAYR 392	C352 Cys->Dha (-34), **C360 Aminochrome (+147)**, C365 Cys->Dha (-34), C368 Trioxidation (+48), C377 Trioxidation (+48)	1179.4941	4	4,713.95	98.40%	27.2	14.08	1
350 VTcEGGNGLGcGFAFcREcKEAYHEGEcSAVFEASG TTTQAYR 392	352 Cys->Dha (-34), C360 Cys->Dha (-34), **C365 Indolequinone (+145)**, C368 Trioxidation (+48), C377 Trioxidation (+48)	1178.9937	4	4,711.95	96.10%	29.3	11.1	1

Figure 3.11: Summary of dopamine metabolite adduct detection in aminochrome-treated r-parkin samples highlights residue cysteine 95.

MASCOT software was used to infer peptide identities from raw LC-MS/MS data. Results were further validated and analyzed using Scaffold 4 and Scaffold PTM software. (**A**) The total spectrum count of peptides assigned to parkin, as well as the percent coverage of the parkin protein in each sample are compared between an experiment in which unmodified cysteines were blocked with IAA and one in which the samples were not treaded with IAA. (**B**) All unique peptides identified with dopamine metabolite adducts are listed with validating information. The table lists one sample occurrence of peptides that were identified as dopamine modified multiple

times. The “Quantity” column lists the total number of occurrences for that particular modified peptide across MS runs 9A, 10A, and 12B.

Decreased parkin spectra observed in aminochrome-treated fractions

Another way to analyze the MS data is to consider the total spectral count of all peptides matched to parkin. Using this method, there are fewer parkin peptides detected in aminochrome-treated samples compared to control samples. This is evident when we measure the total spectral count of all parkin peptides (Figure 3.12 A), or only the subset of peptides that were ever detected to have dopamine metabolite PTMs (Figure 3.12 B; the sum of the modified and unmodified forms of these particular peptides was considered for this analysis). Since protein digestion and injection into the LC-MS/MS instrument are identical for each band, we can assume that the amount of protein injected in each sample should be similar. Therefore, this decrease in parkin in treated samples suggests that many peptides carrying PTMs were not statistically identified by the MS software as being parkin peptides.

Using the total number of parkin spectra corresponding to a particular peptide, I can measure the percentage of those spectra that were identified with a dopamine metabolite PTM. Using these percentages, no significant difference is observed in the modification ratio between monomeric parkin and the HMW (gel-excluded) parkin from the same wells (Figure 3.12 C). However, the variability in percentage of parkin peptides with a dopamine-modification in the HMW samples is greater than that in the monomeric fraction. This is consistent with a greater degree of complexity and variability in parkin modification in parkin species that aggregate.

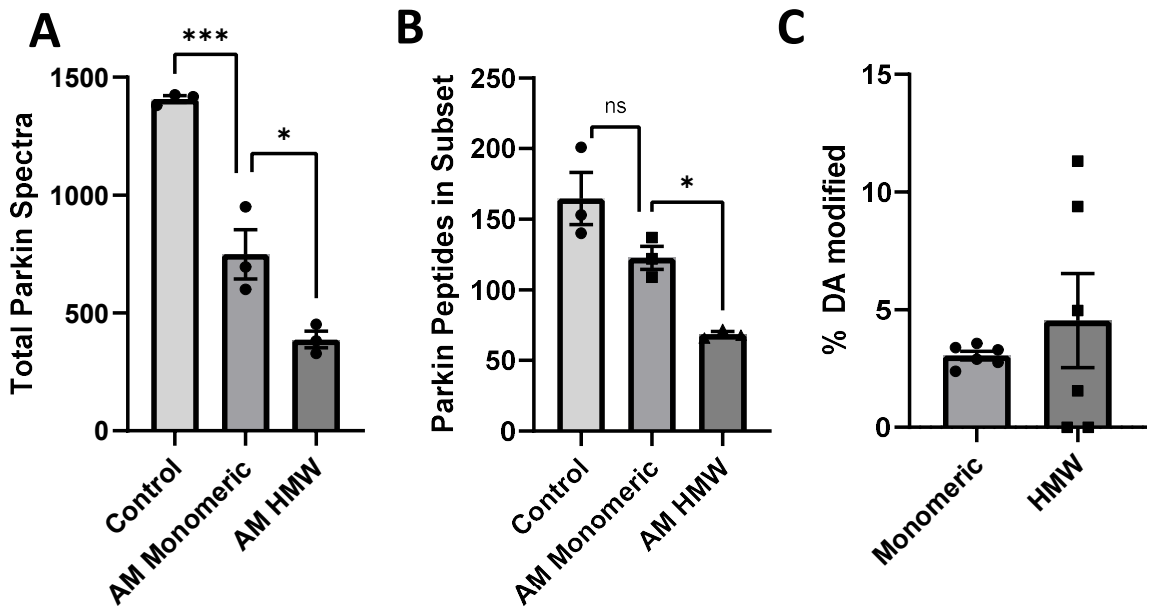

Figure 3.12: Fewer unmodified r-parkin spectra are identified in aminochrome-treated fractions than in control samples.

Spectrum counts were extracted from Scaffold and quantified by fraction. (**A**) Total number of spectra matched to parkin in each fraction (n=3; Data from MS Run 9A is shown). (**B**) The total parkin spectra in the subset of unique amino acid sequences that ever had a dopamine metabolite PTM in MS Run 10A (n=3). Note that the totals include all identified versions of these parkin sequences (modified + unmodified). (**C**) Based on the subset of peptides that ever had a dopamine metabolite PTM in MS Run 9A and MS Run 10A, the percentage of peptides with a dopamine modification were calculated and compared between the monomeric parkin bands and the HMW gel-excluded bands. Data points represent the modification percentage in a single sample (n=6). Statistics for A and B were calculated using an ordinary one-way ANOVA with the Tukey multiple comparison test. Statistics for C were calculated using an unpaired t-test (n.s.). Error bars represent mean +/- SEM.

Additional oxidation-related PTMs are observed on parkin following aminochrome treatment

In addition to probing for dopamine metabolite adducts in our samples, I also included common oxidative PTMs and contaminants in our MASCOT searches. This serves two purposes. One, it increases our coverage and detection of dopamine adducts by identifying parkin peptides that contain both a dopamine modification and one of the other common PTMs. Secondly, it allows for secondary outcomes to be analyzed. As discussed in the introduction, oxidized dopamine metabolites can harm cellular metabolism in various ways. They can form covalent adducts with proteins and disrupt protein function; however; they also further promote the formation of other oxidized metabolites, leading to elevated oxidative stress. Three oxidation-related PTMs that can form include cysteine trioxidation (sulfonic acid), cysteine to dehydroalanine conversion, and methionine oxidation (Figure 3.13). Using spectral count data from MASCOT and Scaffold PTM, I compared the number of spectra corresponding to parkin peptides with these PTMs between control samples and the monomeric or HMW bands from aminochrome-treated parkin samples. This revealed significantly increased ratios of all three oxidative PTMs in the aminochrome treated fractions (Figure 3.14).

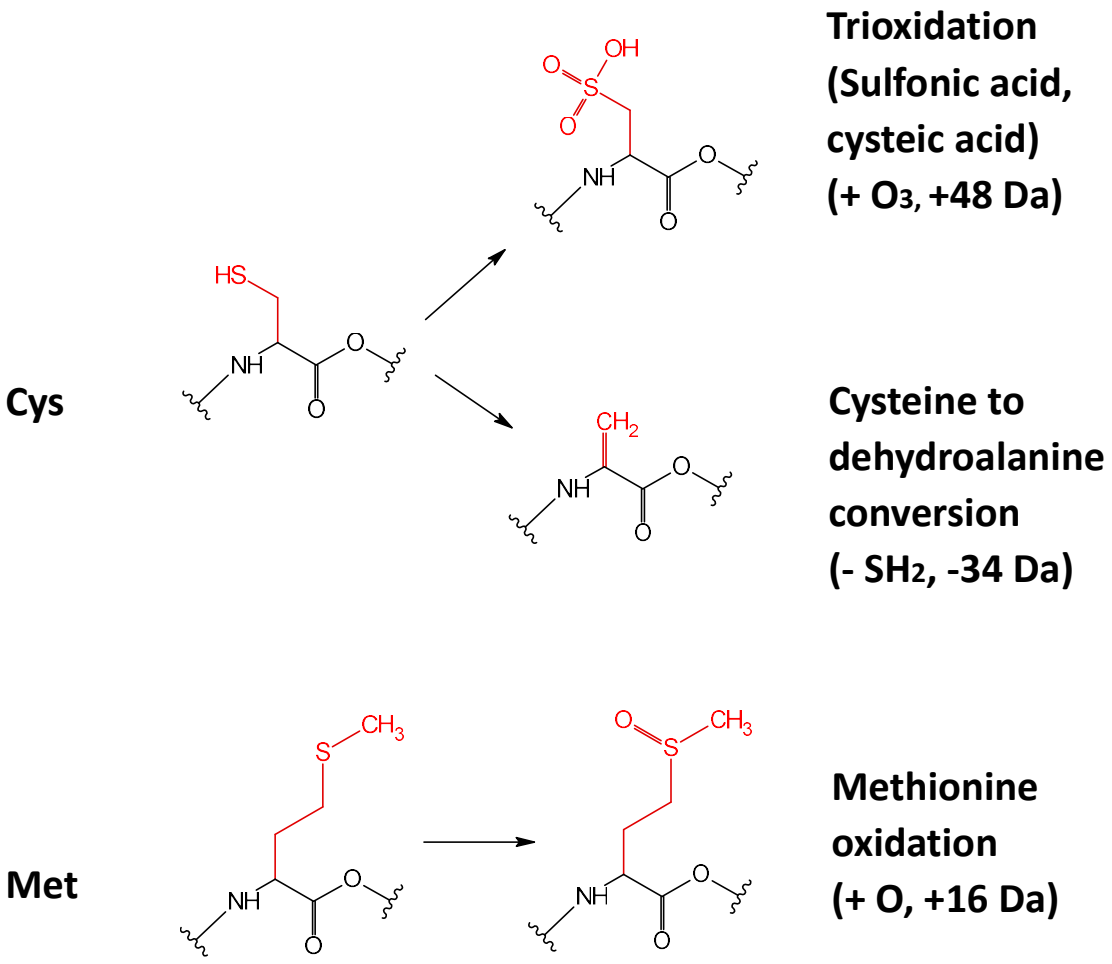

Figure 3.13: Structures of common oxidative PTMs.

Three common modifications to cysteine and methionine residues are shown, along with the characteristic mass shift they add or subtract from an unmodified cysteine residue. The presence of these modifications are predicted statistically using MASCOT software.

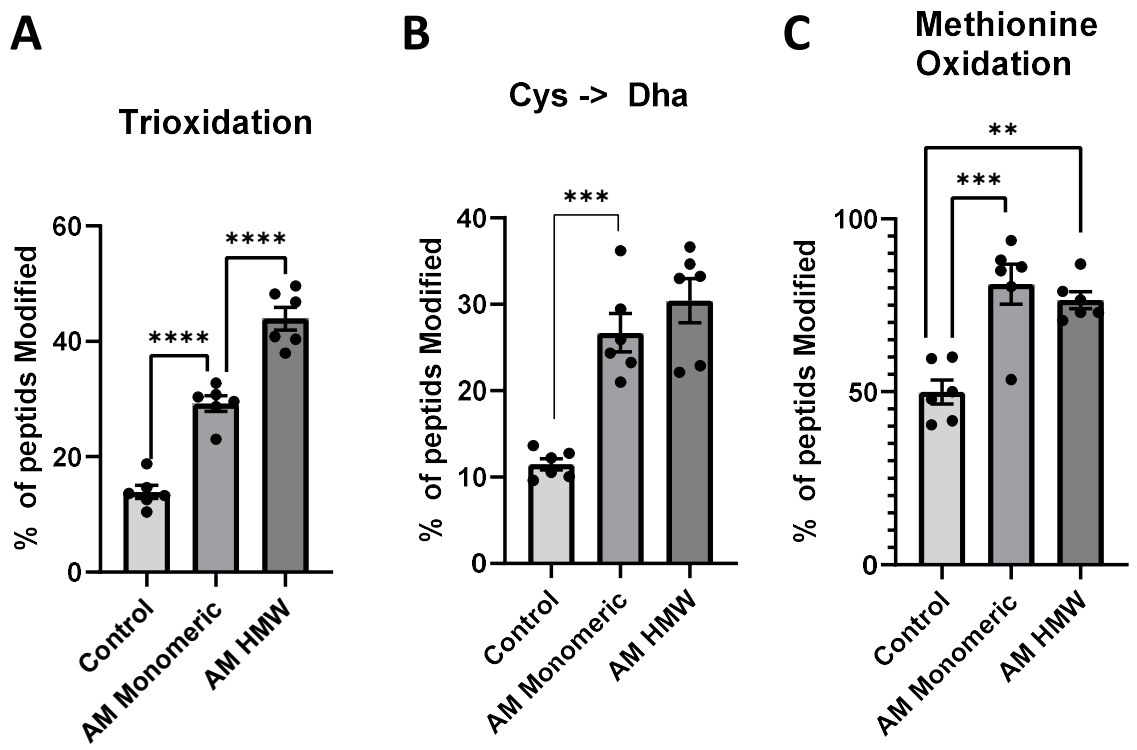

Figure 3.14: The percentage of parkin peptides possessing an oxidative PTM is increased in aminochrome-treated samples.

Spectrum count data was extracted from Scaffold PTM. Percentages represent the number of modified spectra for each specific PTM divided by the total number of parkin spectra (modified + unmodified) for the specific a.a. sequences that were ever detected as modified. Individual data points represent, within a single sample, the modification percentage of (**A**) cysteine trioxidation (+48), (**B**) cysteine to dehydroalanine conversion (-34), and (**C**) methionine oxidation (+16). Statistics were calculated using an ordinary one-way ANOVA with the Tukey multiple comparison test. Error bars represent mean +/- SEM (n=6).

EDTA treatment increases parkin's sensitivity to dopamine modification

I hypothesized that slightly denatured parkin may be even more susceptible to covalent modification by dopamine. In order to test this, I treated r-parkin with a low dose of EDTA (200 μM), a metal chelator, for 30 minutes at 37°C. Since parkin is structurally stabilized by four zinc ions, it would be expected that a low dose of EDTA would, at least partially, cause parkin to unfold. Following pre-treatment with EDTA, r-parkin was exposed to 200 μM aminochrome or water (control) for 30 minutes at 37°C. Multiple identical samples for each treatment were prepared.

Some samples from each treatment were visualized on a membrane by NBT staining to detect quinone-protein species. This revealed a clear increase in staining in EDTA treated samples compared to control samples (Figure 3.15 A).

The remaining samples were run on a gel and subjected to silver staining. Interestingly, this revealed a distinct "laddering" effect in the aminochrome treated samples with EDTA pre-treatment that was not previously observed in standard (non-EDTA pre-treated) aminochrome-treated samples. Four bands were excised from each aminochrome treated lane and prepared for LC-MS/MS analysis. These included: monomeric parkin, two intermediate HMW bands, and a gel-excluded band from the very top of the lane (Figure 3.15 B).

Analysis of the MS data using Scaffold PTM revealed evidence of 61 dopamine-modified peptides with modifications occurring at 7 cysteine residues. 93% (57/61) of the dopamine-metabolite PTMs were at C95 (Figure 3.15 C).

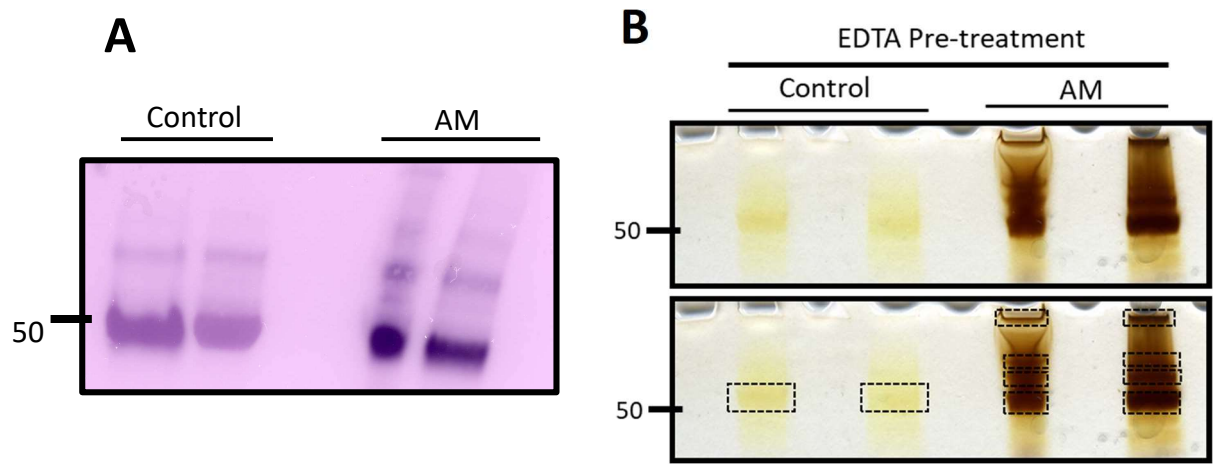

C

Peptide sequence	Variable Modifications	Observed m/z	Spectrum charge	Actual peptide mass (AMU)	Peptide Identification probability	Mascot Ion Score	Scaffold Peptide Score	Quantity
76 KGQE**m**NATGGDDPRNAAGG**c**EREPQSLTR 104	M80 Oxidation (+16), **C95 Indolequinone (+145)**	802.3541	4	3,205.39	99.40%	28.2	29.55	1
76 KGQE**m**NATGGDDPRNAAGG**c**EREPQSLTR 104	M80 Oxidation (+16), **C95 Aminochrome (+147)**	802.8554	4	3,207.39	99.70%	33.3	41.69	4
90 NAAGG**c**EREPQSLTR 104	**C95 Indolequinone (+145)**	867.3880	2	1,732.76	99.70%	59.5	130.03	31
90 NAAGG**c**EREPQSLTR 104	**C95 Aminochrome (+147)**	579.2650	3	1,734.77	99.70%	37.3	87.17	19
90 NAAGG**c**EREPQSLTR 104	**C95 Dopamine Quinone (+151)**	580.6098	3	1,738.81	99.50%	27.7	72.14	2
164 VQ**c**ST**c**RQATLTLTQGPS**c**WDDVLIPNR 191	**C166 Aminochrome (+149), C169 Dopamine Quinone (+151), C182 Indolequinone (+145)**	888.4120	4	3,549.62	99.50%	32	11.71	1
212 **c**GAHPTSDKETSVALHLIATNSRNIT**c**ITCTDVR 245	**C212 Dopamine Quinone (+151), C238 Dopamine Quinone (+151)**	1310.9731	3	3,929.90	99.10%	27.8	19.84	1
235 NIT**c**IT**c**TDVRSPVLVFQ**c**NSR 256	**C238 Indolequinone (+145)**, C241 Cys->Dha (-34), C253 Trioxidation (+48)	1314.6143	2	2,627.21	99.20%	26.3	38.93	1
276 QFVHDPQLGYSLP**c**VAG**c**PNSLIK 299	C289 Cys->Dha (-34), **C293 Indolequinone (+145)**	899.7746	3	2,696.30	99.70%	38.1	45.87	1

Figure 3.15: R-parkin is modified by dopamine metabolites facilitated by EDTA treatment to partially unfold the protein

R-parkin was treated with 200 µM EDTA for 30 minutes, followed by incubation with water (control) or 200 µM aminochrome (AM for 1 hr at 37°C. (**A**) Samples were subjected to NBT staining to detect protein-quinone species. (**B**) Identical samples were resolved by SDS-PAGE (non-reducing conditions) and visualized by silver staining. Indicated bands were excised and prepared for LC-MS/MS analysis. (**C**) MASCOT software was used to infer peptide identities from raw LC-MS/MS data. Results were further validated and analyzed using Scaffold 4 and Scaffold PTM software. All unique peptides identified with dopamine metabolite adducts in EDTA pre-treated samples from MS run 10B are listed with validating information. The table

lists one sample occurrence of peptides that were identified as dopamine modified multiple times. The ‘Quantity” column lists the total number of occurrences for that particular peptide.

Taking only the peptides that were ever found to be dopamine modified, I calculated the percentage of each unique peptide that was modified by dopamine. No difference in modification percentage was observed between the four bands excised from each EDTA pre-treated aminochrome sample (Figure 3.16 B). However, when the modification percentage of all bands from the standard (no EDTA) aminochrome samples was compared to that from the EDTA pre-treated samples, a significantly greater modification percentage is observed in the EDTA pre-treated parkin samples (Figure 3.16 C). This suggests that partially denatured parkin more readily forms covalent adducts with dopamine and its oxidized metabolites.

I again analyzed secondary oxidative modifications (trioxidation, cysteine to dehydroalanine conversion, and methionine oxidation) that may result from aminochrome treatment. This revealed a trend towards increased modification percentage for all three modifications; however only trioxidation modification shows a significant difference between the control samples and fractions from the three aminochrome treated bands (Figure 3.16 D-F).

The comparison of the four individual bands from the EDTA pre-treated samples (Figure 3.16, D-F) were shown as separate sub-fractions in order to better display the effect, or lack thereof, of the distinct protein bands on these metrics. While statistical tests were applied to these groups, the results are likely underpowered due to being limited to a sample size of n=2. Future work could increase sample number to confirm these results.

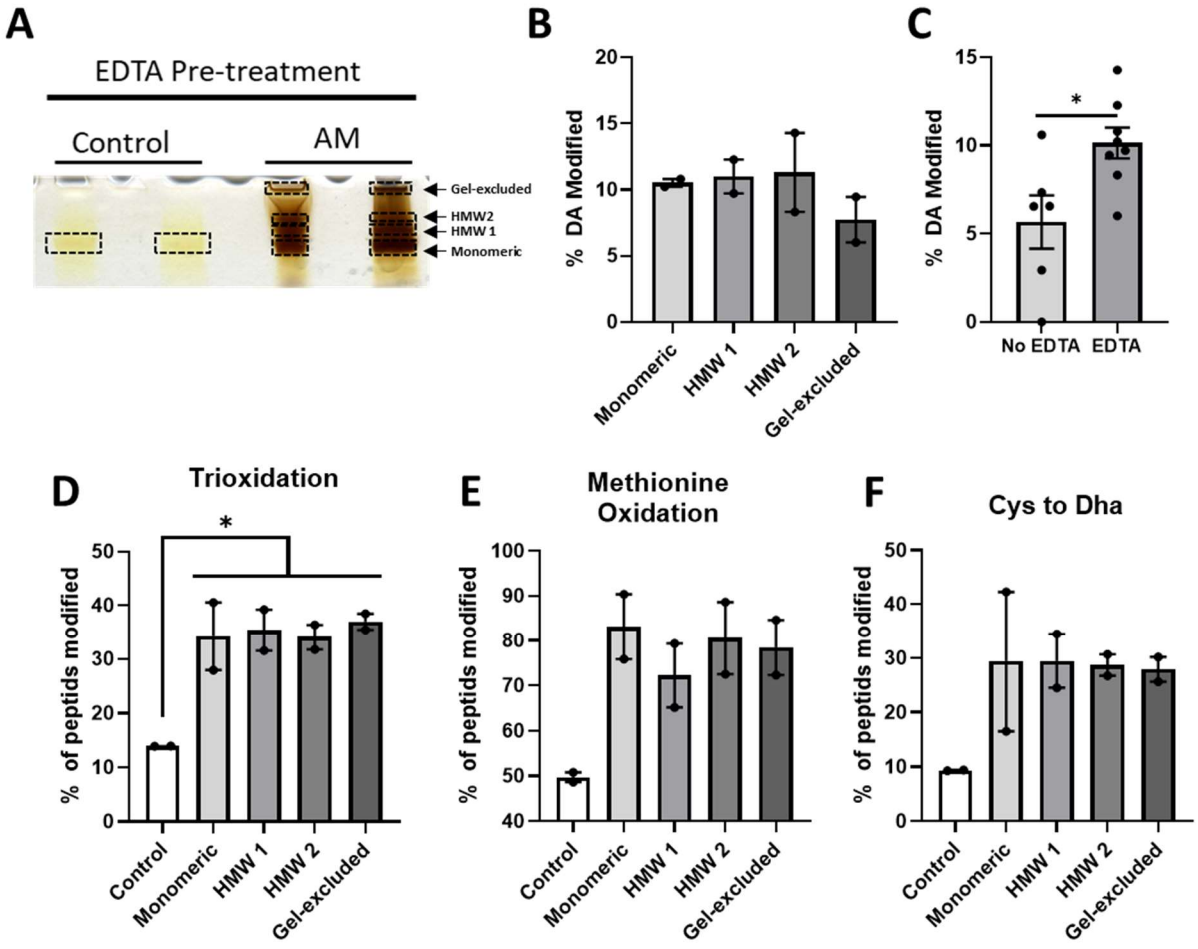

Figure 3.16: An increased percentage of parkin peptides are modified by dopamine when the parkin is exposed to EDTA to partially unfold the protein.

Following LC-MS/MS analysis of r-parkin samples treated with EDTA and then aminochrome, the raw data was analyzed using MASCOT to infer peptide identities and Scaffold PTM for further analysis. (**A**) The same silver stain shown in Figure 3.15 B is shown again with the bands labelled that correspond to EDTA fractions compared here. (**B-F**) Modification percentages for dopamine and other oxidative PTMs were calculated as the number of spectra corresponding to

modified parkin peptides divided by the number of spectra corresponding to all parkin peptides (modified + unmodified) in the subset of peptides ever detected as modified in that MS run. (**B**) Modification percentage is compared for the four dopamine-metabolite PTMs between the four bands obtained from EDTA/AM treated samples (n=2). (**C**) Among aminochrome-treated samples, modification percentage is compared between the various non EDTA-treated samples (n=6; MS runs 9A and 10A) and the distinct bands from the EDTA pre-treated samples (n=8; MS run 10B) (**D-F**) The modification percentage is compared between control and the our AM-treated bands indicated in A for EDTA pre-treated samples (n=2). Results are shown for (**D**) trioxidation, (**E**) methionine oxidation, and (**F**) cysteine to dehydroalanine conversion. Statistics for B and D-F were calculated using an ordinary one-way ANOVA with the Tukey multiple comparison test. Statistics for C were calculated using an unpaired t-test. Error bars represent mean +/- SEM.

Parkin promotes the formation of melanin dependant on C95

Previous experiments in our lab optimized and implemented an absorbance-based assay, measuring absorbance at 405 nm, to quantify the spontaneous auto-oxidation of dopamine to melanin. It was observed that the presence of r-parkin increased the rate melanin formation. Over the course of multiple experiments, I have validated and expanded this observation. I measured the effect of parkin concentration on melanin formation and confirmed that it promotes formation in a dose-dependant manner (Figure 3.17 A). GSH, particularly at a high concentration, inhibits the formation of melanin (Figure 3.17 B). I also found that DJ-1, another PD-linked redox-sensitive protein, is not able to promote melanin formation.

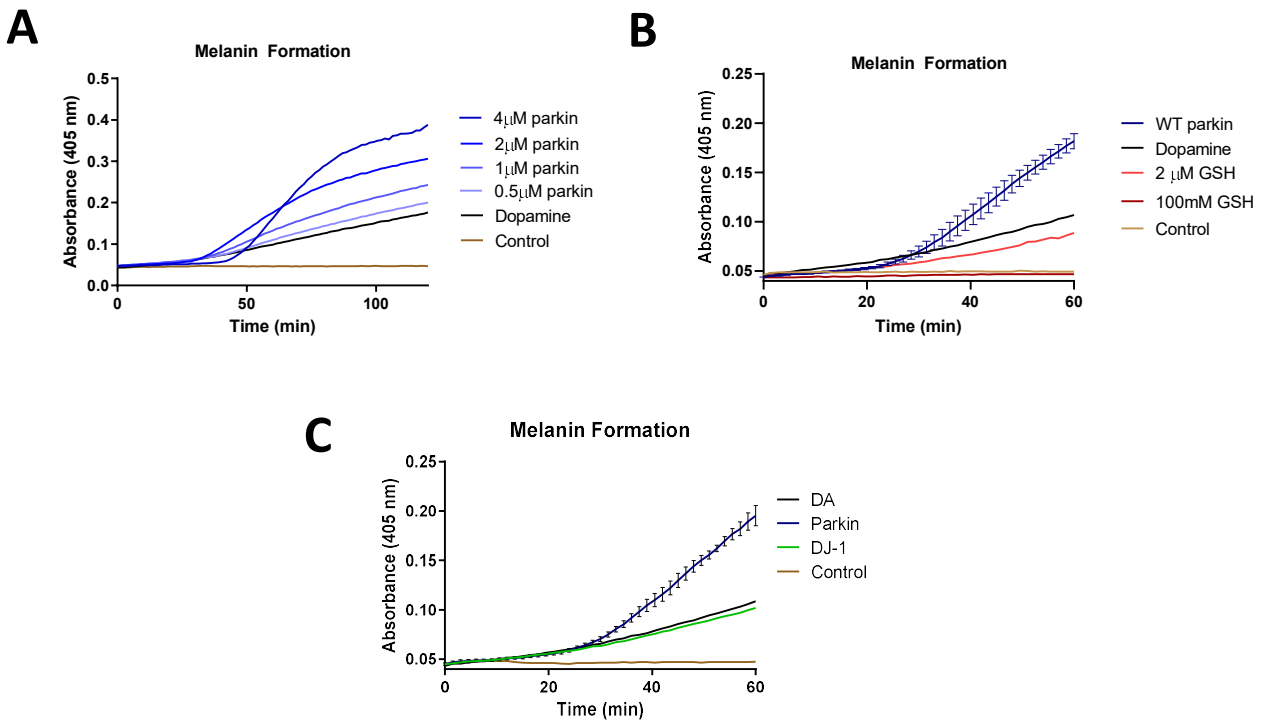

Figure 3.17: Wild-type r-parkin promotes the formation of melanin *in vitro* in a dose-dependant manner.

Melanin formation was monitored *in vitro* by measuring absorbance at 405 nm every 1.5 minutes. Unless otherwise indicated, protein concentration was 2 µM. Dopamine concentration in all wells (expect the controls/blank) was 10 mM. Control samples contained the same buffers as other samples without the addition of dopamine. Melanin formation was measured with dopamine alone or dopamine plus (**A**) 0.5-4 µM WT parkin, (**B**) WT parkin and GSH (2 µM and 100 mM), (**C**) WT parkin and recombinant DJ-1. Error bars, representing the mean +/- SEM (n=3), are only shown for select samples for clarity.

Given my observation that C95 is preferentially detected as dopamine-modified in LC-MS/MS experiments, I hypothesized that an r-parkin protein with a mutation at C95 would not promote melanin formation to the same degree as WT parkin. To test this, our lab introduced a cysteine to alanine mutation at residue 95 into the r-parkin protein. The mutagenesis was performed by Dr. Bojan Shutinoski. WT and C95A parkin were grown in parallel using the same *E. coli* expression system that was used to produce our recombinant protein for all experiments presented here. The protein is initially transcribed with an N-terminal His-SUMO tag which is used to isolate and purify parkin by binding to Ni-agarose beads. The tag is then typically cleaved using a ULP1 protease. The first observation I made when attempting to purify the C95A parkin protein was that the tag was not able to be cleaved (Figure 3.18 A,B). Our lab has since confirmed that this is not due to an unintended mutation in that region of the protein. However, if the tag is intentionally left on, the protein appears to be stable (Figure 3.18 C). I then confirmed using WT parkin that its ability to promote melanin formation is not impacted by the presence or absence of the His-SUMO tag (Figure 3.18 D). I then tested both WT and C95A parkin, both with the His-SUMO tag left on, using the melanin assay and observed that C95A parkin was not able to promote melanin formation beyond the autooxidation of dopamine alone (Figure 3.18 E), suggesting that C95 is critical for parkin-mediated melanin formation. The ability of various proteins tested to promote the formation of melanin are compared with absorbance values plotted relative to dopamine alone (Figure 3.18 F). Importantly, I confirmed that none of the proteins tested increased absorbance in the absence of dopamine (Figure 3.18 G).

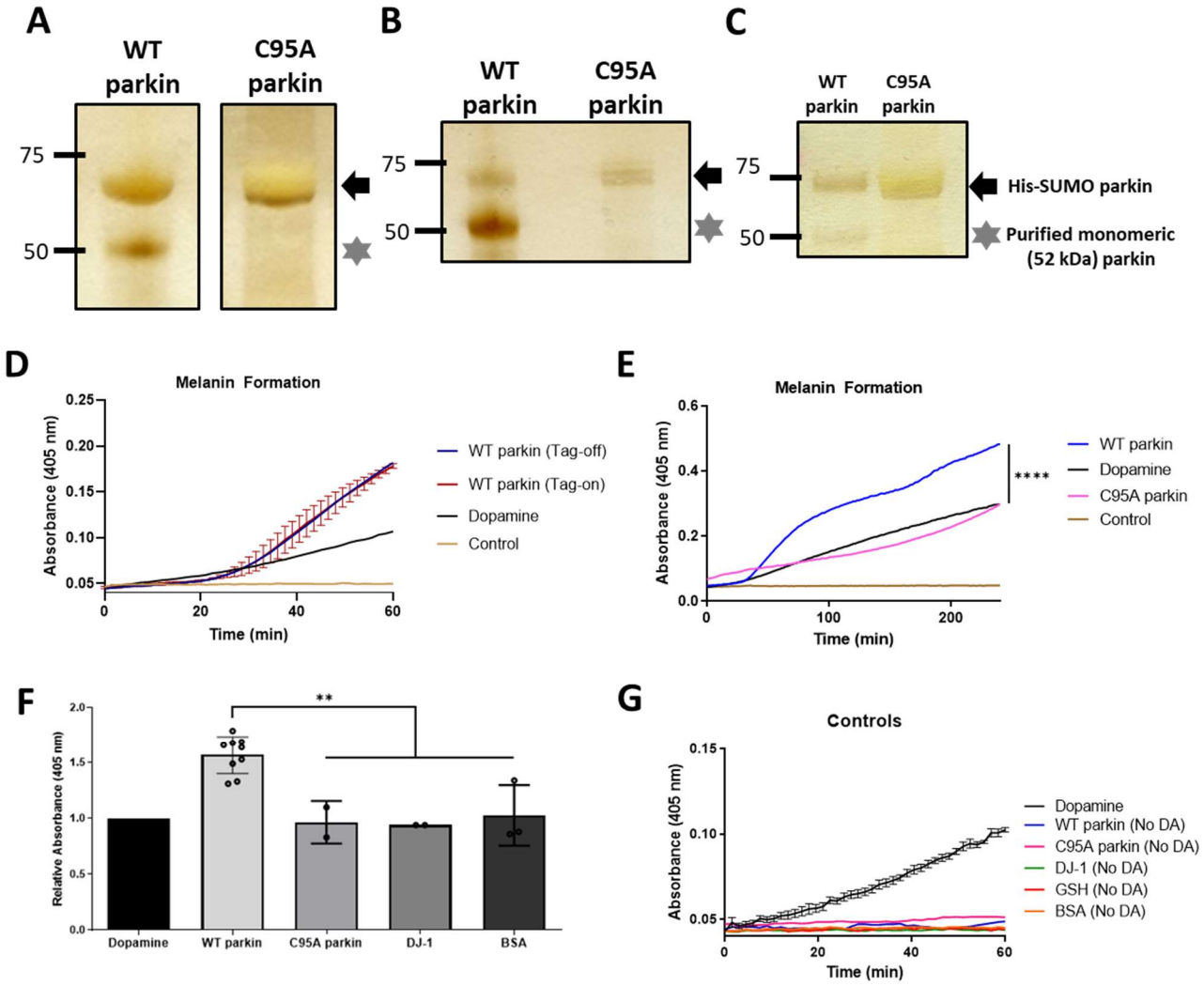

Figure 3.18: R-parkin carrying a mutation at residue C95 is no longer able to promote melanin formation.

WT and C95A parkin were grown in parallel using an established bacterial expression system. Purified proteins were visualized by silver staining. Various controls were run to confirm the melanin formation results, and proteins were visualized by SDS-PAGE and silver staining. (**A**) A low concentration of ULP1 protease (designed to cleave the HIS-SUMO tag off of the recombinant protein constructs) was added to WT and C95A parkin protein samples and

incubated overnight. (**B**) ULP1 was added to WT and C95A parkin samples for 40 minutes at 37°C. (**C**) WT and C95A parkin samples were purified without adding any protease. (**D-G**) Melanin formation was monitored in vitro by measuring absorbance at 405 nm every 1.5 minutes. Control samples contained the same buffers as other samples without the addition of dopamine. Error bars represent mean +/- SEM (n=3). Error bars are omitted for clarity on certain graphs. (**D**) WT parkin with its His-SUMO tag cleaved by ULP1 protease or with the tag left on are compared in their ability to promote melanin formation. No statistical difference was observed. (**E**) WT and C95A parkin are compared in their ability to promote melanin formation. (**F**) The absorbance after 1 hour is plotted for WT parkin, C95A parkin, DJ-1, and BSA relative to dopamine (the absorbance at 1 hour of dopamine alone is set to1). (**G**) Various proteins are compared using the melanin assay in the absence of any dopamine added. Statistics were calculated using an ordinary one-way ANOVA with the Tukey multiple comparison test.

Cysteine 95 is important for parkin-dependant protection against dopamine stress in cells

Following the discovery that dopamine metabolites form adducts primarily at C95 on parkin, a colleague in our lab, Dr. Daniel El Kodsi, also tested a C95A parkin mutant in human, dopamine-producing M17 neuroblastoma cells. Previous work using this model showed that M17 cells transfected with WT parkin protected against dopamine stress. One metric by which we can measure cell health is based on the relative concentration of H_2O_2 following treatment with 200 μM dopamine. This is the same concentration of aminochrome that r-parkin was treated with in my *in vitro* experiments. The plasmid encoding p.C95A human parkin protein was transiently transfected into M17 cells treated with 200 μM dopamine along with M17 cells expressing WT parkin and FLAG cDNA only. As previously shown, cells expressing FLAG had a significant increase in H_2O_2 concentration following dopamine treatment, while cells expressing WT parkin had no increase. Cells expressing p.C95A parkin showed a slight reduction in H_2O_2 concentration following dopamine treatment compared to those expressing FLAG. ROS levels were still significantly higher than in cells expressing WT parkin (Figure 3.19 A). This suggests that WT parkin is able to prevent an increase in ROS due to dopamine autooxidation and that this is partially dependant on its intact C95 residue.

Like WT parkin, the p.C95A parkin mutant promoted cell survival compared to cells transfected with the FLAG vector following dopamine stress. The cells transfected with the mutant parkin appeared to trend towards lesser survival compared to those M17 cells transfected with WT parkin; however, the difference is not significant at current numbers. Expression and stability of WT and p.C95A parkin were confirmed by Western blot (Figure 3.19 C).

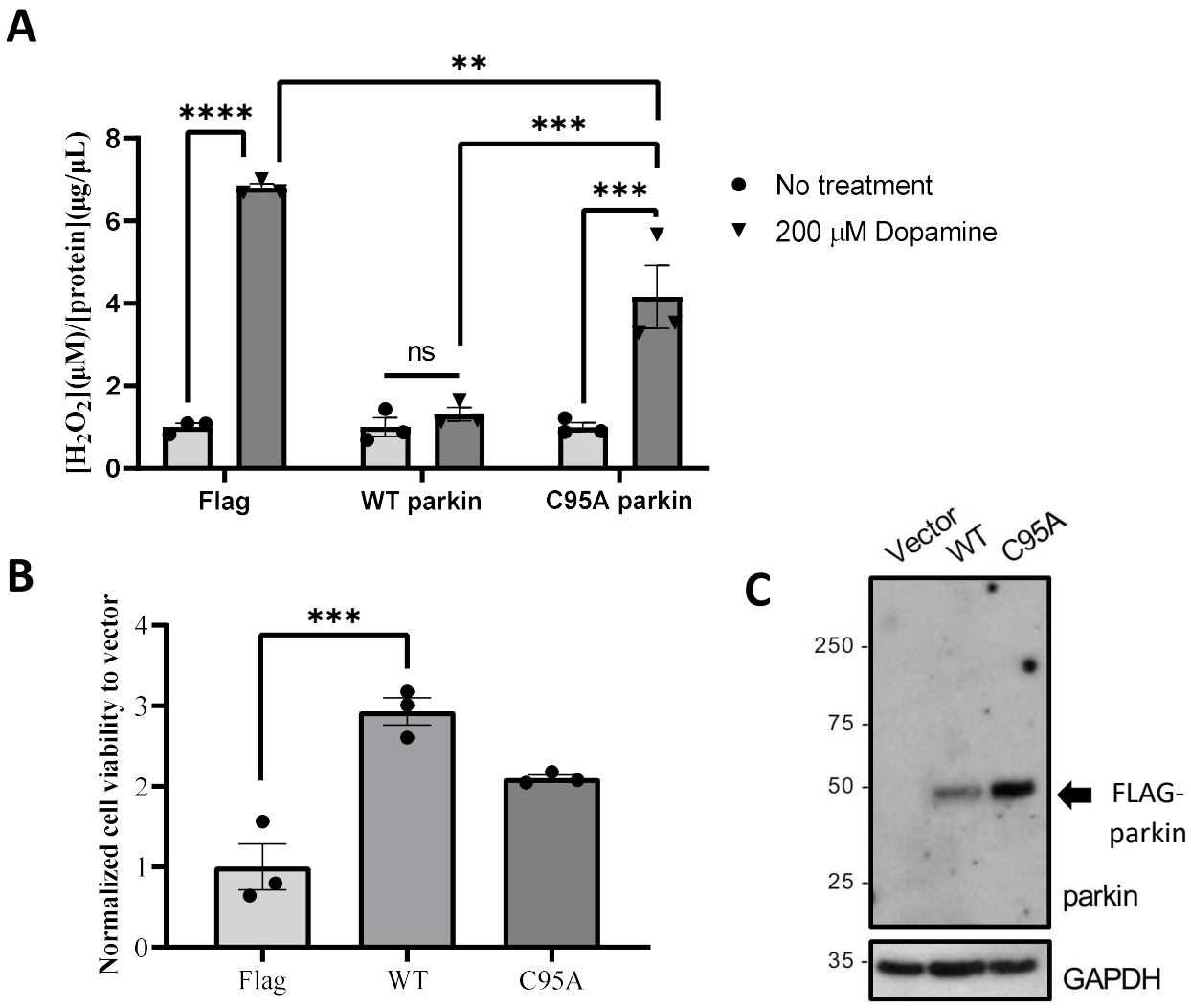

Figure 3.19: M17 cells expressing p.C95A parkin do not protect against ROS generation following dopamine stress as well as does wild-type parkin protein.

WT parkin, C95A mutant parkin, and FLAG vector were transfected into M17 cells and treated with 200 μM dopamine. (**A**) H_2O_2 concentration was quantified. Results are shown as mean +/- SEM (n=3) and dopamine-treated samples are normalized to their respective untreated samples. Statistics were calculated using an ordinary one-way ANOVA with the Tukey multiple comparison test. (**B**) Cell viability was measured using normalized relative fluorescence units

(RFUs) and viability was plotted relative to the cells transfected with FLAG. Results are shown as mean +/- SEM (n=3). Statistics were calculated using a two-way ANOVA with the Sidak multiple comparison test. (**C**) Parkin expression and stability was confirmed by Western blot (IB: Prk8, 1:5000). This M17 cell work was performed by Dr. Daniel El Kodsi with assistance from Dr. Bojan Shutinoski and Nathalie Lengacher.

Parkin's linker region is not well-conserved between mice and humans

The selective vulnerability of C95 to dopamine modification in our MS experiments is especially interesting since this is the one cysteine residue that is not conserved in mouse parkin. In order to further analyze and quantify the differences between the parkin protein in humans, primates, rodents, and common fruit flies, I performed a sequence alignment (Figure 3.20). This demonstrated qualitatively that much of parkin's sequence is very well-conserved across species, especially at cysteine residues. Across human, all three primate sequences analyzed, rats, and mice, 34 of 35 cysteines are conserved. The one that was not is C95, which is absent in mouse and rat parkin. This initial alignment suggested that the entire linker region of parkin may be less conserved in the rodent species. To quantify this, I aligned only human and mouse parkin and then quantified the percentage of amino acids that were conserved across parkin's domains (Figure 3.21). This revealed that all four RING domains as well as the Ubl domain had 86-93% of their amino acids conserved between mice and humans; however, the linker region between the Ubl domain and RING0 had only 56% similarity.

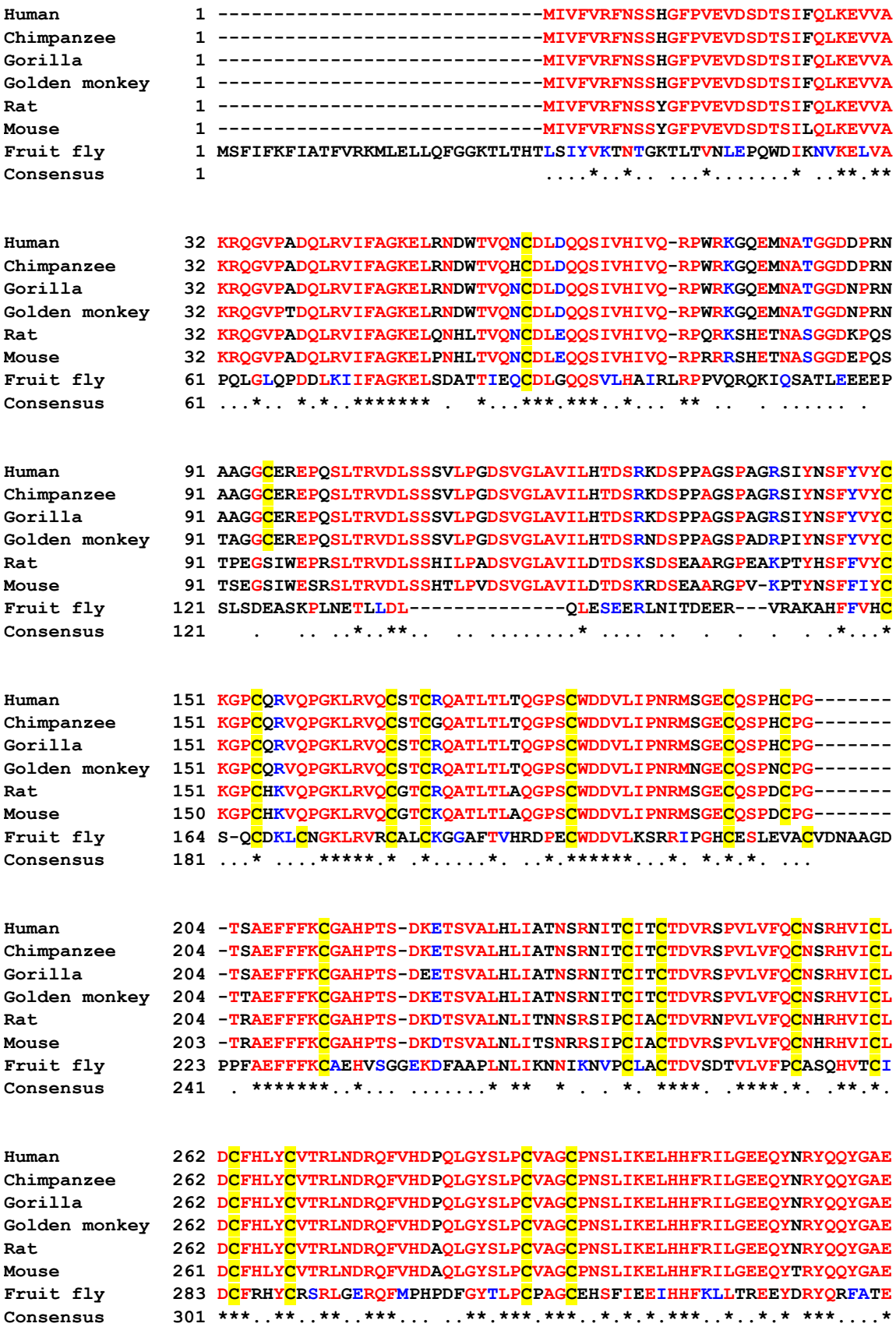
Human 1 ----------MIVFVRFNSSHGFPVEVDSDTSIFQLKEVVA
Chimpanzee 1 ----------MIVFVRFNSSHGFPVEVDSDTSIFQLKEVVA
Gorilla 1 ----------MIVFVRFNSSHGFPVEVDSDTSIFQLKEVVA
Golden monkey 1 ----------MIVFVRFNSSHGFPVEVDSDTSIFQLKEVVA
Rat 1 ----------MIVFVRFNSSYGFPVEVDSDTSIFQLKEVVA
Mouse 1 ----------MIVFVRFNSSYGFPVEVDSDTSILQLKEVVA
Fruit fly 1 MSFIFKFIATFVRKMLELLQFGGKTLTHTLSIYVKTNTGKTLTVNLEPQWDIKNVKELVA
Consensus 1 ....*..*.. ...*.......* ..**.**
Human 32 KRQGVPADQLRVIFAGKELRNDWTVQNCDLDQQSIVHIVQ-RPWRKGQEMNATGGDDPRN
Chimpanzee 32 KRQGVPADQLRVIFAGKELRNDWTVQHCDLDQQSIVHIVQ-RPWRKGQEMNATGGDDPRN
Gorilla 32 KRQGVPADQLRVIFAGKELRNDWTVQNCDLDQQSIVHIVQ-RPWRKGQEMNATGGDNPRN
Golden monkey 32 KRQGVPTDQLRVIFAGKELRNDWTVQNCDLDQQSIVHIVQ-RPWRKGQEMNATGGDNPRN
Rat 32 KRQGVPADQLRVIFAGKELQNHLTVQNCDLEQQSIVHIVQ-RPQRKSHETNASGGDKPQS
Mouse 32 KRQGVPADQLRVIFAGKELPNHLTVQNCDLEQQSIVHIVQ-RPRRRSHETNASGGDEPQS
Fruit fly 61 PQLGLQPDDLKIIFAGKELSDATTIEQCDLGQQSVLHAIRLRPPVQRQKIQSATLEEEEP
Consensus 61 ...*.. *.*..******* . *...***.***..*... ** .. . .
Human 91 AAGGCEREPQSLTRVDLSSSVLPGDSVGLAVILHTDSRKDSPPAGSPAGRSIYNSFYVYC
Chimpanzee 91 AAGGCEREPQSLTRVDLSSSVLPGDSVGLAVILHTDSRKDSPPAGSPAGRSIYNSFYVYC
Gorilla 91 AAGGCEREPQSLTRVDLSSSVLPGDSVGLAVILHTDSRKDSPPAGSPAGRSIYNSFYVYC
Golden monkey 91 TAGGCEREPQSLTRVDLSSSVLPGDSVGLAVILHTDSRNDSPPAGSPADRPIYNSFYVYC
Rat 91 TPEGSIWEPRSLTRVDLSSHILPADSVGLAVILDTDSKSDSEAARGPEAKPTYHSFFVYC
Mouse 91 TSEGSIWESRSLTRVDLSSHTLPVDSVGLAVILDTDSKRDSEAARGPV-KPTYNSFFIYC
Fruit fly 121 SLSDEASKPLNETLLDL--------------QLESEERLNITDEER---VRAKAHFFVHC
Consensus 121 . .. ..*..**.. .. ..* ....*...*
Human 151 KGPCQRVQPGKLRVQCSTCRQATLTLTQGPSCWDDVLIPNRMSGECQSPHCPG-------
Chimpanzee 151 KGPCQRVQPGKLRVQCSTCGQATLTLTQGPSCWDDVLIPNRMSGECQSPHCPG-------
Gorilla 151 KGPCQRVQPGKLRVQCSTCRQATLTLTQGPSCWDDVLIPNRMSGECQSPHCPG-------
Golden monkey 151 KGPCQRVQPGKLRVQCSTCRQATLTLTQGPSCWDDVLIPNRMNGECQSPNCPG-------
Rat 151 KGPCHKVQPGKLRVQCGTCRQATLTLAQGPSCWDDVLIPNRMSGECQSPDCPG-------
Mouse 150 KGPCHKVQPGKLRVQCGTCKQATLTLAQGPSCWDDVLIPNRMSGECQSPDCPG-------
Fruit fly 164 S-QCDKLCNGKLRVRCALCKGGAFTVHRDPECWDDVLKSRRIPGHCESLEVACVDNAAGD
Consensus 181 ...* ....*****.* .*.....*. ..*.******...*. *.*.*. ...
Human 204 -TSAEFFFKCGAHPTS-DKETSVALHLIATNSRNITCITCTDVRSPVLVFQCNSRHVICL
Chimpanzee 204 -TSAEFFFKCGAHPTS-DKETSVALHLIATNSRNITCITCTDVRSPVLVFQCNSRHVICL
Gorilla 204 -TSAEFFFKCGAHPTS-DEETSVALHLIATNSRNITCITCTDVRSPVLVFQCNSRHVICL
Golden monkey 204 -TTAEFFFKCGAHPTS-DKETSVALHLIATNSRNITCITCTDVRSPVLVFQCNSRHVICL
Rat 204 -TRAEFFFKCGAHPTS-DKDTSVALNLITNNSRSIPCIACTDVRNPVLVFQCNHRHVICL
Mouse 203 -TRAEFFFKCGAHPTS-DKDTSVALNLITSNRRSIPCIACTDVRSPVLVFQCNHRHVICL
Fruit fly 223 PPFAEFFFKCAEHVSGGEKDFAAPLNLIKNNIKNVPCLACTDVSDTVLVFPCASQHVTCI
Consensus 241 . *******..*... ....* ** * . . *. ****. .****.*. .**.*.
Human 262 DCFHLYCVTRLNDRQFVHDPQLGYSLPCVAGCPNSLIKELHHFRILGEEQYNRYQQYGAE
Chimpanzee 262 DCFHLYCVTRLNDRQFVHDPQLGYSLPCVAGCPNSLIKELHHFRILGEEQYNRYQQYGAE
Gorilla 262 DCFHLYCVTRLNDRQFVHDPQLGYSLPCVAGCPNSLIKELHHFRILGEEQYNRYQQYGAE
Golden monkey 262 DCFHLYCVTRLNDRQFVHDPQLGYSLPCVAGCPNSLIKELHHFRILGEEQYNRYQQYGAE
Rat 262 DCFHLYCVTRLNDRQFVHDAQLGYSLPCVAGCPNSLIKELHHFRILGEEQYNRYQQYGAE
Mouse 261 DCFHLYCVTRLNDRQFVHDAQLGYSLPCVAGCPNSLIKELHHFRILGEEQYTRYQQYGAE
Fruit fly 283 DCFRHYCRSRLGERQFMPHPDFGYTLPCPAGCEHSFIEEIHHFKLLTREEYDRYQRFATE
Consensus 301 ***..**..**..***... ..**.***.***..*.*.*.***..*..*.* ***....*

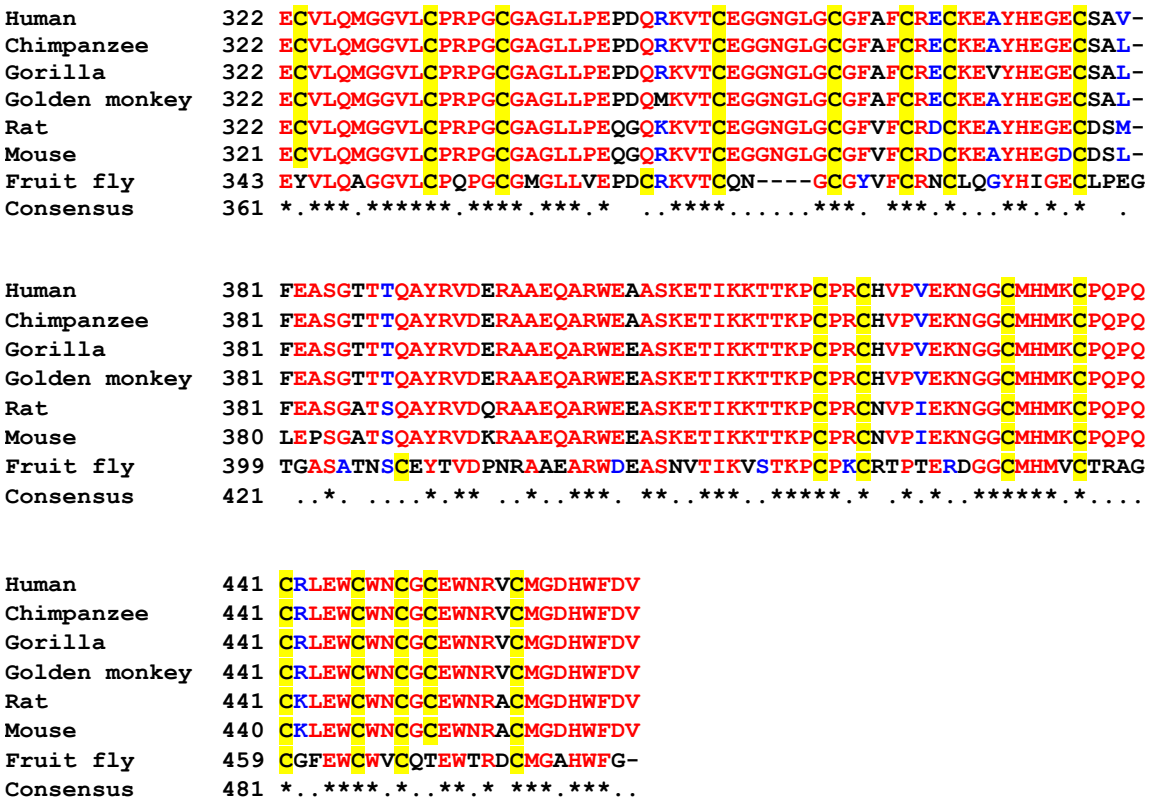

Figure 3.20: Parkin's sequence, including 34/35 cysteine residues, is well conserved between human, primate, and rodent parkin proteins.

The human parkin amino acid sequence was aligned against that of the chimpanzee, western lowland gorilla (Gorilla), golden snub-nosed monkey (Golden monkey), rat, mouse, and common fruit fly (Fruit fly). Cysteine residues are highlighted in yellow. Identical amino acids that are conserved at 6/7 species listed are shown in red. Similar amino acids that are conserved at 6/7 species are shown in blue.

A

```
PRKN_HUMAN    1 MIVFVRFNSSHGFPVEVDSDTSIFQLKEVVAKRQGVPADQLRVIFAGKELRNDWTVQNCDLDQQSIVHIVQRPWRKGQEMNATGGDDPRNAAGGCEREPQ
PRKN_MOUSE    1 MIVFVRFNSSYGFPVEVDSDTSILQLKEVVAKRQGVPADQLRVIFAGKELPNHLTVQNCDLEQQSIVHIVQRPRRRSHETNASGGDEPQSTSEGSIWESR

PRKN_HUMAN  101 SLTRVDLSSSVLPGDSVGLAVILHTDSRKDSPPAGSPAGRSIYNSFYVYCKGPCQRVQPGKLRVQCSTCRQATLTLTQGPSCWDDVLIPNRMSGECQSPH
PRKN_MOUSE  101 SLTRVDLSSHTLPVDSVGLAVILDTDSKRDSEAARGPV-KPTYNSFFIYCKGPCHKVQPGKLRVQCGTCKQATLTLAQGPSCWDDVLIPNRMSGECQSPD

PRKN_HUMAN  201 CPGTSAEFFFKCGAHPTSDKETSVALHLIATNSRNITCITCTDVRSPVLVFQCNSRHVICLDCFHLYCVTRLNDRQFVHDPQLGYSLPCVAGCPNSLIKE
PRKN_MOUSE  200 CPGTRAEFFFKCGAHPTSDKDTSVALNLITSNRRSIPCIACTDVRSPVLVFQCNHRHVICLDCFHLYCVTRLNDRQFVHDAQLGYSLPCVAGCPNSLIKE

PRKN_HUMAN  301 LHHFRILGEEQYNRYQQYGAEECVLQMGGVLCPRPGCGAGLLPEPDQRKVTCEGGNGLGCGFAFCRECKEAYHEGECSAVFEASGTTTQAYRVDERAAEQ
PRKN_MOUSE  300 LHHFRILGEEQYTRYQQYGAEECVLQMGGVLCPRPGCGAGLLPEQGQRKVTCEGGNGLGCGFVFCRDCKEAYHEGDCDSLLEPSGATSQAYRVDKRAAEQ

PRKN_HUMAN  401 ARWEAASKETIKKTTKPCPRCHVPVEKNGGCMHMKCPQPQCRLEWCWNCGCEWNRVCMGDHWFDV
PRKN_MOUSE  400 ARWEEASKETIKKTTKPCPRCNVPIEKNGGCMHMKCPQPQCKLEWCWNCGCEWNRACMGDHWFDV
```

B

	Ubl	Linker	RING0	RING1	IBR	RING2
A.A. Range	1-76	77-140	141-225	226-327	328-378	410-465
Identical AA's	68/76	36/64	73/85	92/102	45/51	52/56
% Similar	89%	56%	86%	90%	88%	93%

Figure 3.21: Linker region of parkin is less conserved between mice and humans than other domains.

(**A**) Amino acid sequences for human and mouse parkin were aligned. All cysteine residues are highlighted in yellow. The C95 residue on human parkin and corresponding S95 residue on mouse parkin is indicated by a red box. (**B**) The number of amino acids conserved between mouse and human parkin in various domains are presented and the percent similarity was calculated for each.

Chapter 4 Discussion

This thesis has sought to further characterize a redox function for the cysteine rich, PD-linked parkin protein. Previous research in our lab demonstrated that the unique sensitivity of parkin's cysteine residues to oxidation confers benefit to the survival of at-risk neurons. I hypothesized that by using mass spectrometry, I could quantitatively measure the redox state of parkin's cysteine residues, as well as detect covalent adducts of dopamine and its oxidized metabolites on parkin. Through various optimization steps and experiments, I was able to quantitatively measure a decrease in the proportion of free cysteines in r-parkin that had been exposed to ROS and in parkin proteins that had transitioned into the insoluble pellet compared to control samples and soluble species, respectively. Further, I was able to detect adducts of four similar chemical structures corresponding to oxidized dopamine metabolites on parkin's cysteine residues.

Reactivity of cysteine residues

Cysteine is arguably the most intriguing amino acid in terms of its diversity of physiological functions. Its functionality stems largely from the sulfur atom of its thiol group and the distance of the free electron pair from its nucleus, which allows for deprotonation at physiological pH. Cysteine's diverse functionality includes the ability to stabilize protein structures through intramolecular and intermolecular disulfide bonds. Cysteines bind metals within various proteins, including iron in cytochromes [121], copper in plastocyanin [122], and zinc in

zinc-finger domains as well as RING domains [123], among others. Cysteines act as the functional residue in the catalytic pockets of various biochemical enzymes. Further, cysteines act as key antioxidants in cells through oxidation of their thiol groups. This can occur through the formation of disulfide bonds, or through PTMs such as oxidation to sulfenic- (SOH), sulfinic- (SO_2H), or sulfonic (SO_3H) acid. Nitrotyrosination by nitric oxide, or even the covalent attachment of lipids represent additional, possible cysteine modifications [124].

As a result of its reactivity and critical functions, cysteine residues, while relatively rare compared to other amino acids (approximately 2.3% within the human proteome [125]), are present in 97% of human proteins. In total, there are approximately 260,000 cysteines in the *homo sapiens* proteome (roughly 13 per protein) [124]. Further, the positions of cysteine residues within proteins tends to be highly conserved between species [126], as I have highlighted here for parkin.

LC-MS/MS Data Processing

This section outlines the MS data processing pipeline used in my experiments and outlines the pros and cons of some common MS quantification techniques. In LC-MS/MS experiments, following separation by liquid chromatography, both the full spectra (MS1) and the tandem MS spectra (MS/MS or MS2) are acquired for each individual peptide. During data processing, three different steps are required. These include peptide peak identification, database search, and quantification. The peak identification step includes applying particular pre-set thresholds such as charge state, signal to noise ratio, and minimal and maximal mass to the set of spectra identified. This filtering process generates a new list of MS2 spectra which are searched against spectra from a database containing a list of proteins from the organism of interest (*homo*

sapiens in my experiments). This is the step where a set of variable modifications can be appended to the spectra and peptide masses as they are searched against the database. The identified peptides are also scored by various statistical parameters to asses the quality of matches [124].

The final step is quantification. This is not straightforward, and much research has been performed to try and optimize and improve the process. A major challenge represents the fact that ionization efficiency can vary considerably between peptides, including the same peptide with and without a PTM. Quantification can be performed using either MS1 or MS2 spectra. The spectral count data that I have presented here represents a common form of MS2 quantification. This method is based on the count (i.e. number of observations) of an identified fragment peptide; however, this method is commonly considered to only be semi-quantitative. Quantification has also been attempted using summed intensities of MS2 peaks; however, this approach suffers from the fact that the spectrum may not have been acquired at the peak of the elution curve, which can lead to significant variation in measured intensities. One solution to this is to quantify MS1 peak area. Since MS1 peaks are elution curves, the peptide can be monitored during the full elution time, and the intensity is based on the area under a curve that has a predefined shape, rather than a single intensity measurement as is the case for MS2 spectra. This also means that there is no need to identify a high number spectra for a given peptide in order to quantify it. The MaxQuant platform that I have employed to quantify IAA intensity in the H_2O_2 treated r-parkin experiments utilizes MS1 peak quantification [124].

In the results presented here, I have utilized both spectral count (Scaffold PTM) and MS1 peak integration (MaxQuant) to quantify PTMs on parkin. This was done acknowledging that

spectral count data are considered to be semi-quantitative. Spectral count data have been presented for the experiments exploring dopamine-metabolite adducts on parkin. Since the primary focus of these experiments were the detection of dopamine-metabolite PTMs themselves, I focused my optimization on that detection. The quantification of those PTMs as a percentage of peptides in order to compare various monomeric vs. HMW bands, or EDTA pre-treated vs. standard samples, were secondary outcomes to the presence of dopamine metabolite adducts themselves. There are no indicators that the spectral count data is not representative. In fact, since comparisons were made based on the same modified peptides between samples, error due to differing ionization efficiency as discussed above would have been minimized or eliminated. Nevertheless, that data generated here were based on semi-quantitative spectral counts is a relative limitation of my work. Future work could confirm the quantification trends by optimizing a more fully quantitative method for this application.

Under Aim 1 experiments, which analyzed IAA tagging of control and H_2O_2 treated r-parkin, a more robust method of quantification was the primary outcome. Our lab had previously shown that both IAA and NEM PTMs could be detected on parkin's cysteines by LC-MS/MS analysis. Therefore, in order to extend the findings, I optimized and utilized MS1 intensity data generated by the MaxQuant platform in order to compare the degree of IAA modification on parkin across samples. This technique yielded promising results by demonstrating that the intensity of IAA modified parkin peptides decreased following H_2O_2 treatment and following parkin's transition from the soluble to the insoluble fraction.

Differentially labelling reduced vs. oxidized cysteines

In addition to a method of accurately quantifying PTM intensity, we needed a robust molecule that could covalently bind to reduced, but not oxidized, cysteines. Many unique cysteine-tagging probes have been developed over the past few decades, which are reviewed in detail by Hoch et al [124]. One methodology that was considered for this project is known as the ICAT (isotope-coded affinity tag) approach. This utilizes an ICAT reagent consisting of an iodoacetamide (IAA) derivative connected to a biotin tag by a cleavable linker. Importantly, this reagent comes in two forms, one that is a standard "light" C-12 version, while the other has is a "heavy" version with nine C-13 isotopes incorporated. Using this approach, I would be able to differentially label reduced vs. reversibly oxidized cysteines using the same molecule, but I could differentiate them based on the 9 Da mass difference. As discussed previously, an advantage of differentially labelling with molecules as similar as possible minimizes error due to technical MS factors such as ionization efficiency. Here, we decided to use IAA alone to label cysteines due to the availability of ICAT reagents not being conducive to the timeline of my project. Further, I did not need the enrichment capabilities of the biotin-tag for this *in vitro* work using r-parkin. However, as future work seeks to extend these findings using cellular and *in vivo* models such as tissues from murine and human brain, enrichment will become a more important factor. In addition to ICAT reagents, other cysteine-reactive probes could be explored for this task. Some recent examples use an approach known as "click chemistry" where a small molecule is used to bind to free cysteines, followed by the addition of a larger enrichment tag. This allows the small molecule to bind to the maximum number of free cysteines, which are often located deep in small pockets within a protein.

Recently published work by the Chouchani team presents a novel method of quantifying cysteine oxidation across an entire proteome [127]. This method uses a newly synthesized cystine-reactive phosphate tag, consisting of a non-hydrolyzable phosphate moiety, an IAA-based cysteine alkylating warhead, and a linker to tune hydrophobicity and permit rapid purification. Labelled cysteine-containing peptides can later be enriched by immobilized metal-affinity chromatography for MS analysis. This technique is compatible with tandem mass tag (TMT)-multiplexing which also uses isobaric tags to differentially label several experimental fractions, or differentially label before and after a sample is treated with a reducing agent. While sharing many functional similarities with previous techniques developed to map the cysteine landscape, this new enhanced method was successful in identifying 34,000 unique cysteine sites across 9,400 mouse proteins. This technique ultimately allows for the determination of a tissue-specific cysteine oxidation ratio for individual cysteine sites and would be useful for our own future work exploring parkin's redox benefit *in vivo*.

The purpose was to differentially label reduced and reversibly oxidized cysteine residues in my samples with iodoacetamide (IAA) and n-ethylmaleimide (NEM), respectively. A limitation of my current work is that coverage of NEM modifications on parkin was never sufficient to confidently compare intensities across samples. I did frequently identify NEM modifications, which I interpreted as evidence that parkin's cysteines could indeed be identified in both reduced and oxidized states, as expected; however, the coverage of NEM modification events would need to be much greater for an accurate MaxQuant analysis. For IAA modifications, nearly every cysteine was identified with a modification in any given run, allowing for more confident comparison of MaxQuant intensity values between control and H_2O_2 treated samples, or between soluble and insoluble fractions. While the conclusion that parkin's

cysteines are reactive to changes in redox environment would be even stronger if there was a corresponding increase in NEM intensity in samples that had a decrease in IAA intensity, the decrease in IAA intensity alone does still show that fewer of parkin's cysteines are in a redox-reduced state following H_2O_2 treatment, or following parkin's transition into the insoluble pellet. This suggests that more cysteines were present in an oxidized state.

Effect of parkin cysteine oxidation

Aside from the unique vulnerability (or exposure) of C95 to modification by dopamine, trends for which cysteine residues are more prone to oxidation were not as readily apparent. I discussed above that NEM coverage was not conducive to quantitative MaxQuant analysis. Instead, I investigated the MS2 spectral count data obtained from Scaffold PTM to see if there were any trends. There did appear to be an increase in NEM modifications at C238, C260, and C263. However, there were no identifiable trends between control and treated sample, between soluble or insoluble fractions, or any corresponding decrease in IAA spectral counts. Therefore, this observations should be interpreted with caution. Nevertheless, future work to validate the role of these residues would be interesting. Overall, it appears that oxidation likely occurs at most or all of parkin's cysteines rather than one or a few specific vulnerable residues. This would better explain parkin's observed ability to reduce H_2O_2 to water considerably more efficiently than GSH, which contains a single cysteine.

A question that remains unanswered is whether there exists is any sort of oxidation "signature" that correlates with parkin's transition into insolubility. For instance, are there certain cysteines that, when oxidized, disrupt its structure and cause it to lose solubility? I had

hypothesized that cysteines coordinating zinc ions would be more critical to structure and therefore oxidation of those residues might lead to insolubility. Interestingly, all three residues mentioned above that were found with higher than average spectral counts for NEM modifications coordinate a single zinc ion in parkin's RING1 domain. Additional structural studies would be helpful to explore the localization and accessibility of this particular region of parkin, and possibly shed light on its apparent susceptibility to oxidation and the structural impacts of oxidation in this region. Considering that the majority of parkin's cysteines coordinate zinc (28/35), it does not seem likely that oxidation of any one or two of those would instantly lead to insolubility. Rather, I predict that there is a gradient of oxidation rather than a strict threshold that correlates with parkin insolubility.

Optimization of dopamine adduct detection

The detection of dopamine metabolite adducts on parkin was found to be more difficult than the detection of other oxidation-related modifications that I searched for. This section will outline and discuss the challenges I faced and solutions I found in order to detect dopamine metabolite adducts on parkin. I predict that the difficulty in detecting dopamine adducts is largely due to heterogeneity in the chemical structure of any given dopamine PTM. The high reactivity of dopamine quinones suggests that at any given moment in time, the full complement of dopamine metabolites in a sample likely possess numerous distinct chemical structures. This can be problematic in our standard LC-MS/MS workflow which requires that we probe for a maximum of 9 distinct PTMs in a single MASCOT search. Even utilizing the full complement of 9 PTMs can greatly increase statistical complexity due to a large number of possible PTM

combinations on a single trypsin-digested peptide, increasing the risk of incorrect identifications by the MASCOT software. This complexity is further increased on peptides that contain multiple cysteine residues, as well as in instances where a trypsin cleavage point is missed. If trypsin digestion is 100% efficient, 14 of parkin's cysteines occur as the only cysteine on that particular digested peptide, while 12 appear on peptides with 2 cysteines and 9 appear on peptides with 3 total cysteines. However, in practice, many of the "single" cysteine peptides are small digested peptides that tend to have one or two missed cleavage points, resulting in multiple cysteines per digested peptide. For most MASCOT searches, peptides with 1 or 2 missed cleavages are included in the results, whereas those with more than that are excluded. In order for a peptide to be detected and assigned to parkin, all PTMs present must be included in the list of MASCOT variable modifications. This can lead to minor variation in the number of spectra identified if the complement of variable modifications is altered, as shown in Figure 3.5. It's important to note that in cases where multiple trials of the same experiment were presented, the MASCOT parameter set was kept the same.

The detection of dopamine metabolite adducts on whole proteins has not been well established. As such, there are limited examples available in the literature. Challenges involved in the proteomic detection of any catechol quinone and current examples are reviewed by Chen and Li [128]. A few papers have presented dopamine-mediated mass shifts identified by MS, but to my knowledge only one has detected a distinct chemical mass shift at a particular cysteine residue in a manner consistent with our PTM identification workflow. That study identified an adduct of 151.06 Da at cysteine residues on GCase [108]. This mass shift corresponds to a dopamine quinone adduct, which I used as one of my MASCOT variable modifications along with three other mass adduct structures.

Following several optimization runs, I detected parkin peptides with mass shifts matching that expected for DAQ and aminochrome adducts on various cysteine residues, as predicted by the MASCOT software (MS runs 4 and 7). However, these detections occurred in aminochrome treated samples as well as control samples; hence the conclusion that these were largely mass adducts due to artifacts of the same size as dopamine (MASSAD). Another observation which suggested that I may not be detecting true dopamine adducts was that the predicted PTMs in these samples were highly concentrated on peptides that contained multiple cysteine residues. Specifically, C332 and C337 appeared to be the most vulnerable to modification. These two cysteines appear on a large peptide spanning from aa 315-348 (with no missed trypsin digestion points) that also contains a third cysteine (C323). Even after it was demonstrated that these adduct detections were likely MASSADs, it remains unclear why this peptide in particular seems to be especially vulnerable to these false detections, while other peptides that also containing 3 cysteines show less vulnerability. Going forward, I needed a method of preparing and analyzing our samples that would not produce false positives. I predicted that if I could eliminate the MASSADs observed thus far, I would be able to detect fewer, but more relevant *bona fide* adducts in dopamine-treated samples.

I next demonstrated that the MASSADs resulted from the addition of cysteine-modifying compounds such as IAA and NEM. In some initial optimization experiments, following treatment of r-parkin with dopamine or aminochrome, I subsequently treated samples with IAA, DTT, and NEM as I had done with H_2O_2 treated samples. The advantage of this is that I could measure changes in cysteine oxidation state following treatment that is not due to a covalent dopamine adduct. Further, blocking any unreacted cysteines is a common MS practice because it reduces cross reactions during MS analysis, thereby reducing complexity and increasing protein

coverage. This fingerprinting approach has potential to yield interesting data due to its ability to detect changes in cysteine oxidation beyond physical dopamine adducts; however, I opted to reduce PTM complexity and eliminate this step in order to prevent MASSADs.

In light of this observation that cysteine-modifying compounds can lead to MASSADs and thereby limit the ability to infer true modifications caused by aminochrome treatment, I prepared samples that were never treated with DTT, IAA, NEM, or acrylamide during the initial experiment or during the MS preparation stage. Three identical runs were prepared and analyzed using this revised method (MS runs 9A, 10, 12B). Together, these runs revealed evidence of many spectra with mass shifts matching that expected for my four predicted dopamine metabolite adducts. None were detected in any control samples, thereby increasing my confidence that these spectra represent true dopamine-modified parkin peptides.

Many dopamine metabolite adducts were detected across the three MS runs (designated as 9A, 10, 12B). Across 15 individual MS samples that were treated with only aminochrome (no EDTA), a total of 53 dopamine-metabolite adducts were detected. Across 8 individual MS samples that were treated with a low dose of EDTA and then aminochrome, 61 dopamine-metabolite adducts were detected. In total, 103/114 dopamine-metabolite adducts were found at C95. The other 11 occurred across C166, C169, C182, C212, C238, C293, C360, C365 of human r-parkin. Of note, all these cysteines except for C95 and C182 coordinate zinc ions. These adducts detected here are likely an underrepresentation of the true scope of dopamine modifications on parkin due to the limits of our PTM detection workflow, namely our limit to 4 dopamine metabolite structures in these searches. Future unbiased searches would be helpful to explore the full extent of modifications on parkin following dopamine stress.

Unique Susceptibility of C95

The observation from the MS data that most of the frequent dopamine-metabolite PTMs occurred at C95 is very interesting to us. This cysteine residue is located in the linker region of parkin, which as shown in Figure 3.20 is conserved among primates but not across other species. Based on my current data, one cannot completely exclude the possibility that some technical phenomenon makes dopamine adducts on this peptide more readily detected ('selection bias'). For example, C95 lies within a trypsin-digested peptide that is relatively short (8 amino acids if no trypsin cleavage points are missed, more commonly 15 amino acids with 1 missed trypsin cleavage) and only contains one cysteine residue. Compared to peptides with multiple cysteines, the complexity of PTMs and peptide m/z values is likely to be far less, and therefore more likely to be detectable in the context of limited MASCOT parameter sets. However, there are several cysteines on parkin that reside on trypsin-digested peptides with only one cysteine residue, so if all cysteines were equally modified by dopamine or aminochrome, we would expect that other single-cysteine peptides would also be readily detected. While the aforementioned factors may help explain the limited number of dopamine metabolite adducts at other parkin cysteine residues, namely those with multiple cysteine residues, I believe that my current data represents compelling evidence that C95 is in fact uniquely susceptible to modification by dopamine.

In addition to identifying dopamine-metabolite adducts primarily at C95, I found that r-parkin with a cysteine to alanine mutation at C95 didn't have the same ability as WT r-parkin to promote the formation of melanin *in vitro*. Parallel work in our lab showed that C95A parkin transfected into M17 neuroblastoma cells did not protect as well as WT parkin against dopamine-induced ROS. This further supports the importance of this residue in protecting neurons against dopamine-toxicity.

The C95 residue on parkin has previously been identified in our lab as being oxidized. It has also been detected as being glutathionylated in both GST-tagged, human parkin [41] and in *post mortem* human brain [42]. This residue has also previously been identified with nitrotyrosination and sulfhydration (conversion of an -SH group of cysteine to -SSH) PTMs [129]. While C95 has not been identified as being particularly vulnerable to these other modifications to the degree that I have identified here for modification by dopamine, this nevertheless suggests that this cysteine residue may be uniquely reactive.

The suggestion that C95 is uniquely susceptible to modification by dopamine is highly relevant because it may help to explain the formation of neuromelanin. It is known that mice and rats do not form neuromelanin in the SN [94]. These species also do not accurately replicate a human parkin-deficient PD phenotype, including a lack of dopamine neuron loss [130]. Interestingly, C95 is the only cysteine that is not conserved between humans and rodents, as was highlighted in Figure 3.21. The results I present here suggest that C95 may represent a critical amino acid that protects vulnerable dopaminergic neurons in human brain. It is plausible that, through their altered handling of dopamine metabolites, rodent species have compensatory mechanisms to reduce dopamine stress in the absence of the C95 residue in parkin's linker region, or even in the absence of parkin altogether. It is known that the handling of cytosolic dopamine is different between humans and rodents. For example, dopamine is mostly oxidized by MAO-B in humans, while in rodents it is oxidized primarily by MAO-A. Furthermore, there is evidence that mice in particular can metabolize dopamine using both MAO isoforms under conditions of high dopamine stress [131]. Similarly, more efficient COMT function in non-human mammals has been suggested to result in fewer cytosolic dopamine metabolites. Their shorter lifespan may also limit the consequences of reactive dopamine metabolites. All of these factors

suggest that the protective effects that C95 on human parkin has on reducing stress due to harmful dopamine metabolites may not be critical in rodent species. Similarly, the sheer divergence in the amino acid composition of this linker region between human and mouse parkin is consistent with potentially varying biological functions and significance.

A recent paper, described above for the development of a novel cysteine redox probe, also explored the propensity of specific cysteines for oxidation based on the composition of amino acids directly surrounding it (+/- 4 amino acids) [127]. At physiological pH, cysteines exist in equilibrium between the thiol (-SH) and thiolate ($-S^-$) forms, with the protonated thiol slightly favoured. Deprotonated thiolates would be expected to be more susceptible to modification. The authors found that the nearby presence of a basic amino acid, particularly arginine, correlated with increased susceptibility to oxidative modification. This is presumably due to its positive charge which stabilizes the negative charge of the cysteine thiolate. On the contrary, the negative charge of acidic amino acids (aspartic and glutamic acids) appeared to make cysteines less vulnerable to modification, presumably by destabilizing the negative charge of the cysteine thiolate form. This research was performed in the context of reversible oxidative modifications; however, it would seem plausible that factors favouring the deprotonated cysteine thiolate would also make residues more vulnerable to dopamine modification. The amino acid composition directly surrounding C95 on parkin is as follows: alanine, alanine, glycine, glycine, **cysteine**, *glutamic acid, arginine, glutamic acid*, proline. The presence of two glutamic acid residues and one arginine are opposing factors based on the above hypothesis, so it remains unclear how important of factor local charge state is for C95's unique susceptibility to dopamine modification. Nevertheless, this remains an important consideration as we further uncover the unique role of parkin's C95 residue.

Another potential explanation for the unique susceptibility of C95 includes increased accessibility due to its location on parkin's linker region and the fact that it does not coordinate a zinc ion. Notably, 28/35 of parkin's cysteines coordinate zinc ions. Of the remaining 7 cysteines, 6 of those are located in relatively close proximity to those that coordinate zinc. This may leave C95 as the cystine residue most accessible to dopamine modification. It is also possible that dopamine modification at C95 may leave parkin in a relatively stable state, whereas modification at other residues might have a more detrimental effect on parkin's structure and/or solubility. In my experiments that were successful in detecting dopamine metabolite adducts (i.e. those that I can confidently assert are not MASSADs), soluble and insoluble parkin were not separated by centrifugation. The intent was that this would capture both fractions and increase the chances of detecting dopamine PTMs. However, I cannot rule out that portions of the parkin sample may have been modified in ways such that it was not detected. This could result from alterations in trypsin cleavage, or simply because the modifications were too complex for my current workflow, as discussed above.

Of the 14 human parkin structures currently available in the Protein Data Bank [132], none include the linker region between the Ubl domain and RING0 that contains C95. This is presumably due to the flexibility of this particular region, making crystal formation difficult. One low resolution structure of full-length rat parkin was published with the linker region present in the protein; however, the region was completely disordered in the structure [133]. As a result of this difficulty in visualizing the structure of this region, relatively little is known about its function and importance. However, my present results suggest that this linker region, particularly the C95 residue, may play a very important role in protecting neurons from dopamine stress. This further suggests that additional focus should be placed on better understanding the structural

implications of this region of parkin. The importance of better understanding the structure of parkin's linker region, in combination with the effect of local charge state as explored above, is further highlighted by our observation that a cysteine to alanine mutation at residue 95 seems to impact the ability of ULP1 to cleave the N-terminal His-SUMO tag on our recombinant parkin protein. This suggests that this mutation may impact structure more than generally anticipated.

Future work in our lab seeks to employ a newly developed technique that utilizes a functionalized hydroxydopamine (6-OHDA) quinone that can modify cysteines and allow for enhanced detection [104]. This synthetic dopamine variant, developed at the University of Ottawa, can modify cysteines like naturally occurring dopamine, and can subsequently be functionalized using an established copper-catalyzed azide-alkyne cycloaddition approach. This allows for fluorescence-mediated visualization in-gel or via microscopy, as well as affinity purification of dopamine-modified proteins. A recently published paper utilizing this technique identified 201 proteins targeted by dopamine in a mouse neuronal cell culture, among which were many proteins involved in the respiratory electron transport chain and oxidative phosphorylation [104]. This technique will be especially useful as we expand our findings into cell cultures as it will not only allow us to detect and quantify modification of parkin, but also other cellular proteins. By using this dopamine variant along with fluorescence microscopy, we can gain a better understanding if the intracellular localization of proteins covalently modified by dopamine metabolites. This would complement recent work in our lab which has shown, using newly developed, monoclonal parkin antibodies and human brain tissue, that parkin is highly enriched in neuromelanin granules within the human SN, further suggesting a possible role for parkin in the formation of neuromelanin in human midbrain [42].

As the speed, sensitivity, robustness, and availability of proteomics equipment continues to improve, it is reasonable to expect that our knowledge of dopamine and other PTMs will increase rapidly. These advancements could also hold promise as diagnostic and predictive tools. For example, protein adduction levels of major blood proteins such as hemoglobin and human serum albumin by catechol estrogens has been measured and proposed as a biomarker of estrogen homeostasis. [128,134]. The detection of dopamine-related PTMs that we expect to be significant in the context of PD would likely occur primarily in the SN and LC and therefore detection may be significantly more difficult; nevertheless, it is possible that increased PTMs due to oxidative stress, including other oxidized quinones, may be detectable either systemically or in various neuronal populations, and may correlate with the development of PD. As technical capabilities continue to improve, oxidative and dopamine-mediated protein modification could represent potential biomarkers.

Scientific Implications

Until now, the field has largely viewed any occurrences of parkin oxidation as "loss of function", as it is viewed and interpreted in the context of its E3 ubiquitin ligase function. Our lab has presented, in two manuscripts recently submitted, a large body of evidence showing that parkin can mediate redox balance via its cysteine residues. We propose that loss of this redox function may be responsible for the selective neurodegeneration of oxidatively demanding dopaminergic neurons in parkin-linked PD. However, parkin's role as an E3 ligase and our newly demonstrated role as a redox stabilizer may not be mutually exclusive. In fact, it has been previously demonstrated that low concentrations of pro-oxidants can activate parkin's E3 ligase activity [113], as our lab has since confirmed. The newly found function presented here and in our

manuscripts does not preclude the possibility that parkin's E3 function may be important in specific tissues or at certain timepoints during development (i.e. in younger human brain and murine heart muscle [40] where parkin is mostly soluble). Nevertheless, we propose that deficiency in parkin's antioxidant function best explains the specific neurodegeneration of SN and LC neurons in parkin-linked PD cases.

A previous study crossed a parkin knockout mouse with the Mutator mouse, which develops mitochondrial dysfunction due to accelerated mtDNA mutations. This Mutator parkin knockout cross resulted in neurodegeneration specifically in dopaminergic neurons as well as L-DOPA reversible motor deficit [135]. At the time, this was presented as proof that parkin knockout led to a stronger mitochondrial phenotype; however, mitochondrial dysfunction also leads to elevated oxidative stress, namely high levels of ROS, and loss of a key contributor to the thiol pool would be expected to be detrimental to cells that already experience high oxidative stress. This is an example of a phenotype that we propose is better explained by parkin's contribution to the cellular thiol pool than its E3 function alone.

I suggest above that while C95 seems to have a unique susceptibility to modification by dopamine metabolites and a role in melanin formation, there is no evidence that it is uniquely responsible for parkin's ability to reduce ROS. Additional work is needed to confirm this. Particularly, future experiments will test our newly generated C95A r-parkin protein to see if it has the same ability as WT parkin to reduce hydrogen peroxide *in vitro* (this work is currently ongoing). If it is true that the C95 residue is necessary for parkin's ability to promote melanin formation but is not as critical for its ability to reduce ROS, this would further explain some observations regarding parkin-null mouse models. Parkin-null mice do not show degeneration of dopamine neurons and do not develop parkinsonism. While mice do not develop neuromelanin,

parkin-null mice do show altered markers of redox stress compared to WT controls. For instance, unbiased proteomic studies have showed alterations in various metabolic enzymes [115,136]. It is possible that parkin's role in melanin formation is not needed in rodents due to their short lifespan and altered handling of dopamine. As such, the C95 residue simply may not be required in these species. While parkin plays an important role in reducing other sources of oxidative stress, such as ROS and RNS, other compensatory mechanisms may provide enough antioxidant capacity to prevent significant neurodegeneration in the absence of parkin.

Clinical Implications

Uncovering the essential function of parkin in the vulnerable dopaminergic neurons of the SN and LC is critical for the development of novel and effective therapies to both manage symptoms and alter the course of PD. The field is currently focusing largely on increasing parkin's E3 ligase function through activation via small molecule activators. Evidence from our lab that parkin's solubility decreases with age in healthy humans after age 40 years suggests that efforts to pharmacologically activate parkin may not be effective in older individuals. However, if in fact parkin's function as a contributor to the thiol pool is critical in these demanding dopamine neurons, an increased focus on antioxidants as a therapy and treatment may be warranted in stratified patients. A recently published study developed and tested a cell-permeable parkin protein (iCP-parkin) [137]. This protein had a solubilization domain and showed enhanced solubility and the ability to enter cells. This study showed promising initial results in cell and animal models.

In addition to administering dopamine precursors such as L-DOPA, other PD therapeutics have focussed on preventing dopamine degradation by enzymes such as COMT (ex. Entacapone) [138,139]. Similarly, several clinical trials have tested MAO-B inhibitors (ex. Selegiline, Rasagiline), with varying but limited success [140-142]. While promising in many regards, my results presented here suggest that simply increasing the levels of dopamine in vulnerable neurons may not address the root causes of parkin-linked PD. Particularly, high levels of ROS and RES would likely persist, and theoretically could even be made worse. Treatments that address dopamine shortages while simultaneously providing some sort of antioxidant protection against reactive metabolites could be more useful and should be tested in parkin-deficient humans. Further, considering the early age of onset for parkin-deficient PD patients, gene therapy may be an especially valuable treatment option in the future. Overall, I predict that an increased focus on reducing oxidative stressors such as ROS and RES will hopefully lead to the development of novel and innovative antioxidants, synthetic or protein-based, that will promote survival in these vulnerable dopaminergic neurons.

Future Work

To further characterize parkin's redox capabilities, future work should seek to better understand the unique role that the C95 residue has in protecting neurons. I have suggested that this residue may be particularly important for protecting against dopamine stress but not uniquely critical among parkin's amino acids in protecting against other sources of ROS, but this hypothesis needs to be tested further. As suggested above, a first step would include testing our newly generated C95A r-parkin protein in an in vitro hydrogen peroxide assay to see if it has the same ability as WT r-parkin to reduce peroxide to water. Further, the Ellman's assay could be

used to determine the relative number of free thiol equivalents on C95A parkin compared to WT parkin.

The functionalized hydroxydopamine probe described above can be used to measure and map dopamine metabolite adducts on parkin in cell cultures, and to better understand other proteins that are modified by dopamine and how parkin protects their functions. Further, mapping dopamine adducts on parkin in human brain tissue would represent an important confirmation of my findings. LaVoie et al. previously used biochemical methods to identify catechol-modified parkin from human brain [110], but to date these modifications have not been confirmed by MS or mapped to specific cysteine residues. Our current MS protocols could be applied for this; however, given the high amounts of parkin I required in order to detect adducts and the negative implications of adduct heterogeneity, it is likely that further optimization steps at enrichment would be necessary in order to detect dopamine modifications in human tissue.

A previously published paper, using *in vitro* activity assays, demonstrated reductions in the activity of key metabolic enzymes, lactate dehydrogenase and malate dehydrogenase, due to modification by dopamine [109]. Based on my results, I would expect the presence of parkin to improve outcomes following dopamine stress. Further, the C95A parkin mutant seemingly wouldn't protect the activity of other metabolic enzymes. Future work could test this by replicating these assays using WT *vs.* C95A parkin-encoding cDNA plasmids.

Regarding my results showing a reduction in free cysteines in oxidized and insoluble parkin, ongoing work in our lab is seeking to similarly measure the redox state of parkin's cysteines in *post mortem* human brain tissue. The proportion of reduced cysteines can be measured by IAA intensity as was done here as well as by optimizing and implementing other available cysteine-reactive probes as described previously. This work will also probe for other

non-reversible oxidative modifications using the same PTM detection techniques, which I optimized for the study of dopamine metabolites.

Conclusion

This thesis has advanced our understanding of parkin's role as a redox regulator by measuring post-translational modifications at its cysteine residues following treatment with oxidative species and dopamine stressors. This was accomplished through *in vitro* experiments as well as specialized LC-MS/MS methods that were optimized and implemented for this purpose. In Aim 1, the relative number of reduced cysteines was found to decrease following treatment with H_2O_2, a source of ROS, and in parkin that had transitioned from the soluble to the insoluble fraction. In Aim 2, following treatment with aminochrome, oxidized dopamine metabolite adducts were mapped to specific cysteine residues on parkin, with the primate-specific C95 residue showing particular vulnerability to modification by dopamine adducts. Mutations at this residue impacted parkin's ability to promote melanin formation as well as its ability to promote survival in human, dopaminergic M17 cells following dopamine stress. In parallel work (not shown here), we have demonstrated that wild-type parkin is spatially closely involved in the generation of neuromelanin, which begins in young adulthood [42].

Overall, this project highlights the importance of parkin's contribution to the thiol-based antioxidant forces in vulnerable, dopaminergic neurons that generate high levels of ROS, RNS, and RES. The specificity of the C95 may help to explain melanin formation in human but not rodent midbrains as well as potentially explain the lack of a PD-phenotype in parkin-deficient rodent models. This also suggests the need for future research into the structural implications of C95 embedded within the linker region between parkin's UBL and RING0 domains. Further characterization of parkin's redox functions, and the potential for antioxidants (synthetic molecules or parkin protein replacement) to be used as PD treatments holds the promise to improve the often decades-long suffering of subjects living with young-onset parkin-linked PD.

Manuscripts

Much of the research presented in this thesis has contributed to two manuscripts that have recently been submitted for publication. Versions of these manuscripts are currently available on BioRxiv at the links provided below.

Tokarew, Jacqueline M.; El-Kodsi, Daniel N.; Lengacher Nathalie A.; **Fehr, Travis K**.; …; Tomlinson, Julianna J.; Schlossmacher, Michael G. **Age-Associated Insolubility of Parkin in Human Midbrain is Linked to Redox Balance and Sequestration of Reactive Dopamine Metabolites**. (Submitted, November 2020). Preprint (BioRxiv 2020.02.19.953034; doi: https://doi.org/10.1101/2020.11.20.392175).

El Kodsi, Daniel N.; Tokarew, Jacqueline M.; Sengupta, Rajib; Lengacher, Nathalie A.; Ng, Andy C.; Boston, Heather; Jiang, Qiubo; Palmberg, Carina; Pileggi, Chantel; Shutinoski, Bojan; Li, Juan; Nguyen, Angela P.; **Fehr, Travis K**.; …; Tomlinson, Julianna J.; Schlossmacher, Michael G. **Parkinson Disease-Linked Parkin Mediates Redox Reactions That Lower Oxidative Stress in Mammalian Brain.** (Manuscript in preparation). Preprint (BioRxiv 2020.11.20.392175; doi: https://doi.org/10.1101/2020.04.26.062380).

Chapter 5 Appendix

Appendix 1 List of all LC-MS/MS runs performed

MS Run	Project Tracking #	Date Submitted	Number of Samples	Treatment	LC-MS/MS Method	Injection Volume	Analysis Software	Results Overview
1	DP823	2018-10-22	8	H2O2 and DA	CID_40_v4	10%	Skyline	No DA adducts detected, low NEM detection
2	DP833	2018-12-07	8	H2O2 and DA	CID_30_v4	1 uL	Skyline, Scaffold PTM	No DA detected, low peptide coverage across samples 1-6
3	DP837	2019-01-18	4	DA	CID			Very low peptide coverage
4	DP843	2019-02-13	12	DA - Soluble vs Pellet	CID_30_v6; HCD_45_v2	1 uL; 5 uL	Scaffold PTM	Evidence of many AM (+149) and DAQ (+151) modifications, no control sample
5A	DP861	2019-05-21	6	DA - Soluble vs Pellet	HCD_45_v2	1 uL	Scaffold PTM	No DA detacted at high probability
5B	DP861	2019-05-21	6	H2O2 - Soluble vs Pellet	HCD_45_v2	1 uL	MaxQuant	Complete IAA intenisty data
6	DP868	2019-07-25	4	DA	HCD_45_v2	15%	Scaffold PTM	Very few DA modifications detected
7	DP890	2019-11-15	6	DA - Soluble vs Pellet	HCD_45_v2	20%	Scaffold PTM	Evidence of many DA (All 4 PTMs) modifications in all samples, including controls
8	DP895	2019-11-29	6	Cys-modifying compounds	HCD_45_v2	30%	MASCOT	Presumably "false positive" DA modifications detected in IAA, NEM, acrylamide, and TCEP samples
9A	DP900	2020-01-16	9	AM (WT Parkin)	HCD_45_v2	30%	Scaffold 3; Scaffold PTM	14 DA modifcations observed, all in treated samples
9B	DP900	2020-01-16	5	AM (321C truncated parkin)	HCD_45_v2	30%	Scaffold 3; Scaffold PTM	Very few DA modifications detected
10A	DP908	2020-02-05	9	AM	HCD_45_v2	30%	Scaffold PTM	Many DA modiifactions detected in treated sampels, none in controls
10B	DP908	2020-02-05	10	EDTA, AM	HCD_45_v2	30%	Scaffold PTM	Many DA modiifactions detected in treated sampels, none in controls
11	DP 917	2020-06-22	8	H2O2	X3_HCD_45_v2	0.3 uL	Scaffold PTM, MaxQuant	Much lower coverage than previous run, unable to extract confident MaxQuant intenities
12A	DP923	2020-08-06	6	H2O2	X3_HCD_45_v2	0.3 uL	Scaffold PTM, MaxQuant	Coverage was again very low. A normalization procedure used by the Core Facility to determine sufficient injection was used. Clearly parkin requires significantly higher injection for quantification
12B	DP923	2020-08-06	4	AM	X3_HCD_45_v2	0.3 uL	Scaffold PTM	Additional DA adducts detected

Appendix 2 Spectra corresponding to each unique peptide with a dopamine-metabolite PTM

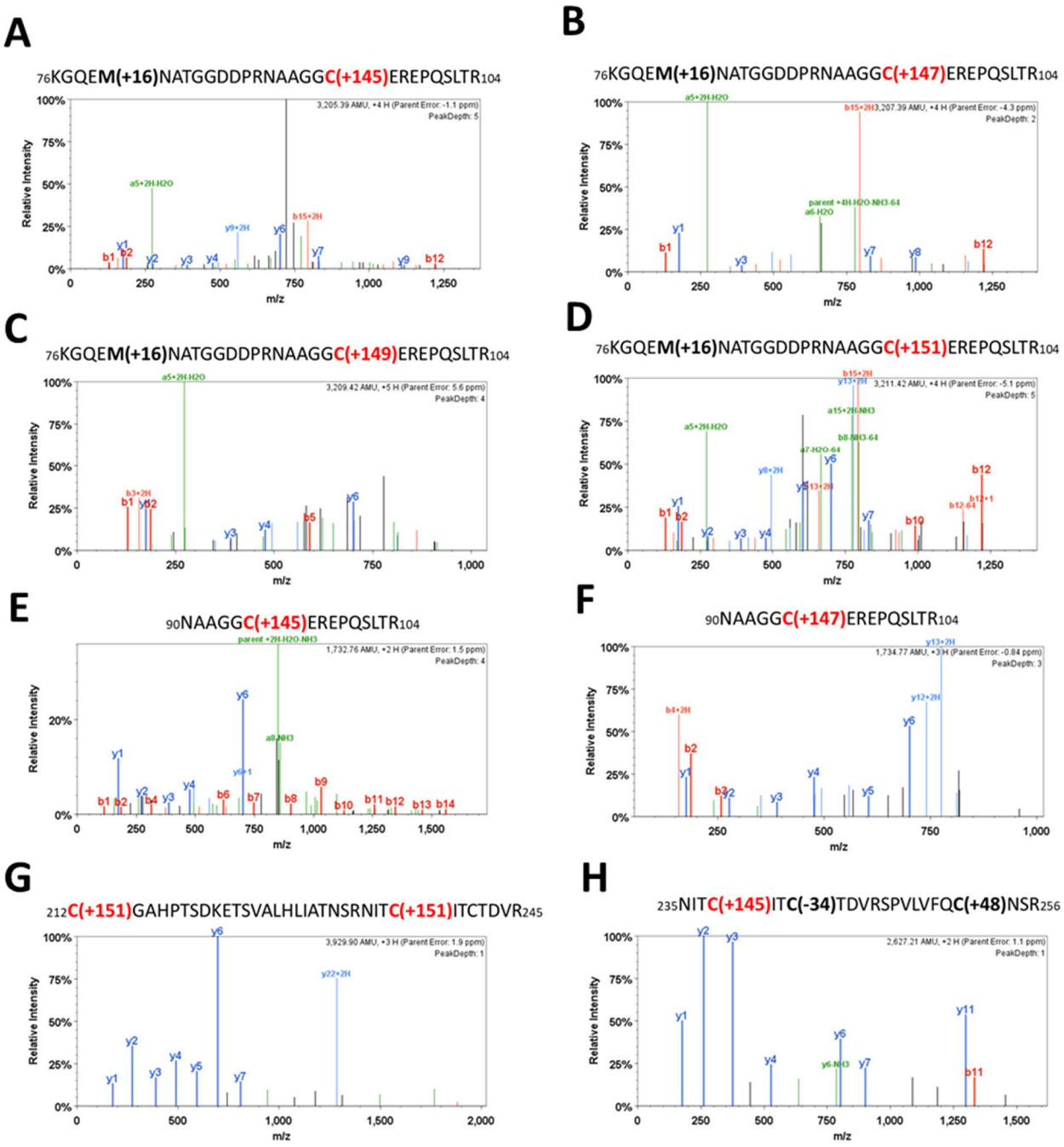

I

276QFVHDPQLGYSLP**C(-34)**VAG**C(+145)**PNSLIK299

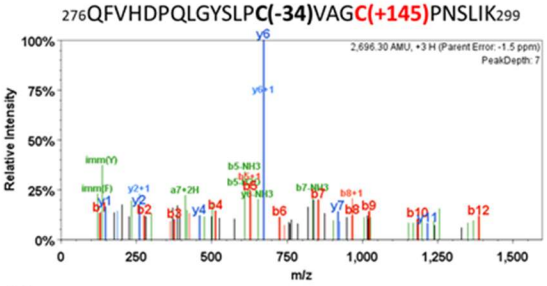

J

350VT**C(-34)**EGGNGLG**C(+147)**GFAF**C(-34)**
RE**C(+48)**KEAYHHEGE**C(+48)**SAVFEASGTTTQAYR392

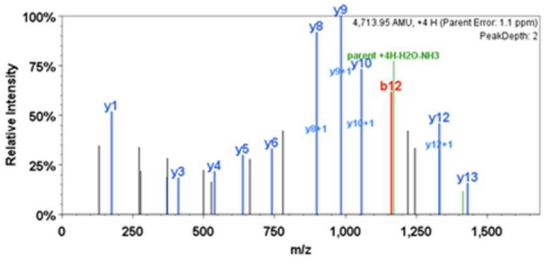

K

350VT**C(-34)**EGGNGLG**C(-34)**GFAF**C(+145)**
RE**C(+48)**KEAYHHEGE**C(+48)**SAVFEASGTTTQAYR392

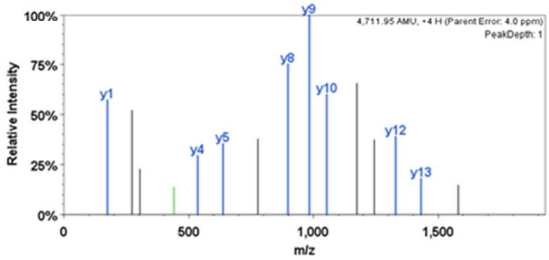

Appendix 3 List of all dopamine-metabolite adducts detected

MS run 9B

Peptide sequence	Variable modifications identified by spectrum	Observed m/z	Spectrum charge	Actual peptide mass (AMU)	Peptide Identification Probability	Mascot Ion Score	Scaffold Peptide Score
76 KGQE**m**NATGGDDPRNAAGG**c**EREPQSLTR 104	M80 Oxidation (+16), **C95 Aminochrome (+147)**	803.10895	4	3,208.41	99.70%	30.7	29.3
76 KGQE**m**NATGGDDPRNAAGG**c**EREPQSLTR 104	M80 Oxidation (+16), **C95 Dopamine Quinone (+151)**	803.86255	4	3,211.42	97.80%	28.4	64.11
90 NAAGG**c**EREPQSLTR 104	C95 **Indolequinone (+145)**	578.59387	3	1,732.76	99.50%	25.7	77.8
90 NAAGG**c**EREPQSLTR 104	C95 **Indolequinone (+145)**	578.59399	3	1,732.76	99.70%	29.1	81.39
90 NAAGG**c**EREPQSLTR 104	C95 **Indolequinone (+145)**	867.38672	2	1,732.76	99.70%	29.6	70.61
90 NAAGG**c**EREPQSLTR 104	C95 **Indolequinone (+145)**	867.38733	2	1,732.76	99.70%	31.1	93.74
90 NAAGG**c**EREPQSLTR 104	C95 **Indolequinone (+145)**	867.38751	2	1,732.76	98.80%	21.5	32.17
90 NAAGG**c**EREPQSLTR 104	C95 **Indolequinone (+145)**	867.38629	2	1,732.76	99.60%	26.6	58.04
90 NAAGG**c**EREPQSLTR 104	C95 **Aminochrome (+147)**	579.26563	3	1,734.78	98.00%	21.2	69.64
90 NAAGG**c**EREPQSLTR 104	C95 **Aminochrome (+147)**	579.26532	3	1,734.77	99.70%	29.8	75.44
90 NAAGG**c**EREPQSLTR 104	C95 **Aminochrome (+147)**	579.26642	3	1,734.78	99.00%	24.7	82.52
90 NAAGG**c**EREPQSLTR 104	C95 **Aminochrome (+147)**	579.26666	3	1,734.78	99.70%	30.8	69.64
90 NAAGG**c**EREPQSLTR 104	C95 **Dopamine Quinone (+151)**	580.60907	3	1,738.81	96.20%	22.4	71.37
90 NAAGG**c**EREPQSLTR 104	C95 **Dopamine Quinone (+151)**	580.6098	3	1,738.81	95.50%	20.3	58.55

MS run 10

Peptide sequence	Variable modifications identified by spectrum	Observed m/z	Spectrum charge	Actual peptide mass (AMU)	Peptide Identification probability	Mascot Ion score	Scaffold Peptide Score
76 KGQE**m**NATGGDDPRNAAGG**c**EREPQSLTR 104	M80 Oxidation (+16), **C95 Indolequinone (+145)**	802.35407	4	3,205.39	99.40%	28.2	29.55

76 KGQE**m**NATGGDDPRNAAGG**c**EREPQSLTR 104	M80 Oxidation (+16), **C95 Aminochrome (+147)**	802.85907	4	3,207.41	98.70%	24	42.56
76 KGQE**m**NATGGDDPRNAAGG**c**EREPQSLTR 104	M80 Oxidation (+16), **C95 Aminochrome (+147)**	803.11017	4	3,208.41	99.30%	26.5	39.26
76 KGQE**m**NATGGDDPRNAAGG**c**EREPQSLTR 104	M80 Oxidation (+16), **C95 Aminochrome (+147)**	802.85877	4	3,207.41	96.90%	22.5	52.18
76 KGQE**m**NATGGDDPRNAAGG**c**EREPQSLTR 104	M80 Oxidation (+16), **C95 Aminochrome (+147)**	802.85541	4	3,207.39	99.70%	33.3	41.69
76 KGQE**m**NATGGDDPRNAAGG**c**EREPQSLTR 104	M80 Oxidation (+16), **C95 Aminochrome (+149)**	642.89172	5	3,209.42	97.40%	27.7	18.71
90 NAAGG**c**EREPQSLTR 104	**C95 Indolequinone (+145)**	578.59375	3	1,732.76	99.70%	31.7	74.5
90 NAAGG**c**EREPQSLTR 104	**C95 Indolequinone (+145)**	578.59375	3	1,732.76	99.70%	35.2	76.09
90 NAAGG**c**EREPQSLTR 104	**C95 Indolequinone (+145)**	867.38702	2	1,732.76	99.70%	49.5	122.39
90 NAAGG**c**EREPQSLTR 104	**C95 Indolequinone (+145)**	578.59363	3	1,732.76	99.60%	26.4	88.23
90 NAAGG**c**EREPQSLTR 104	**C95 Indolequinone (+145)**	867.38684	2	1,732.76	99.70%	49.5	129.45
90 NAAGG**c**EREPQSLTR 104	**C95 Indolequinone (+145)**	867.38684	2	1,732.76	99.70%	48.8	113.16
90 NAAGG**c**EREPQSLTR 104	**C95 Indolequinone (+145)**	867.3869	2	1,732.76	99.70%	42.4	102.2
90 NAAGG**c**EREPQSLTR 104	**C95 Indolequinone (+145)**	578.59369	3	1,732.76	99.20%	24.4	76.82
90 NAAGG**c**EREPQSLTR 104	**C95 Indolequinone (+145)**	867.38666	2	1,732.76	99.70%	34	97.44
90 NAAGG**c**EREPQSLTR 104	**C95 Indolequinone (+145)**	867.38886	2	1,732.76	99.70%	37.5	93.44
90 NAAGG**c**EREPQSLTR 104	**C95 Indolequinone (+145)**	867.38739	2	1,732.76	99.70%	52.1	114.98
90 NAAGG**c**EREPQSLTR 104	**C95 Indolequinone (+145)**	578.59406	3	1,732.76	99.70%	33.5	83.77
90 NAAGG**c**EREPQSLTR 104	**C95 Indolequinone (+145)**	867.38715	2	1,732.76	99.70%	57.9	144.77
90 NAAGG**c**EREPQSLTR 104	**C95 Indolequinone (+145)**	867.38709	2	1,732.76	99.70%	50.3	115.41
90 NAAGG**c**EREPQSLTR 104	**C95 Indolequinone (+145)**	578.59381	3	1,732.76	99.70%	29.6	76.36
90 NAAGG**c**EREPQSLTR 104	**C95 Indolequinone (+145)**	867.38709	2	1,732.76	99.70%	45	118.48
90 NAAGG**c**EREPQSLTR 104	**C95 Indolequinone (+145)**	867.38666	2	1,732.76	99.70%	43.9	98.46
90 NAAGG**c**EREPQSLTR 104	**C95 Indolequinone (+145)**	867.38666	2	1,732.76	99.70%	52.5	90.21
90 NAAGG**c**EREPQSLTR 104	**C95 Indolequinone (+145)**	578.59387	3	1,732.76	99.70%	30.4	74.37
90 NAAGG**c**EREPQSLTR 104	**C95 Indolequinone (+145)**	867.38733	2	1,732.76	99.70%	42.3	108.09
90 NAAGG**c**EREPQSLTR 104	**C95 Indolequinone (+145)**	867.38855	2	1,732.76	99.70%	51.3	98.53
90 NAAGG**c**EREPQSLTR 104	**C95 Indolequinone (+145)**	578.59393	3	1,732.76	99.70%	27.1	85.98

90 NAAGGcEREPQSLTR 104	**C95 Indolequinone (+145)**	578.59393	3	1,732.76	99.70%	27.5	83.05
90 NAAGGcEREPQSLTR 104	**C95 Indolequinone (+145)**	867.38666	2	1,732.76	99.70%	39.3	104.67
90 NAAGGcEREPQSLTR 104	**C95 Indolequinone (+145)**	578.59381	3	1,732.76	98.00%	22.7	81.37
90 NAAGGcEREPQSLTR 104	**C95 Indolequinone (+145)**	867.38745	2	1,732.76	99.70%	34.2	101.03
90 NAAGGcEREPQSLTR 104	**C95 Indolequinone (+145)**	578.59338	3	1,732.76	99.70%	31.4	77.61
90 NAAGGcEREPQSLTR 104	**C95 Indolequinone (+145)**	578.59338	3	1,732.76	99.40%	25.6	80.33
90 NAAGGcEREPQSLTR 104	**C95 Indolequinone (+145)**	867.38776	2	1,732.76	99.70%	37.9	90.21
90 NAAGGcEREPQSLTR 104	**C95 Indolequinone (+145)**	867.38641	2	1,732.76	99.70%	37.5	87.68
90 NAAGGcEREPQSLTR 104	**C95 Indolequinone (+145)**	867.38763	2	1,732.76	99.70%	46.4	93.52
90 NAAGGcEREPQSLTR 104	**C95 Indolequinone (+145)**	867.38751	2	1,732.76	99.70%	47.8	100.07
90 NAAGGcEREPQSLTR 104	**C95 Indolequinone (+145)**	578.59338	3	1,732.76	99.40%	25.1	71.88
90 NAAGGcEREPQSLTR 104	**C95 Indolequinone (+145)**	578.59338	3	1,732.76	99.70%	28.2	73.52
90 NAAGGcEREPQSLTR 104	**C95 Indolequinone (+145)**	867.38751	2	1,732.76	99.70%	31.9	74.18
90 NAAGGcEREPQSLTR 104	**C95 Indolequinone (+145)**	578.59326	3	1,732.76	99.70%	28.3	66.84
90 NAAGGcEREPQSLTR 104	**C95 Indolequinone (+145)**	578.59326	3	1,732.76	94.60%	22.4	62.49
90 NAAGGcEREPQSLTR 104	**C95 Indolequinone (+145)**	578.5943	3	1,732.76	95.80%	21.6	63.65
90 NAAGGcEREPQSLTR 104	**C95 Indolequinone (+145)**	867.38831	2	1,732.76	99.70%	33.1	93.36
90 NAAGGcEREPQSLTR 104	**C95 Indolequinone (+145)**	578.59314	3	1,732.76	98.50%	25.7	83.31
90 NAAGGcEREPQSLTR 104	**C95 Indolequinone (+145)**	578.5943	3	1,732.76	99.50%	24.6	76.94
90 NAAGGcEREPQSLTR 104	**C95 Indolequinone (+145)**	867.38623	2	1,732.76	99.70%	52.4	111.54
90 NAAGGcEREPQSLTR 104	**C95 Indolequinone (+145)**	578.5932	3	1,732.76	95.60%	22.6	70.18
90 NAAGGcEREPQSLTR 104	**C95 Indolequinone (+145)**	867.38794	2	1,732.76	99.70%	31.5	82.59
90 NAAGGcEREPQSLTR 104	**C95 Indolequinone (+145)**	578.59442	3	1,732.76	99.70%	28.8	81.57
90 NAAGGcEREPQSLTR 104	**C95 Indolequinone (+145)**	867.388	2	1,732.76	99.70%	59.5	130.03
90 NAAGGcEREPQSLTR 104	**C95 Indolequinone (+145)**	578.59271	3	1,732.76	98.50%	24.2	73.44
90 NAAGGcEREPQSLTR 104	**C95 Indolequinone (+145)**	867.38574	2	1,732.76	99.70%	34.6	73.17
90 NAAGGcEREPQSLTR 104	**C95 Indolequinone (+145)**	578.59308	3	1,732.76	99.70%	30	74.94
90 NAAGGcEREPQSLTR 104	**C95 Indolequinone (+145)**	578.92725	3	1,733.76	99.70%	35.2	77.46
90 NAAGGcEREPQSLTR 104	**C95 Indolequinone (+145)**	867.88757	2	1,733.76	99.70%	35.8	87.51

90 NAAGGcEREPQSLTR 104	**C95 Aminochrome (+147)**	579.26556	3	1,734.77	97.00%	21.6	66.63
90 NAAGGcEREPQSLTR 104	**C95 Aminochrome (+147)**	579.26563	3	1,734.78	99.70%	29	58.02
90 NAAGGcEREPQSLTR 104	**C95 Aminochrome (+147)**	579.26587	3	1,734.78	97.40%	20.8	63.22
90 NAAGGcEREPQSLTR 104	**C95 Aminochrome (+147)**	579.2655	3	1,734.77	94.90%	17.8	62.43
90 NAAGGcEREPQSLTR 104	**C95 Aminochrome (+147)**	868.39484	2	1,734.78	95.90%	18.4	40.15
90 NAAGGcEREPQSLTR 104	**C95 Aminochrome (+147)**	579.26563	3	1,734.78	99.70%	28.5	65.33
90 NAAGGcEREPQSLTR 104	**C95 Aminochrome (+147)**	579.26587	3	1,734.78	99.70%	29.7	69.64
90 NAAGGcEREPQSLTR 104	**C95 Aminochrome (+147)**	868.39459	2	1,734.77	96.70%	19.6	35.86
90 NAAGGcEREPQSLTR 104	**C95 Aminochrome (+147)**	579.26502	3	1,734.77	99.70%	29.1	79.41
90 NAAGGcEREPQSLTR 104	**C95 Aminochrome (+147)**	579.26502	3	1,734.77	99.70%	33	73.38
90 NAAGGcEREPQSLTR 104	**C95 Aminochrome (+147)**	579.26611	3	1,734.78	99.70%	34.6	87.71
90 NAAGGcEREPQSLTR 104	**C95 Aminochrome (+147)**	579.26605	3	1,734.78	99.70%	36.2	83.56
90 NAAGGcEREPQSLTR 104	**C95 Aminochrome (+147)**	579.26447	3	1,734.77	99.70%	30.4	80.87
90 NAAGGcEREPQSLTR 104	**C95 Aminochrome (+147)**	579.26459	3	1,734.77	99.70%	28.9	83.09
90 NAAGGcEREPQSLTR 104	**C95 Aminochrome (+147)**	579.2652	3	1,734.77	99.50%	25.4	64.87
90 NAAGGcEREPQSLTR 104	**C95 Aminochrome (+147)**	579.26611	3	1,734.78	96.40%	20.3	70.67
90 NAAGGcEREPQSLTR 104	**C95 Aminochrome (+147)**	868.39557	2	1,734.78	98.70%	22.9	51.3
90 NAAGGcEREPQSLTR 104	**C95 Aminochrome (+147)**	579.26611	3	1,734.78	99.70%	28.3	77.97
90 NAAGGcEREPQSLTR 104	**C95 Aminochrome (+147)**	868.89581	2	1,735.78	95.20%	19.8	27.53
90 NAAGGcEREPQSLTR 104	**C95 Aminochrome (+147)**	579.26624	3	1,734.78	99.20%	26.2	71.83
90 NAAGGcEREPQSLTR 104	**C95 Aminochrome (+147)**	579.59869	3	1,735.77	96.80%	23.9	76.63
90 NAAGGcEREPQSLTR 104	**C95 Aminochrome (+147)**	579.26477	3	1,734.77	99.70%	34.5	82.14
90 NAAGGcEREPQSLTR 104	**C95 Aminochrome (+147)**	579.26392	3	1,734.77	99.70%	27.7	85.01
90 NAAGGcEREPQSLTR 104	**C95 Aminochrome (+147)**	579.26495	3	1,734.77	99.70%	37.3	87.17
90 NAAGGcEREPQSLTR 104	**C95 Aminochrome (+147)**	579.60022	3	1,735.78	98.90%	24.8	69.51
90 NAAGGcEREPQSLTR 104	**C95 Dopamine Quinone (+151)**	435.70874	4	1,738.81	96.00%	19.2	53.67
90 NAAGGcEREPQSLTR 104	**C95 Dopamine Quinone (+151)**	580.6098	3	1,738.81	99.50%	27.7	72.14
162 LRVQcSTcRQATLTLTQGPSCWDDVLIPNR 191	**C166 Aminochrome (+149)**, C169 Cys->Dha (-34)	1164.249	3	3,489.73	99.30%	83.9	42.91

162 LRVQcSTcRQATLTLTQGPSCWDDVLIPNR 191	**C166 Aminochrome (+149)**, C169 Cys->Dha (-34)	1164.2529	3	3,489.74	99.10%	78.4	25.84
162 LRVQcSTcRQATLTLTQGPSCWDDVLIPNR 191	**C166 Aminochrome (+149)**, C169 Cys->Dha (-34)	1164.2566	3	3,489.75	99.30%	69	40.57
162 LRVQcSTcRQATLTLTQGPScWDDVLIPNR 191	**C166 Aminochrome (+149)**, **C169 Dopamine Quinone (+151)**, C182 Cys->Dha (-34)	1214.6033	3	3,640.79	99.20%	31.4	25.73
164 VQcSTcRQATLTLTQGPScWDDVLIPNR 191	**C166 Aminochrome (+149), C169 Dopamine Quinone (+151), C182 Indolequinone (+145)**	888.41199	4	3,549.62	99.50%	32	11.71
212 cGAHPTSDKETSVALHLIATNSRNITcITCTDVR 245	**C212 Dopamine Quinone (+151), C238 Dopamine Quinone (+151)**	1310.9731	3	3,929.90	99.10%	27.8	19.84
212 cGAHPTSDKETSVALHLIATNSRNITcITCTDVR 245	**C212 Dopamine Quinone (+151), C238 Dopamine Quinone (+151)**	1310.975	3	3,929.90	98.60%	30	10.39
235 NITcITcTDVRSPVLVFQcNSR 256	**C238 Indolequinone (+145)**, C241 Cys->Dha (-34), C253 Trioxidation (+48)	1314.6143	2	2,627.21	99.20%	26.3	38.93
276 QFVHDPQLGYSLPcVAGcPNSLIK 299	C289 Cys->Dha (-34), **C293 Indolequinone (+145)**	899.7746	3	2,696.30	99.70%	38.1	45.87
350 VTcEGGNGLGcGFAFcREcKEAYHEGEcSAVFEASGTTTQAYR 392	C352 Cys->Dha (-34), **C360 Aminochrome (+147)**, C365 Cys->Dha (-34), C368 Trioxidation (+48), C377 Trioxidation (+48)	1179.4941	4	4,713.95	98.40%	27.2	14.08
350 VTcEGGNGLGcGFAFcREcKEAYHEGEcSAVFEASGTTTQAYR 392	352 Cys->Dha (-34), C360 Cys->Dha (-34), **C365 Indolequinone (+145)**, C368 Trioxidation (+48), C377 Trioxidation (+48)	1178.9937	4	4,711.95	96.10%	29.3	11.1

MS Run 13

Peptide sequence	Variable modifications identified by spectrum	Observed m/z	Spectrum charge	Actual peptide mass (AMU)	Peptide Identification probability	Mascot Ion score	Scaffold Peptide Score
90 NAAGGcEREPQSLTR 104	**C95 Indolequinone (+145)**	578.92767	3	1,733.76	98.57%	24.81	66.19
90 NAAGGcEREPQSLTR 104	**C95 Indolequinone (+145)**	867.38696	2	1,732.76	100.00%	45.98	123.45
90 NAAGGcEREPQSLTR 104	**C95 Indolequinone (+145)**	578.59338	3	1,732.76	99.94%	29.58	73.97
90 NAAGGcEREPQSLTR 104	**C95 Indolequinone (+145)**	867.3855	2	1,732.76	100.00%	45.43	100.55
90 NAAGGcEREPQSLTR 104	**C95 Indolequinone (+145)**	867.888	2	1,733.76	100.00%	38.85	82.5

References

1 Obeso, J. A. *et al.* Past, present, and future of Parkinson's disease: A special essay on the 200th Anniversary of the Shaking Palsy. *Mov Disord* **32**, 1264-1310, doi:10.1002/mds.27115 (2017).

2 Canada, P. H. A. o. (Ottawa, 2014).

3 Ascherio, A. & Schwarzschild, M. A. The epidemiology of Parkinson's disease: risk factors and prevention. *Lancet Neurol* **15**, 1257-1272, doi:10.1016/S1474-4422(16)30230-7 (2016).

4 Bonifati, V. *et al.* Mutations in the DJ-1 gene associated with autosomal recessive early-onset parkinsonism. *Science* **299**, 256-259, doi:10.1126/science.1077209 (2003).

5 Kitada, T. *et al.* Mutations in the parkin gene cause autosomal recessive juvenile parkinsonism. *Nature* **392**, 605-608, doi:10.1038/33416 (1998).

6 Polymeropoulos, M. H. *et al.* Mutation in the alpha-synuclein gene identified in families with Parkinson's disease. *Science* **276**, 2045-2047, doi:10.1126/science.276.5321.2045 (1997).

7 Valente, E. M. *et al.* Hereditary early-onset Parkinson's disease caused by mutations in PINK1. *Science* **304**, 1158-1160, doi:10.1126/science.1096284 (2004).

8 Arkinson, C. & Walden, H. Parkin function in Parkinson's disease. *Science* **360**, 267-268, doi:10.1126/science.aar6606 (2018).

9 Jankovic, J. Parkinson's disease: clinical features and diagnosis. *J Neurol Neurosurg Psychiatry* **79**, 368-376, doi:10.1136/jnnp.2007.131045 (2008).

10 Goedert, M., Spillantini, M. G., Del Tredici, K. & Braak, H. 100 years of Lewy pathology. *Nat Rev Neurol* **9**, 13-24, doi:10.1038/nrneurol.2012.242 (2013).

11 Birkmayer, W. & Hornykiewicz, O. [The L-3,4-dioxyphenylalanine (DOPA)-effect in Parkinson-akinesia]. *Wien Klin Wochenschr* **73**, 787-788 (1961).

12 Hornykiewicz, O. [The tropical localization and content of noradrenalin and dopamine (3-hydroxytyramine) in the substantia nigra of normal persons and patients with Parkinson's disease]. *Wien Klin Wochenschr* **75**, 309-312 (1963).

13 Oertel, W. & Schulz, J. B. Current and experimental treatments of Parkinson disease: A guide for neuroscientists. *J Neurochem* **139 Suppl 1**, 325-337, doi:10.1111/jnc.13750 (2016).

14 Lewitt, P. A. Levodopa for the treatment of Parkinson's disease. *N Engl J Med* **359**, 2468-2476, doi:10.1056/NEJMct0800326 (2008).

15 Connolly, B. S. & Lang, A. E. Pharmacological treatment of Parkinson disease: a review. *JAMA* **311**, 1670-1683, doi:10.1001/jama.2014.3654 (2014).

16 Kalia, L. V. & Lang, A. E. Parkinson's disease. *Lancet* **386**, 896-912, doi:10.1016/S0140-6736(14)61393-3 (2015).

17 Mak, M. K., Wong-Yu, I. S., Shen, X. & Chung, C. L. Long-term effects of exercise and physical therapy in people with Parkinson disease. *Nat Rev Neurol* **13**, 689-703, doi:10.1038/nrneurol.2017.128 (2017).

18 Doherty, K. M. *et al.* Parkin disease: a clinicopathologic entity? *JAMA Neurol* **70**, 571-579, doi:10.1001/jamaneurol.2013.172 (2013).

19 Johansen, K. K., Torp, S. H., Farrer, M. J., Gustavsson, E. K. & Aasly, J. O. A Case of Parkinson's Disease with No Lewy Body Pathology due to a Homozygous Exon Deletion in Parkin. *Case Rep Neurol Med* **2018**, 6838965, doi:10.1155/2018/6838965 (2018).

20 Healy, D. G., Abou-Sleiman, P. M. & Wood, N. W. PINK, PANK, or PARK? A clinicians' guide to familial parkinsonism. *Lancet Neurol* **3**, 652-662, doi:10.1016/S1474-4422(04)00905-6 (2004).

21 Lohmann, E. *et al.* How much phenotypic variation can be attributed to parkin genotype? *Ann Neurol* **54**, 176-185, doi:10.1002/ana.10613 (2003).

22 West, A. *et al.* Identification and characterization of the human parkin gene promoter. *J Neurochem* **78**, 1146-1152, doi:10.1046/j.1471-4159.2001.00512.x (2001).

23 Dove, K. K. & Klevit, R. E. Structural Biology: Parkin's Serpentine Shape Revealed in the Year of the Snake. *Curr Biol* **23**, R691-693, doi:10.1016/j.cub.2013.07.039 (2013).

24 Cruts, M., Theuns, J. & Van Broeckhoven, C. Locus-specific mutation databases for neurodegenerative brain diseases. *Hum Mutat* **33**, 1340-1344, doi:10.1002/humu.22117 (2012).

25 Wauer, T. & Komander, D. Structure of the human Parkin ligase domain in an autoinhibited state. *EMBO J* **32**, 2099-2112, doi:10.1038/emboj.2013.125 (2013).

26 Yi, W. *et al.* The landscape of Parkin variants reveals pathogenic mechanisms and therapeutic targets in Parkinson's disease. *Hum Mol Genet* **28**, 2811-2825, doi:10.1093/hmg/ddz080 (2019).

27 *PRKN*.

28 Hershko, A. & Ciechanover, A. The ubiquitin system. *Annu Rev Biochem* **67**, 425-479, doi:10.1146/annurev.biochem.67.1.425 (1998).

29 Narendra, D., Walker, J. E. & Youle, R. Mitochondrial quality control mediated by PINK1 and Parkin: links to parkinsonism. *Cold Spring Harb Perspect Biol* **4**, doi:10.1101/cshperspect.a011338 (2012).

30 Lazarou, M., Jin, S. M., Kane, L. A. & Youle, R. J. Role of PINK1 binding to the TOM complex and alternate intracellular membranes in recruitment and activation of the E3 ligase Parkin. *Dev Cell* **22**, 320-333, doi:10.1016/j.devcel.2011.12.014 (2012).

31 Deas, E. *et al.* PINK1 cleavage at position A103 by the mitochondrial protease PARL. *Hum Mol Genet* **20**, 867-879, doi:10.1093/hmg/ddq526 (2011).

32 Greene, A. W. *et al.* Mitochondrial processing peptidase regulates PINK1 processing, import and Parkin recruitment. *EMBO Rep* **13**, 378-385, doi:10.1038/embor.2012.14 (2012).

33 Yamano, K. & Youle, R. J. PINK1 is degraded through the N-end rule pathway. *Autophagy* **9**, 1758-1769, doi:10.4161/auto.24633 (2013).

34 Matsuda, N. *et al.* PINK1 stabilized by mitochondrial depolarization recruits Parkin to damaged mitochondria and activates latent Parkin for mitophagy. *J Cell Biol* **189**, 211-221, doi:10.1083/jcb.200910140 (2010).

35 Lin, W. & Kang, U. J. Characterization of PINK1 processing, stability, and subcellular localization. *J Neurochem* **106**, 464-474, doi:10.1111/j.1471-4159.2008.05398.x (2008).

36 Zhou, C. *et al.* The kinase domain of mitochondrial PINK1 faces the cytoplasm. *Proc Natl Acad Sci U S A* **105**, 12022-12027, doi:10.1073/pnas.0802814105 (2008).

37 Sauve, V. *et al.* Mechanism of parkin activation by phosphorylation. *Nat Struct Mol Biol* **25**, 623-630, doi:10.1038/s41594-018-0088-7 (2018).

38 Narendra, D. P. *et al.* PINK1 is selectively stabilized on impaired mitochondria to activate Parkin. *PLoS Biol* **8**, e1000298, doi:10.1371/journal.pbio.1000298 (2010).

39 Vives-Bauza, C. *et al.* PINK1-dependent recruitment of Parkin to mitochondria in mitophagy. *Proc Natl Acad Sci U S A* **107**, 378-383, doi:10.1073/pnas.0911187107 (2010).

40 Gong, G. *et al.* Parkin-mediated mitophagy directs perinatal cardiac metabolic maturation in mice. *Science* **350**, aad2459, doi:10.1126/science.aad2459 (2015).

41 El Kodsi, D. N. *et al.* Parkinson Disease-Linked Parkin Mediates Redox Reactions That Lower Oxidative Stress In Mammalian Brain. *bioRxiv*, 2020.2004.2026.062380, doi:10.1101/2020.04.26.062380 (2020).

42 Tokarew, J. M. *et al.* Oxidative Modifications of Parkin Underlie its Selective Neuroprotection in Adult Human Brain. *bioRxiv*, 2020.2002.2019.953034, doi:10.1101/2020.02.19.953034 (2020).

43 Mochizuki, H. & Yasuda, T. Iron accumulation in Parkinson's disease. *J Neural Transm (Vienna)* **119**, 1511-1514, doi:10.1007/s00702-012-0905-9 (2012).

44 Nakamura, T., Naguro, I. & Ichijo, H. Iron homeostasis and iron-regulated ROS in cell death, senescence and human diseases. *Biochim Biophys Acta Gen Subj* **1863**, 1398-1409, doi:10.1016/j.bbagen.2019.06.010 (2019).

45 Zecca, L. *et al.* The role of iron and copper molecules in the neuronal vulnerability of locus coeruleus and substantia nigra during aging. *Proc Natl Acad Sci U S A* **101**, 9843-9848, doi:10.1073/pnas.0403495101 (2004).

46 Zucca, F. A. *et al.* Neuromelanin and iron in human locus coeruleus and substantia nigra during aging: consequences for neuronal vulnerability. *J Neural Transm (Vienna)* **113**, 757-767, doi:10.1007/s00702-006-0453-2 (2006).

47 Earle, K. M. Studies on Parkinson's disease including x-ray fluorescent spectroscopy of formalin fixed brain tissue. *J Neuropathol Exp Neurol* **27**, 1-14, doi:10.1097/00005072-196801000-00001 (1968).

48 Surmeier, D. J., Guzman, J. N., Sanchez-Padilla, J. & Goldberg, J. A. The origins of oxidant stress in Parkinson's disease and therapeutic strategies. *Antioxid Redox Signal* **14**, 1289-1301, doi:10.1089/ars.2010.3521 (2011).

49 Chan, C. S., Gertler, T. S. & Surmeier, D. J. A molecular basis for the increased vulnerability of substantia nigra dopamine neurons in aging and Parkinson's disease. *Mov Disord* **25 Suppl 1**, S63-70, doi:10.1002/mds.22801 (2010).

50 Guzman, J. N., Sanchez-Padilla, J., Chan, C. S. & Surmeier, D. J. Robust pacemaking in substantia nigra dopaminergic neurons. *J Neurosci* **29**, 11011-11019, doi:10.1523/JNEUROSCI.2519-09.2009 (2009).

51 Viola, H. M. & Hool, L. C. Cross-talk between L-type Ca2+ channels and mitochondria. *Clin Exp Pharmacol Physiol* **37**, 229-235, doi:10.1111/j.1440-1681.2009.05277.x (2010).

52 Surmeier, D. J. Calcium, ageing, and neuronal vulnerability in Parkinson's disease. *Lancet Neurol* **6**, 933-938, doi:10.1016/S1474-4422(07)70246-6 (2007).

53 Bolam, J. P. & Pissadaki, E. K. Living on the edge with too many mouths to feed: why dopamine neurons die. *Mov Disord* **27**, 1478-1483, doi:10.1002/mds.25135 (2012).

54 Matsuda, W. *et al.* Single nigrostriatal dopaminergic neurons form widely spread and highly dense axonal arborizations in the neostriatum. *J Neurosci* **29**, 444-453, doi:10.1523/JNEUROSCI.4029-08.2009 (2009).

55 Parent, M. & Parent, A. Relationship between axonal collateralization and neuronal degeneration in basal ganglia. *J Neural Transm Suppl*, 85-88 (2006).

56 Gauthier, J., Parent, M., Levesque, M. & Parent, A. The axonal arborization of single nigrostriatal neurons in rats. *Brain Res* **834**, 228-232 (1999).

57 Pissadaki, E. K. & Bolam, J. P. The energy cost of action potential propagation in dopamine neurons: clues to susceptibility in Parkinson's disease. *Front Comput Neurosci* **7**, 13, doi:10.3389/fncom.2013.00013 (2013).

58 Pacelli, C. *et al.* Elevated Mitochondrial Bioenergetics and Axonal Arborization Size Are Key Contributors to the Vulnerability of Dopamine Neurons. *Curr Biol* **25**, 2349-2360, doi:10.1016/j.cub.2015.07.050 (2015).

59 Giguere, N. *et al.* Comparative analysis of Parkinson's disease-associated genes in mice reveals altered survival and bioenergetics of Parkin-deficient dopamine neurons. *J Biol Chem* **293**, 9580-9593, doi:10.1074/jbc.RA117.000499 (2018).

60 Bosco, D. A. *et al.* Elevated levels of oxidized cholesterol metabolites in Lewy body disease brains accelerate alpha-synuclein fibrilization. *Nat Chem Biol* **2**, 249-253, doi:10.1038/nchembio782 (2006).

61 Nakabeppu, Y., Tsuchimoto, D., Yamaguchi, H. & Sakumi, K. Oxidative damage in nucleic acids and Parkinson's disease. *J Neurosci Res* **85**, 919-934, doi:10.1002/jnr.21191 (2007).

62 Puspita, L., Chung, S. Y. & Shim, J. W. Oxidative stress and cellular pathologies in Parkinson's disease. *Mol Brain* **10**, 53, doi:10.1186/s13041-017-0340-9 (2017).

63 Fedorova, M., Bollineni, R. C. & Hoffmann, R. Protein carbonylation as a major hallmark of oxidative damage: update of analytical strategies. *Mass Spectrom Rev* **33**, 79-97, doi:10.1002/mas.21381 (2014).

64 Alam, Z. I. *et al.* A generalised increase in protein carbonyls in the brain in Parkinson's but not incidental Lewy body disease. *J Neurochem* **69**, 1326-1329, doi:10.1046/j.1471-4159.1997.69031326.x (1997).

65 Drose, S. & Brandt, U. The mechanism of mitochondrial superoxide production by the cytochrome bc1 complex. *J Biol Chem* **283**, 21649-21654, doi:10.1074/jbc.M803236200 (2008).

66 Kussmaul, L. & Hirst, J. The mechanism of superoxide production by NADH:ubiquinone oxidoreductase (complex I) from bovine heart mitochondria. *Proc Natl Acad Sci U S A* **103**, 7607-7612, doi:10.1073/pnas.0510977103 (2006).

67 Richter, C., Park, J. W. & Ames, B. N. Normal oxidative damage to mitochondrial and nuclear DNA is extensive. *Proc Natl Acad Sci U S A* **85**, 6465-6467, doi:10.1073/pnas.85.17.6465 (1988).

68 Cadenas, E. & Davies, K. J. Mitochondrial free radical generation, oxidative stress, and aging. *Free Radic Biol Med* **29**, 222-230, doi:10.1016/s0891-5849(00)00317-8 (2000).

69 Lee, H. C., Chang, C. M. & Chi, C. W. Somatic mutations of mitochondrial DNA in aging and cancer progression. *Ageing Res Rev* **9 Suppl 1**, S47-58, doi:10.1016/j.arr.2010.08.009 (2010).

70 Forno, L. S., Langston, J. W., DeLanney, L. E., Irwin, I. & Ricaurte, G. A. Locus ceruleus lesions and eosinophilic inclusions in MPTP-treated monkeys. *Ann Neurol* **20**, 449-455, doi:10.1002/ana.410200403 (1986).

71 Langston, J. W., Forno, L. S., Rebert, C. S. & Irwin, I. Selective nigral toxicity after systemic administration of 1-methyl-4-phenyl-1,2,5,6-tetrahydropyrine (MPTP) in the squirrel monkey. *Brain Res* **292**, 390-394, doi:10.1016/0006-8993(84)90777-7 (1984).

72 Langston, J. W., Irwin, I., Langston, E. B. & Forno, L. S. 1-Methyl-4-phenylpyridinium ion (MPP+): identification of a metabolite of MPTP, a toxin selective to the substantia nigra. *Neurosci Lett* **48**, 87-92, doi:10.1016/0304-3940(84)90293-3 (1984).

73 Javitch, J. A., D'Amato, R. J., Strittmatter, S. M. & Snyder, S. H. Parkinsonism-inducing neurotoxin, N-methyl-4-phenyl-1,2,3,6 -tetrahydropyridine: uptake of the metabolite N-methyl-

4-phenylpyridine by dopamine neurons explains selective toxicity. *Proc Natl Acad Sci U S A* **82**, 2173-2177, doi:10.1073/pnas.82.7.2173 (1985).

74 Mizuno, Y., Sone, N. & Saitoh, T. Effects of 1-methyl-4-phenyl-1,2,3,6-tetrahydropyridine and 1-methyl-4-phenylpyridinium ion on activities of the enzymes in the electron transport system in mouse brain. *J Neurochem* **48**, 1787-1793, doi:10.1111/j.1471-4159.1987.tb05737.x (1987).

75 Pirooznia, S. K. *et al.* PARIS induced defects in mitochondrial biogenesis drive dopamine neuron loss under conditions of parkin or PINK1 deficiency. *Mol Neurodegener* **15**, 17, doi:10.1186/s13024-020-00363-x (2020).

76 Betarbet, R. *et al.* Chronic systemic pesticide exposure reproduces features of Parkinson's disease. *Nat Neurosci* **3**, 1301-1306, doi:10.1038/81834 (2000).

77 Floor, E. & Wetzel, M. G. Increased protein oxidation in human substantia nigra pars compacta in comparison with basal ganglia and prefrontal cortex measured with an improved dinitrophenylhydrazine assay. *J Neurochem* **70**, 268-275, doi:10.1046/j.1471-4159.1998.70010268.x (1998).

78 Chung, S. Y. *et al.* Parkin and PINK1 Patient iPSC-Derived Midbrain Dopamine Neurons Exhibit Mitochondrial Dysfunction and alpha-Synuclein Accumulation. *Stem Cell Reports* **7**, 664-677, doi:10.1016/j.stemcr.2016.08.012 (2016).

79 Kinumi, T., Kimata, J., Taira, T., Ariga, H. & Niki, E. Cysteine-106 of DJ-1 is the most sensitive cysteine residue to hydrogen peroxide-mediated oxidation in vivo in human umbilical vein endothelial cells. *Biochem Biophys Res Commun* **317**, 722-728, doi:10.1016/j.bbrc.2004.03.110 (2004).

80 Canet-Aviles, R. M. *et al.* The Parkinson's disease protein DJ-1 is neuroprotective due to cysteine-sulfinic acid-driven mitochondrial localization. *Proc Natl Acad Sci U S A* **101**, 9103-9108, doi:10.1073/pnas.0402959101 (2004).

81 Trist, B. G. *et al.* Amyotrophic lateral sclerosis-like superoxide dismutase 1 proteinopathy is associated with neuronal loss in Parkinson's disease brain. *Acta Neuropathol* **134**, 113-127, doi:10.1007/s00401-017-1726-6 (2017).

82 Trist, B. G. *et al.* Accumulation of dysfunctional SOD1 protein in Parkinson's disease is not associated with mutations in the SOD1 gene. *Acta Neuropathol* **135**, 155-156, doi:10.1007/s00401-017-1779-6 (2018).

83 Trist, B. G., Hare, D. J. & Double, K. L. A Proposed Mechanism for Neurodegeneration in Movement Disorders Characterized by Metal Dyshomeostasis and Oxidative Stress. *Cell Chem Biol* **25**, 807-816, doi:10.1016/j.chembiol.2018.05.004 (2018).

84 Smeyne, M. & Smeyne, R. J. Glutathione metabolism and Parkinson's disease. *Free Radic Biol Med* **62**, 13-25, doi:10.1016/j.freeradbiomed.2013.05.001 (2013).

85 Ambani, L. M., Van Woert, M. H. & Murphy, S. Brain peroxidase and catalase in Parkinson disease. *Arch Neurol* **32**, 114-118, doi:10.1001/archneur.1975.00490440064010 (1975).

86 Carlsson, A., Lindqvist, M., Magnusson, T. & Waldeck, B. On the presence of 3-hydroxytyramine in brain. *Science* **127**, 471, doi:10.1126/science.127.3296.471 (1958).

87 Haber, S. N. The place of dopamine in the cortico-basal ganglia circuit. *Neuroscience* **282**, 248-257, doi:10.1016/j.neuroscience.2014.10.008 (2014).

88 Ehringer, H. & Hornykiewicz, O. [Distribution of noradrenaline and dopamine (3-hydroxytyramine) in the human brain and their behavior in diseases of the extrapyramidal system]. *Klin Wochenschr* **38**, 1236-1239, doi:10.1007/bf01485901 (1960).

89 Hornykiewicz, O. Dopamine miracle: from brain homogenate to dopamine replacement. *Mov Disord* **17**, 501-508, doi:10.1002/mds.10115 (2002).

90 Giguere, N., Burke Nanni, S. & Trudeau, L. E. On Cell Loss and Selective Vulnerability of Neuronal Populations in Parkinson's Disease. *Front Neurol* **9**, 455, doi:10.3389/fneur.2018.00455 (2018).

91 Zarow, C., Lyness, S. A., Mortimer, J. A. & Chui, H. C. Neuronal loss is greater in the locus coeruleus than nucleus basalis and substantia nigra in Alzheimer and Parkinson diseases. *Arch Neurol* **60**, 337-341, doi:10.1001/archneur.60.3.337 (2003).

92 Daubner, S. C., Le, T. & Wang, S. Tyrosine hydroxylase and regulation of dopamine synthesis. *Arch Biochem Biophys* **508**, 1-12, doi:10.1016/j.abb.2010.12.017 (2011).

93 Montioli, R., Cellini, B., Dindo, M., Oppici, E. & Voltattorni, C. B. Interaction of human Dopa decarboxylase with L-Dopa: spectroscopic and kinetic studies as a function of pH. *Biomed Res Int* **2013**, 161456, doi:10.1155/2013/161456 (2013).

94 Levin, E. Y., Levenberg, B. & Kaufman, S. The enzymatic conversion of 3,4-dihydroxyphenylethylamine to norepinephrine. *J Biol Chem* **235**, 2080-2086 (1960).

95 Vendelboe, T. V. *et al.* The crystal structure of human dopamine beta-hydroxylase at 2.9 A resolution. *Sci Adv* **2**, e1500980, doi:10.1126/sciadv.1500980 (2016).

96 Monzani, E. *et al.* Dopamine, Oxidative Stress and Protein-Quinone Modifications in Parkinson's and Other Neurodegenerative Diseases. *Angew Chem Int Ed Engl* **58**, 6512-6527, doi:10.1002/anie.201811122 (2019).

97 Herrera, A., Munoz, P., Steinbusch, H. W. M. & Segura-Aguilar, J. Are Dopamine Oxidation Metabolites Involved in the Loss of Dopaminergic Neurons in the Nigrostriatal System in Parkinson's Disease? *ACS Chem Neurosci* **8**, 702-711, doi:10.1021/acschemneuro.7b00034 (2017).

98 Zucca, F. A. *et al.* Interactions of iron, dopamine and neuromelanin pathways in brain aging and Parkinson's disease. *Prog Neurobiol* **155**, 96-119, doi:10.1016/j.pneurobio.2015.09.012 (2017).

99 Zhang, S., Wang, R. & Wang, G. Impact of Dopamine Oxidation on Dopaminergic Neurodegeneration. *ACS Chem Neurosci* **10**, 945-953, doi:10.1021/acschemneuro.8b00454 (2019).

100 Cartier, E. A. *et al.* A biochemical and functional protein complex involving dopamine synthesis and transport into synaptic vesicles. *J Biol Chem* **285**, 1957-1966, doi:10.1074/jbc.M109.054510 (2010).

101 Lohr, K. M., Masoud, S. T., Salahpour, A. & Miller, G. W. Membrane transporters as mediators of synaptic dopamine dynamics: implications for disease. *Eur J Neurosci* **45**, 20-33, doi:10.1111/ejn.13357 (2017).

102 Segura-Aguilar, J. A new mechanism for protection of dopaminergic neurons mediated by astrocytes. *Neural Regen Res* **10**, 1225-1227, doi:10.4103/1673-5374.162750 (2015).

103 Segura-Aguilar, J. *et al.* Protective and toxic roles of dopamine in Parkinson's disease. *J Neurochem* **129**, 898-915, doi:10.1111/jnc.12686 (2014).

104 Farzam, A. *et al.* A functionalized hydroxydopamine quinone links thiol modification to neuronal cell death. *Redox Biol* **28**, 101377, doi:10.1016/j.redox.2019.101377 (2020).

105 Zucca, F. A. *et al.* Neuromelanin organelles are specialized autolysosomes that accumulate undegraded proteins and lipids in aging human brain and are likely involved in Parkinson's disease. *NPJ Parkinsons Dis* **4**, 17, doi:10.1038/s41531-018-0050-8 (2018).

106 Graham, D. G. Oxidative pathways for catecholamines in the genesis of neuromelanin and cytotoxic quinones. *Mol Pharmacol* **14**, 633-643 (1978).

107 Tse, D. C., McCreery, R. L. & Adams, R. N. Potential oxidative pathways of brain catecholamines. *J Med Chem* **19**, 37-40, doi:10.1021/jm00223a008 (1976).

108 Burbulla, L. F. *et al.* Dopamine oxidation mediates mitochondrial and lysosomal dysfunction in Parkinson's disease. *Science* **357**, 1255-1261, doi:10.1126/science.aam9080 (2017).

109 Yu, G. *et al.* In vivo protein targets for increased quinoprotein adduct formation in aged substantia nigra. *Exp Neurol* **271**, 13-24, doi:10.1016/j.expneurol.2015.04.019 (2015).

110 LaVoie, M. J., Ostaszewski, B. L., Weihofen, A., Schlossmacher, M. G. & Selkoe, D. J. Dopamine covalently modifies and functionally inactivates parkin. *Nat Med* **11**, 1214-1221, doi:10.1038/nm1314 (2005).

111 LaVoie, M. J., Cortese, G. P., Ostaszewski, B. L. & Schlossmacher, M. G. The effects of oxidative stress on parkin and other E3 ligases. *J Neurochem* **103**, 2354-2368, doi:10.1111/j.1471-4159.2007.04911.x (2007).

112 Chung, K. K. *et al.* S-nitrosylation of parkin regulates ubiquitination and compromises parkin's protective function. *Science* **304**, 1328-1331, doi:10.1126/science.1093891 (2004).

113 Yao, D. *et al.* Nitrosative stress linked to sporadic Parkinson's disease: S-nitrosylation of parkin regulates its E3 ubiquitin ligase activity. *Proc Natl Acad Sci U S A* **101**, 10810-10814, doi:10.1073/pnas.0404161101 (2004).

114 Whitworth, A. J. *et al.* Increased glutathione S-transferase activity rescues dopaminergic neuron loss in a Drosophila model of Parkinson's disease. *Proc Natl Acad Sci U S A* **102**, 8024-8029, doi:10.1073/pnas.0501078102 (2005).

115 Palacino, J. J. *et al.* Mitochondrial dysfunction and oxidative damage in parkin-deficient mice. *J Biol Chem* **279**, 18614-18622, doi:10.1074/jbc.M401135200 (2004).

116 Aguirre, J. D., Dunkerley, K. M., Mercier, P. & Shaw, G. S. Structure of phosphorylated UBL domain and insights into PINK1-orchestrated parkin activation. *Proc Natl Acad Sci U S A* **114**, 298-303, doi:10.1073/pnas.1613040114 (2017).

117 Kumar, A. *et al.* Disruption of the autoinhibited state primes the E3 ligase parkin for activation and catalysis. *EMBO J* **34**, 2506-2521, doi:10.15252/embj.201592337 (2015).

118 Spratt, D. E. *et al.* A molecular explanation for the recessive nature of parkin-linked Parkinson's disease. *Nat Commun* **4**, 1983, doi:10.1038/ncomms2983 (2013).

119 Shevchenko, A., Tomas, H., Havlis, J., Olsen, J. V. & Mann, M. In-gel digestion for mass spectrometric characterization of proteins and proteomes. *Nat Protoc* **1**, 2856-2860, doi:10.1038/nprot.2006.468 (2006).

120 Cox, J. & Mann, M. MaxQuant enables high peptide identification rates, individualized p.p.b.-range mass accuracies and proteome-wide protein quantification. *Nat Biotechnol* **26**, 1367-1372, doi:10.1038/nbt.1511 (2008).

121 Werck-Reichhart, D. & Feyereisen, R. Cytochromes P450: a success story. *Genome Biol* **1**, REVIEWS3003, doi:10.1186/gb-2000-1-6-reviews3003 (2000).

122 Han, J. *et al.* Resonance Raman spectra of plastocyanin and pseudoazurin: evidence for conserved cysteine ligand conformations in cupredoxins (blue copper proteins). *Biochemistry* **30**, 10904-10913, doi:10.1021/bi00109a014 (1991).

123 Berg, J. M. Zinc finger domains: hypotheses and current knowledge. *Annu Rev Biophys Biophys Chem* **19**, 405-421, doi:10.1146/annurev.bb.19.060190.002201 (1990).

124 Hoch, D. G., Abegg, D. & Adibekian, A. Cysteine-reactive probes and their use in chemical proteomics. *Chem Commun (Camb)* **54**, 4501-4512, doi:10.1039/c8cc01485j (2018).

125 Miseta, A. & Csutora, P. Relationship between the occurrence of cysteine in proteins and the complexity of organisms. *Mol Biol Evol* **17**, 1232-1239, doi:10.1093/oxfordjournals.molbev.a026406 (2000).

126 Marino, S. M. & Gladyshev, V. N. Cysteine function governs its conservation and degeneration and restricts its utilization on protein surfaces. *J Mol Biol* **404**, 902-916, doi:10.1016/j.jmb.2010.09.027 (2010).

127 Xiao, H. *et al.* A Quantitative Tissue-Specific Landscape of Protein Redox Regulation during Aging. *Cell* **180**, 968-983 e924, doi:10.1016/j.cell.2020.02.012 (2020).

128 Chen, S. H. & Li, C. W. Detection and Characterization of Catechol Quinone-Derived Protein Adducts Using Biomolecular Mass Spectrometry. *Front Chem* **7**, 571, doi:10.3389/fchem.2019.00571 (2019).

129 Vandiver, M. S. *et al.* Sulfhydration mediates neuroprotective actions of parkin. *Nat Commun* **4**, 1626, doi:10.1038/ncomms2623 (2013).

130 Goldberg, M. S. *et al.* Parkin-deficient mice exhibit nigrostriatal deficits but not loss of dopaminergic neurons. *J Biol Chem* **278**, 43628-43635, doi:10.1074/jbc.M308947200 (2003).

131 Fornai, F. *et al.* Striatal dopamine metabolism in monoamine oxidase B-deficient mice: a brain dialysis study. *J Neurochem* **73**, 2434-2440, doi:10.1046/j.1471-4159.1999.0732434.x (1999).

132 Berman, H. M. *et al.* The Protein Data Bank. *Nucleic Acids Res* **28**, 235-242, doi:10.1093/nar/28.1.235 (2000).

133 Trempe, J. F. *et al.* Structure of parkin reveals mechanisms for ubiquitin ligase activation. *Science* **340**, 1451-1455, doi:10.1126/science.1237908 (2013).

134 Fang, C. M. *et al.* Identification of Endogenous Site-specific Covalent Binding of Catechol Estrogens to Serum Proteins in Human Blood. *Toxicol Sci* **148**, 433-442, doi:10.1093/toxsci/kfv190 (2015).

135 Pickrell, A. M. *et al.* Endogenous Parkin Preserves Dopaminergic Substantia Nigral Neurons following Mitochondrial DNA Mutagenic Stress. *Neuron* **87**, 371-381, doi:10.1016/j.neuron.2015.06.034 (2015).

136 Periquet, M., Corti, O., Jacquier, S. & Brice, A. Proteomic analysis of parkin knockout mice: alterations in energy metabolism, protein handling and synaptic function. *J Neurochem* **95**, 1259-1276, doi:10.1111/j.1471-4159.2005.03442.x (2005).

137 Chung, E. *et al.* Intracellular delivery of Parkin rescues neurons from accumulation of damaged mitochondria and pathological alpha-synuclein. *Sci Adv* **6**, eaba1193, doi:10.1126/sciadv.aba1193 (2020).

138 Rascol, O., Lozano, A., Stern, M. & Poewe, W. Milestones in Parkinson's disease therapeutics. *Mov Disord* **26**, 1072-1082, doi:10.1002/mds.23714 (2011).

139 Schapira, A. H. *et al.* Extended-release pramipexole in advanced Parkinson disease: a randomized controlled trial. *Neurology* **77**, 767-774, doi:10.1212/WNL.0b013e31822affdb (2011).

140 Olanow, C. W. *et al.* A double-blind, delayed-start trial of rasagiline in Parkinson's disease. *N Engl J Med* **361**, 1268-1278, doi:10.1056/NEJMoa0809335 (2009).

141 Shoulson, I. DATATOP: a decade of neuroprotective inquiry. Parkinson Study Group. Deprenyl And Tocopherol Antioxidative Therapy Of Parkinsonism. *Ann Neurol* **44**, S160-166 (1998).

142 Siderowf, A. *et al.* Test-retest reliability of the unified Parkinson's disease rating scale in patients with early Parkinson's disease: results from a multicenter clinical trial. *Mov Disord* **17**, 758-763, doi:10.1002/mds.10011 (2002).